

POLITECNICO DI TORINO



Corso di Laurea Magistrale in Ingegneria Energetica e Nucleare

*Computational model for water
management improvement
in Proton Exchange Membrane fuel cells*

Relatore:

Prof. Vittorio Verda

Correlatore:

Ing. Alberto Pizzolato

*Candidato:
Salvatore De Sena*

Dicembre 2018

Abstract

Global energy scenarios foresee an increase in the energy demand and greenhouse gases emissions, unless some significant actions are taken. Switching to a clean and flexible energy carrier like hydrogen is of paramount importance. Fuel cells allow hydrogen to be converted into electricity without any thermal combustion process and with much higher efficiencies than traditional thermal engines. However, the design of cheap, robust and efficient fuel cell devices is still hampered by the complex physical phenomena involved. Hence, it is essential to develop high-fidelity models, able to represent practical operating conditions. In the thesis, a 2D steady-state model of a proton exchange membrane fuel cell is presented, which accounts for fluid-dynamics, species transport, charge conservation, electrochemical kinetics and water in all its forms. The objective of this work is to represent all the physical and chemical aspects that characterize the cell, and to analyse its performance in typical operating conditions. Compared to most previous studies, we fully represent the influence of water in the polymer membrane fuel cell. Besides steam and liquid water, we also consider the water dissolved in the membrane, to account for its influence on the ionic conductivity and on the mass transfer between the three phases. This yielded a framework that correctly predicts the behaviour of the cell at low voltages, considering both the anode dehydration and the diffusive losses. The governing equations are discretized using the finite element method and solved using the commercial software COMSOL Multiphysics[®]. The accuracy of the framework was both verified and validated using numerical and experimental data available in literature. Results show that a thorough model of water in all its phases is essential to predict mass transfer losses at high current densities. Furthermore, we obtained an optimum porosity of the catalyst, by exploring the trade-off between convective and ohmic losses. Finally, our parametric analysis suggested that optimizing the catalyst distribution has high potential for performance improvements.

Summary

1.	Introduction to fuel cell.....	7
1.1.	The thermodynamics of a cell.....	8
1.2	Electrochemical kinetics	11
1.3	Charge conduction	14
1.4	Mass Transport	16
1.5	Polarization curve	18
2.	Proton Exchange Membrane Fuel Cell.....	21
2.1	Bipolar plates	22
2.1.1	Properties of bipolar plates	23
2.1.2	Materials for bipolar plate	23
2.2	The gas diffusion layer	24
2.2.1	Properties of the layer.....	24
2.2.2	Materials for the gas diffusion layer.....	25
2.3	The catalyst layers	26
2.3.1	Properties of the catalysis layers	27
2.3.2	Types of catalysis layers.....	28
2.4	The proton exchange membrane.....	28
2.4.1	Membrane properties	29
3	Water Management in a fuel cell.....	31
3.1	The problem of membrane drying	31
3.2	Transport of water in the membrane.....	33
3.2.1	Electro-osmotic drag.....	34
3.2.2	Back diffusion	34
3.2.3	Transfer of water due to pressure gradients between anode and cathode	35
3.2.4	Water loss due to evaporation phenomena	35
4	Computational model of PEMFC	37
4.1	Introduction to computational model.....	39
4.2	Assumptions for the fuel cell model.....	41
4.3	Governing equations	41
4.4	Equations for the gaseous species.....	42
4.4.1	Continuity's equation.....	42
4.4.1	Brinkman's equation	43
4.4.2	Chemical species transport's equation	45

4.5	Energy equations of the cell.....	49
4.5.1	Charge transport's equation.....	50
4.6	Equations for water management	54
4.6.1	Dissolved water's equation.....	54
4.6.2	Liquid water's equation	58
4.7	Numerical methods	62
4.7.1	Method and program used	62
4.7.2	Parameters and variables	63
5	Result and discussion.....	68
5.1	Model verification.....	68
5.2	Model validation	70
5.3	Analysis in nominal conditions.....	72
5.4	Parametric analysis	79
5.4.1	Variation of operating parameters	79
5.4.2	Variation of design parameters.....	83
6	Conclusion	96
7	Bibliography	98

Nomenclature

Parameters and variable

c	concentration (mol/mm ³)
D	diffusion coefficient
E_{th}	Nernst potential (V)
F	Faraday's constant
h_{fg}	enthalpy of vaporization (J/kg)
k	thermal conductivity (W/mK)
M	Molar mass (kg/mol)
n	number of electrons
P	pressure (Pa)
R	universal gas constant (J/molK)
s	Saturation
S	Source's terms
t	thickness (m)
T	Temperature (K)
u	velocity (m/s)
V_{cell}	cell voltage
w	mass fraction
W	Potenza
L	Work
G	Gibbs free energy
z	Charge numebr
J	Molar specific flow

Greek letters

φ	potential (V)
ε	volume fraction
γ	switch function
λ	polymer water content H ₂ O/SO ₃ ⁻
μ	viscosity (Pa s)
ρ	density (kg/m ³)
σ	ionic conductivity (S/m)
τ	tortuosity
η	efficiency
λ_{H_2}	excess fuel coefficient

Subscripts

a	anode
act	activation
c	cathode
C	carbon
eff	effective
evap	evaporation
H ₂	hydrogen
i	ionic
LV	mass transfer from liquid to vapor
O ₂	oxygen
p	polymer
v	vapor
void	void space
W	water
WD	water dissolved in polymer
WV	water vapor
WL	water liquid
WP	water production
el	electrical
ohm	ohmic effect
diff	diffusion effect
agg	agglomerate

Superscripts

cat	catalyst layer
cp	capillary pores
g	gas phase
gdl	gas diffusion layer
p	polymer phase
v	vapor phase

1. Introduction to fuel cell

Current topics such as the progressive depletion of fossil fuel reserves and the contextual increase in global energy needs, pollution and climate changes of the planet have been at the centre of international debates for several years. In particular, the unconditional increase in fuel prices and the need to reduce greenhouse gas emissions are pushing rapidly to research and experiment with renewable, low-cost and low-impact energy sources. One of the industrial sectors strongly influenced by the energy issue is the automotive world, which is going through a critical phase; today, in fact, the car is considered by the average customer as a costly mean of transport and little respectful of the environment. Therefore, the concept of sustainable mobility, which is based on the use of alternative fuel vehicles, is becoming more and more important recently. In fact, there are some studies that are evaluating the feasibility of realizing complex smart systems, where the fuel cell electric vehicles are used also in fuel cell Vehicle-to-Grid (FCV2G) mode: when there is a peak of electricity demand, the car could be used to produce electricity to inject in the grid. [1]. In this context, in recent years hydrogen has attracted considerable interest as a clean energy resource of the future, and it has strongly pushed research and experimentation of technologies suitable for its use. It is evident that to guarantee the necessary eco-compatibility the hydrogen of the future must be entirely derived from renewable sources, with methodologies that, however, are not today still economically viable and able to compete with the most established industrial techniques derivation of hydrogen from fossil exhaustible sources. It is foreseen a significant increase in usage of Pemfc in the transport sector. In fact, all the major automobile manufacturers are currently investing in research and development of hydrogen fuelled vehicles to be commercialized within 10-15 years. To reach this target, and realize other ambitious projects, fuel cell technology must continue to improve from the point of view of costs and performances [8].

Proton Exchange Membrane Fuel Cells (Pemfc) are among the best solution for both portable and small stationary applications, thanks to their high energy conversion efficiency, high power density and low pollutants emissions [2-5]. During the operation of the fuel cell, it is important to manage the temperature level because of heat release, that affects transport, kinetic and phase-transfer parameters [2-4]. Therefore, numerous mathematical models were developed with the aim of fully understanding the species momentum and thermal transport by coupling water and thermal transport [6,7]. Actually, there are still some challenging limits to be overcome such as the cost of catalyst and the low durability, that are the main reasons why the

wide spread application of Pemfc is difficult today [9]. During past decades, many researchers have made efforts to optimize the performance of Pemfc.

Having a full understanding of how fuel cell works, and how to improve it, can be very important for developing an eco-sustainable future. In the past some have tried to study the cell, building computational models, but they were unable to fully simulate the cell behaviour, since they did not consider the management of water within it. Considering the cell in working conditions at high voltages, the influence of water inside is almost negligible [10], but changing the operating point to higher currents, the movement and the quantity of water in the cell, change the performance completely. The goal of this study is to have a complete model, able to represent all the physical and chemical aspects present in the cell correctly. In this way, it's possible to have a fuel cell model perfectly working, to find the optimal configuration that allows to size efficient hydrogen vehicles.

1.1. The thermodynamics of a cell

The fuel cell is a device with which it is possible to produce, by electrochemical means, the oxidation reaction, with direct production of electrical energy; in some types, the cell works at high temperatures making the thermal energy available, thus operating in cogeneration of electrical and thermal energy.

The most used fuel is hydrogen and the oxidizer are oxygen; the complete chemical reaction is the following:



The reaction product is a mole of water for each mole of oxidized hydrogen.

By spatially separating these reactions, the electrons transferred from the fuel are forced to flow through an external circuit (thus constituting an electric current) and do useful work before they can complete the reaction, as can be seen in Fig. 1.

The reagents can be fed continuously into the cell, from which the reaction products can be continuously discharged; the operation, from the thermodynamic point of view, is therefore

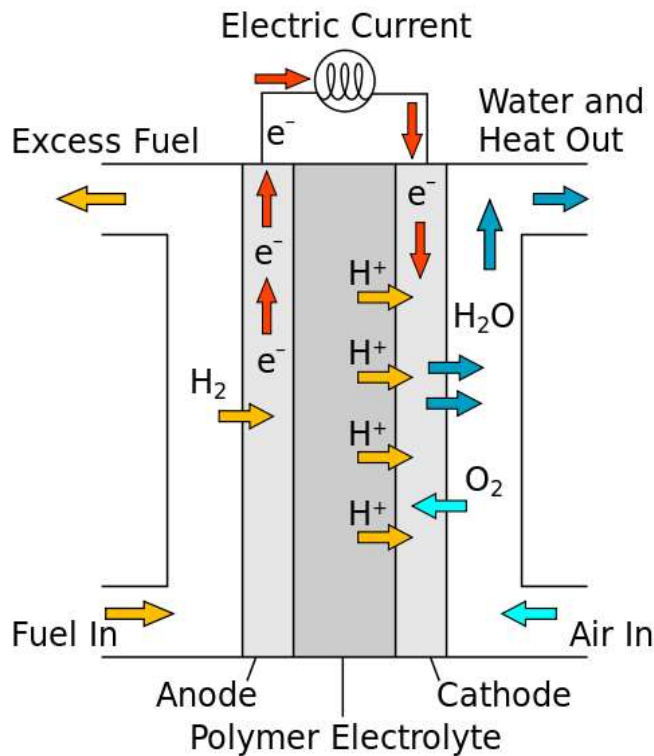


Figure 1 Schematic of a fuel cell

with a steady-state run-off.

From a thermodynamic point of view, the maximum electrical work obtained corresponds to the variation of the Gibbs free energy ΔG ; the reaction is spontaneous and is thermodynamically favoured because the Gibbs free energy of the products is less than the energy of the reagents.

Chemical energy can be defined as the property of a stream of mass characterized by high value of the Gibbs free energy. The classical processes to take advantage of chemical energy in order to produce electrical power is:

- Producing heat at high T (thermo-chemical transformation)
- Producing mechanical power using a shaft in a thermodynamic cycle fed by heat at high T (thermo-mechanical transformation)
- Producing electrical power in alternator (electro-mechanical transformation)

These processes are very complex and inefficient ways to exploit chemical energy. Electrochemical cells are able to directly convert chemical energy into electric energy with low value of irreversibility and high efficiencies, and they can also run in both directions, making it possible to spend energy in order to produce fuel.

Defining n as the number of electrons involved in the reaction, E [V] as the reversible voltage (or electromotive force), F as the Faraday constant (module of the electric charge of a mole of electrons: $F = 96485 \left[\frac{C}{mol} \right]$).

The variation in the Gibbs free energy can be expressed as:

$$\Delta G = -z_F F E \quad (2)$$

$$L_{el} = \frac{W_{el}}{n_r} = \frac{I E}{\frac{I}{z_F F}} = E z_F F \quad (3)$$

where z_F is the number of electrons involved in the reaction, E [V] is the reversible voltage (or electromotive force), $F \left[\frac{C}{mol} \right]$ is the Faraday constant (module of the electric charge of a mole of electrons).

In an isothermal and isobaric process, the variation of the Gibbs free energy expresses the maximum electrical work that can be delivered ($-W_{el}$) max:

$$\Delta G = -W_{el} \quad (4)$$

The ΔH enthalpy variation of a reaction in a fuel cell represents the whole heat released by the constant pressure reaction; defining S as entropy, Q as the heat and T as the temperature in Kelvin:

$$\Delta H = \Delta Q = T \Delta S \quad (5)$$

In an exothermic process, the produced heat, or reaction heat, can be defined as ΔH_{tot} reaction enthalpy; this quantity can be calculated as the difference between the formation enthalpies ΔH_{tot} of the species that make up the reaction products and reagents:

$$\Delta H_{tot} = \Delta H_p - \Delta H_r \quad (6)$$

The efficiency of a generation process is the relationship between the useful energy (or power) and the total energy (or power) developed to produce the useful energy; in the case of fuel cells, the useful energy is expressed by the Gibbs free energy, while the total energy developed in a reversible process is given by the reaction enthalpy:

$$\eta = \frac{\Delta G}{\Delta H_{tot}} = \frac{\Delta g}{\Delta h} \text{ (in molar terms)} \quad (7)$$

The actual yield must take into account the electrical losses inside the load and the fuel losses; the electrical losses are due to internal dissipative phenomena associated with the current circulation and reduce the power produced by the cell. The fuel losses are inevitable to supply the electrochemical reaction completely, it is necessary to supply more reagents than what is required by stoichiometry and therefore there is an efficiency loss in using the fuel. With the factor λ_{H_2} the excess of used fuel is taken into account.

$$\lambda_{H_2} = \frac{G_{H_2}^{eff}}{G_{H_2}^{stoich}} \quad (8)$$

The mass flow rate G is calculated with the Faraday's law:

$$G_{H_2} = \frac{I}{z_f F} M_{H_2} \lambda_{H_2} \quad (9)$$

Efficiency calculated according to the flow rate:

$$\eta = \frac{W_{el}}{G_{H_2} \Delta h} = \frac{IV_c}{\frac{I}{z_f F} M_{H_2} \lambda_{H_2} \Delta h} = \frac{V_c z_f F}{M_{H_2} \lambda_{H_2} \Delta h} \quad (10)$$

In this way it is possible to calculate the efficiency as a function of V_c if the λ_{H_2} is known.

1.2 Electrochemical kinetics

The thermodynamic laws are used in order to study the equilibrium of a reaction, making it possible to predict how much fuel will react, and what power will be produced. The concept of rate of reaction is instead studied with kinetics.

Chemical kinetics studies the "speed" of chemical processes, so the variation over time of the quantity and quality of the chemical species that participate in it (see Fig. 2) and the relationships that bind it to the composition of the system, to temperature, pressure and to other chemical-physical factors; we try to determine the time necessary to obtain a conversion from reagents to products,

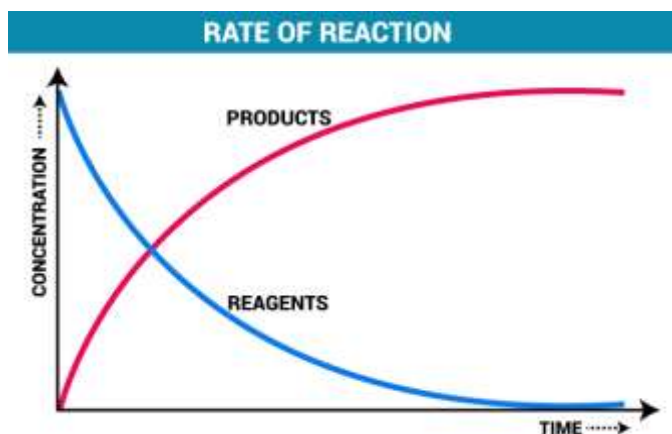


Figure 2 Representation of the variation in the concentration of reagents on time [11]

allowing us to know the mechanism of the reaction, and also the set of steps and intermediate chemical species that creates the reaction in question. The fluid dynamics of the reactant mixture, especially the inlet velocity, and the speed at which the reaction occurs, may combine in a way that won't allow the chemical reaction to reach the equilibrium in the reactor. It is necessary that the reaction rate is high enough to guarantee the achievement of this equilibrium.

The rate of reaction can be changed by 3 factors:

- Temperature (usually the increase of the temperature increases the rate of reaction)
- The concentration of reagents (the increase of the concentration increases the rate of reaction)
- The catalyst: the catalyst only changes the rate of reaction without modifying the equilibria dictated by thermodynamics, its presence only increases the reaction speed.

Usually, a catalyst operates over the reactant molecules through an adsorption process. The interaction between fluid and the catalyst occurs at the level of the surface.

An electrochemical reaction takes place as two different half electrochemical reactions occurring separately in the two electrodes. Each of the electrochemical reactions has its own given kinetic. The kinetic behaviour of a half electrochemical reaction is strictly related to the rate of reaction R . Differently from a normal chemical reaction, for which R is a function of the T only, the rate of reaction R for an electrochemical reaction is a function of T and potential gradient in the electrodes ($R = R(T, \eta)$).

So, it's possible to define:

$$R = k(T)e^{\frac{\alpha F}{RT}v_i z_i \eta} \quad (11)$$

Where k is constant rate, that is a function of T ($k(T) = Ae^{-E_a/RT}$), F is faraday constant, v_i is stoichiometric coefficient of “i” species, Z is charge number of “i” species, η is potential drop in the electrodes, α is transfer coefficient and it is function of symmetry factor (β that is usually equal to 0.5), n_{drs} number of electrons transferred in the rate determining step of reactions.

The potential gradient does not modify directly the activation energy of a reaction (like catalyst) but modifies the energy level of reactants and products phase. The advantages involved by η are subdivided between positive effect at reactants, and positive effect at products, and are expressed by symmetry factor β and its complementary ($1 - \beta$).

Starting from the equation of R , it is possible to obtain an expression stating the relation between the current density “ I ” and voltage drop due to charge transport phenomena taking place when the reaction has been activated.

$$i = i_o \left[e^{\frac{\beta F}{RT}\eta_{act}} - e^{\frac{(1-\beta)F}{RT}\eta_{act}} \right] \quad (12)$$

η_{act} is the activation overvoltage: voltage drop that should be “spent” in order to activate the electrochemical reaction by increasing the rate of reaction.

i_o exchange current density: current density exchanged when the electrochemical reaction is in equilibrium. Higher currents operation is the preferred condition, because the reaction activation is easier. This value depends on many factors:

- l_{tpb}
- *type of nanostructure*
- *Temperature*

l_{tpb} is the length of the three-phase boundary: such a parameter takes into account the surface over which the reaction occurs. In order to make the reactions occur:

- Molecules of reactants must be fed to the point of reaction (in porous phase)
- H^+ ions must be removed from the point of reaction (in ionic phase)
- e^- must be removed from point of reaction (electronic phase)

The point in which the three phases coexist is called three phase boundary. The union of all this point is the l_{tpb} . Larger value of this means larger areas over which the reaction can take place, so larger current density. A diagram of all this is shown in the Fig 3.

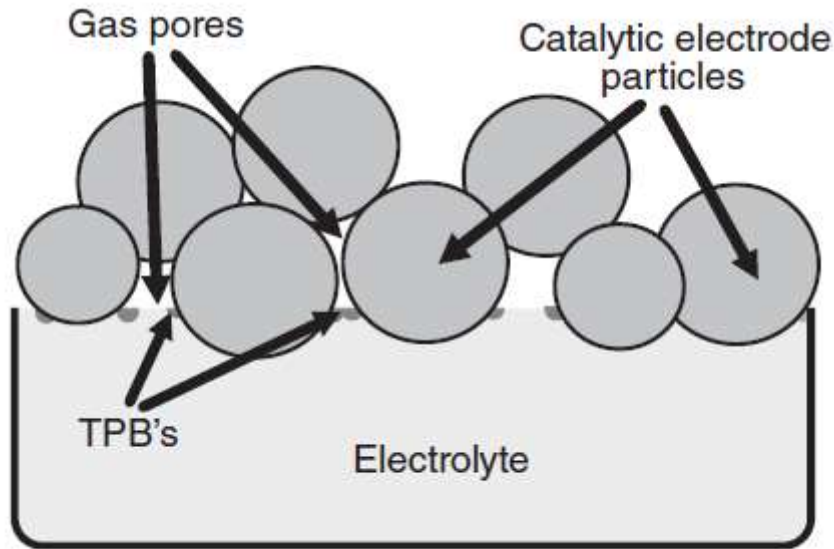


Figure 3 Simplified schematic of electrode–electrolyte interface in a fuel cell, illustrating TPB [11]

1.3 Charge conduction

The electrons are transported in electrodes, according to mechanisms of electrical conduction, produced by the electric field that acts directly on the charges. In the electrolyte takes place the transport of ions according to electrical conduction, diffusion and convection of the charge carriers, but the dominant mechanism is conduction. The electric current density j from Faraday's law is:

$$\begin{aligned} j &= zFJ \\ \sigma &= |z|F c \mu \end{aligned} \tag{13}$$

where z is the number of charges associated with the carrier, F is the constant of Faraday, the product zF is the electric charge of a charge-carrying molecule of the chemical species and allows the transformation from chemical quantities to electrical quantities, J is the flow specific

molar $\left[\frac{mol}{cm^2s}\right]$. The measure of how well the cell allows the charge transport is indicated by the electrical conductivity. In fuel cells I have to consider both ionic and electronic conductivity, that is calculated in siemens σ (S Siemens), while $c \left[\frac{mol}{cm^3}\right]$ is the molar concentration of the charge carriers present in the medium and $\mu \left[\frac{m^2}{Vs}\right]$ expresses their mobility in the medium.

The proton conductivity is much lower than the electrical one, so the voltage losses are mainly due to the motion of the ions rather than the electrons. To increase the efficiency of the cell, the electrolyte must have very high ion conductivity, in order to avoid drop of voltage, but it must not transmit the electrons or allow the reagent gases to permeate.

The requirements that a good electrolyte must have are the following [12]:

- for the material: high ionic conductivity, low electronic conductivity, low crossover, mechanical strength, easy workability, low cost;
- for thickness: low electrical resistance, low crossover, mechanical integrity, uniformity, high discharge voltage.

The ohmic voltage drop caused by charge conduction can be expressed as:

$$\eta_{ohm} = RI = \frac{\rho L}{A} I = \frac{\rho L}{A} (iA) = \rho Li = ASR \quad (14)$$

Where ASR is the Area specific Resistance. It depends on $\rho [\Omega m]$ that is the resistivity of material (the inverse of conductivity).

1.4 Mass Transport

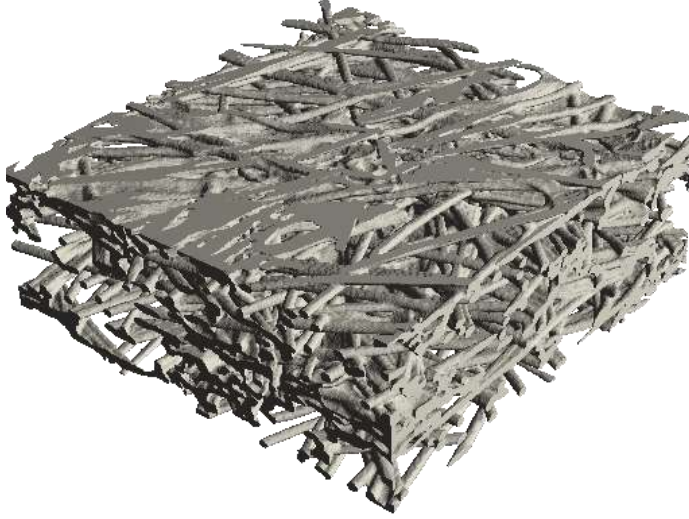


Figure 4 Example of a GDL [29]

The mass transport mechanisms are both convective and diffusive, so the forces involved are, respectively, pressure and concentration gradients. Mass transport takes place initially in the channels, and then it is passed to the GDL (gas diffusion layer represented in Fig. 4) thanks also to the conveyors. In the GDL, where diffusion dominates, the reagents are directed towards the electrodes where the reaction takes place; Concentration gradients are at the origin of diffusive transport, governed by Fick's first law:

$$J = -D_i \nabla C_i \quad (15)$$

where $J \left[\frac{\text{mol}}{\text{m}^2 \text{s}} \right]$ is the molar specific flow, $D_i \left[\frac{\text{m}^2}{\text{s}} \right]$ the molar concentration, and C_i is the concentration of species;

Molecular diffusion processes strictly affect the quantity of reactants in point of reaction. Given a certain molar flow of reactant, which is supplied to the electrode in bulk conditions, the diffusive process through which the fuel molecules are diffused across the electrode pores, will determine the reactant concentration C_i in any of the point of the electrode.

The diffusive process will be strictly related to the diffusive coefficient of the species D_i

$$D_i^{eff} = \left(\frac{\varepsilon}{\tau} \right)^n D_i \quad (16)$$

Where ε is the porosity of the GDL, τ is the tortuosity, and n is a fitting parameter, D_i is the diffusive coefficient of species "i" at bulk condition.

When the current to be delivered becomes larger and larger, the number of reactions in the reaction point increases as well, and the number of molecules needed to drive those reactions grow. In such situation the mechanism of molecular diffusion in the porous structure of the electrodes may become too slow to replace rapidly enough the molecules that have reacted over the electrode surface.

Physically, diffusion phenomena will not be the direct responsible of a potential drop, but rather it will cause a reactant concentration reduction, which could cause a potential drop. It is representable with η_{diff} .

The way to calculate the diffusion of the gas through the porous medium is the Fick equation, but in the case of several components present at the same time, a modified Fick formula is used. Maxwell-Stefan diffusivity equation is used. The Maxwell-Stefan diffusion (or Stefan-Maxwell diffusion) is a model for describing diffusion in multicomponent systems.

This equation can take into account the Knudsen diffusion. It is a mean of diffusion that occurs when the scale length of a system is comparable to or smaller than the mean free path of the particles involved. Consider the diffusion of gas molecules through very small capillary pores. If the pore diameter is smaller than the mean free path of the diffusing gas molecules and the density of the gas is low, the gas molecules collide with the pore walls more frequently than with each other. This process is known as Knudsen flow or Knudsen diffusion [13].

Conveyors then perform the function of current collectors between one cell and the next and have both sides provided with flow channels: one conveys reactants of anode and the other one the cathode

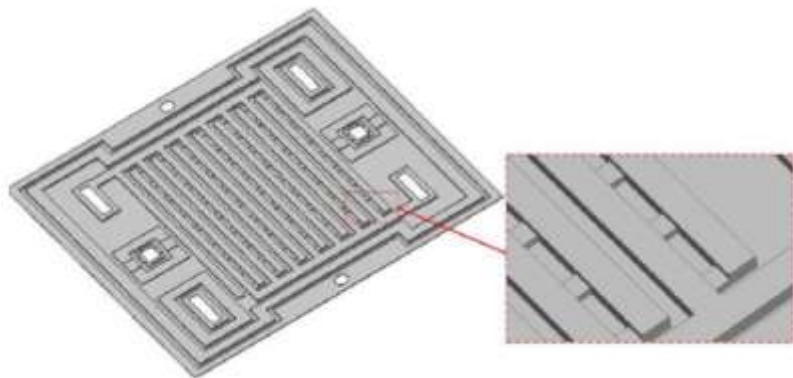


Figure 5 Schematic of a bipolar plate with Conveyors [14]

reactants; therefore, the conveyors are called bipolar plates. The main requirements for the materials are [4]: high resistance to chemical aggression, high chemical compatibility, high electrical and thermal conductivity, high mechanical resistance, easy workability, low cost. The most used material is graphite. There are three flow channel configurations: serial, parallel, or mixed connections; the goal is having a high homogeneity in the conveyance of reagents and products, low inlet pressure, high flow, absence of stagnation areas and accumulation. The Fig. 5 shows some configurations of the flow channels in the bipolar plates. [14]

1.5 Polarization curve

Temperature is a parameter that influences the quantities mentioned in the previous paragraphs; but the temperature distribution must also be taken into account since local deviations may occur from optimal conditions leading to a drop in overall performance, or hot spots may occur with the risk of deteriorating the materials and the cell itself.

The thermal sources due to dissipative phenomena occur in the catalysis layer, in fact during the cell operation, many thermal fluxes are exchanged within the system. Such heat fluxes are generated by the occurrence of the reaction itself and overvoltage [14].

- All the overvoltage effects will generate heat
- The effect of reaction thermodynamics will generate an exothermic or endothermic heat flux, depending on the working regime of the fuel cell. In case of Pemfc use to produce electricity (Galvanic cell) the will be generation of heat flux, so it is always be characterized by an exothermic reaction.

$$\begin{aligned}
 Q_{th} = Q_{react} + Q_{irr} &= \left(-\frac{T\Delta s_{react}}{z_f F} \right) I + \left(\sum_j \eta_j \right) I = \left(-\frac{T\Delta s_{react}}{z_f F} + \sum_j \eta_j \right) I \\
 &= \left(-\frac{\Delta h_{react} - \Delta g_{react}}{z_f F} + \sum_j \eta_j \right) I = \left(-\frac{\Delta h_{react}}{z_f F} - \left(-\frac{\Delta g_{react}}{z_f F} - \sum_j \eta_j \right) \right) I \\
 Q_{th} &= \left(-\frac{\Delta h_{react}}{z_f F} - V_c \right) I \tag{17}
 \end{aligned}$$

1) If we consider an ideal reaction in open-circuit condition, the entropy generation due to the reaction occurrence and transport phenomena is null, so all the chemical energy is totally transformed into electrical efficiency

2) If there will be a real reaction in open circuit conditions, the entropy generation due to the reaction occurrence it would not be null, and there will be a production of heat. So not all chemical energy is transformed in electrical energy.

3) Finally, if we do a real reaction in closed-circuit condition, the entropy generation due to both factors won't be null, so we will obtain a different behaviour of the polarization curve.

	Case 1	Case 2	Case 3
V_c	$-\frac{\Delta h_{react}}{z_f F}$	$-\frac{\Delta g_{react}}{z_f F}$	$OCV - \left(\sum_j \eta_j \right) I$
Q_{th}	0	$\left(-\frac{\Delta h_{react} - \Delta g_{react}}{z_f F} + \sum_j \eta_j \right) I$ $= \left(-\frac{T \Delta S_{react}}{z_f F} \right) I$	$\left(-\frac{\Delta h_{react}}{z_f F} - V_c \right) I$

Table 1 Explanation of the entropy generations according to the irreversibility of the cell and the voltage and current conditions

A final aspect of thermal transport concerns the convective exchange with the environment, which takes into account natural transverse convection and forced longitudinal convection in the flow channels. The first, which takes place through the lateral surface of the cell, is limited by the small longitudinal thickness of the cell and by the edge thickness in the transversal direction, in which there is the heat exchange along the side wall; the second is due to the reaction products carried by diffusion in the electrode and by convection in the flow channels. As we have already seen before, the characteristic curve represents the trend of the voltage as a function of the current density. Irreversible phenomena that subtract potential from the ideal value in operation are called polarizations. At low currents, the characteristic curve is predominantly influenced by the activation bias. In the zone of intermediate values of the current density, there is a fairly linear trend where we can see the influence of the ohmic polarization and the fall can be estimated with the law of Ohm ($\eta_{ohm} = RI$ with R total cell resistance); finally, for high current densities, the reagents are consumed at a speed such that the flow through the electrodes is no longer sufficient to maintain an adequate concentration on the catalysis layer [15]. In Fig. 7 we can see the typical shape of the polarization curve of a fuel cell. The image shows the reasons why there is voltage reduction. In the first part the losses are due to the activation energy, then in the second part are due to the ohmic effect, and then, in the last part, the reduction is due to diffusion difficulties.

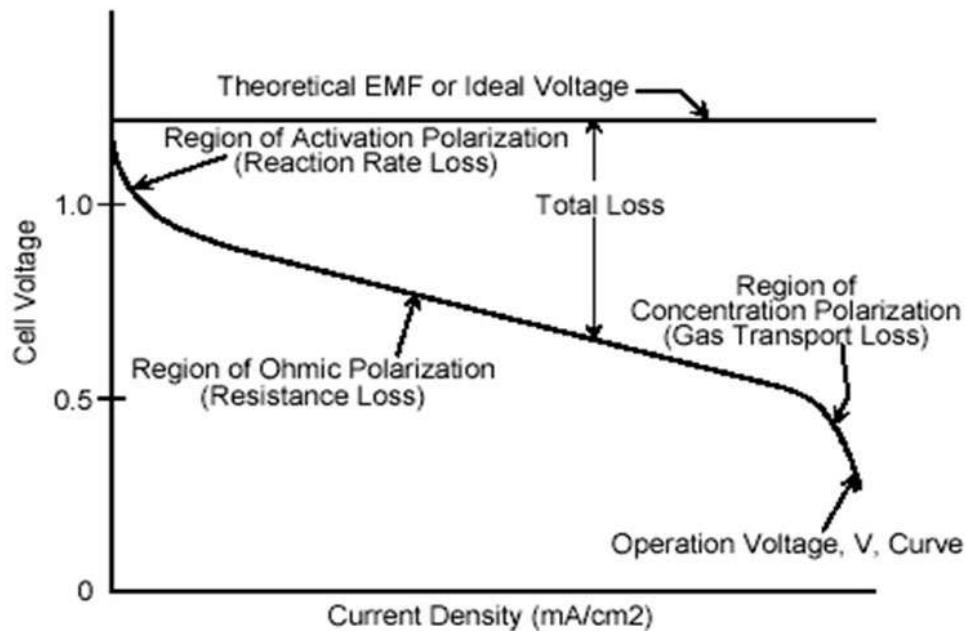


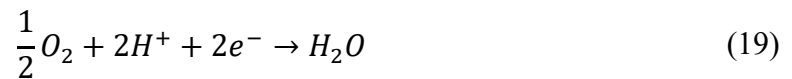
Figure 6 Typical shape of a bias curve

2. Proton Exchange Membrane Fuel Cell

Polymeric membrane cells operate at temperatures between 30 and 120 ° C [16]; the fuel has to be provided continuously and it is used directly without reforming process. The reaction that takes place at the anode is:



While the one that takes place at the cathode is:



therefore, the charge transporter ion is H^+ ; the water produced is expelled to the cathode, with excess air as shown in Fig.7

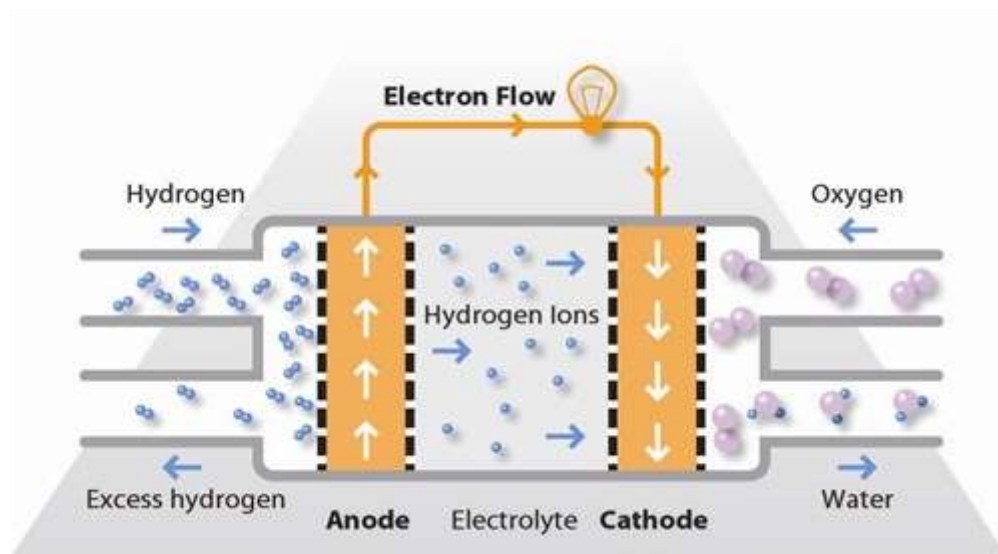


Figure 7 Operation of a Pemfc [24]

Usually the electrical efficiency of a fuel cell is around the 40 or 50 % [17]. These cells have some advantages:

- high power density: $0.3 - 1 \left[\frac{W}{cm^2} \right]$ [(the highest among the fuel cells) [18]
- absence of corrosion problems typical of other types of cells with liquid electrolyte [19]

- relative constructive simplicity
- rapid cold start, on the order of minutes [18].
- High volumetric and gravimetric power density. [20,21]

The cells, however, work at low temperature and this has the disadvantage of having a poor tolerance to the presence of CO in the fuel that would damage the catalysts. Since most of the hydrogen in the world comes from a process called steam reforming, where methane reacts with steam water at very high temperatures (usually 800 ° C) [22,23] and forms hydrogen and carbon monoxide. So, it is very important to make sure that the presence of CO in the flow of hydrogen is practically null, as it is a poison for the platinum catalyst.

The Pemfc-type fuel cell is made up of several components in order to make it possible to transport the gas near the electrolyte, so that the electrochemical reaction can occur. The different components are shown in the Fig. 8 and then explained.

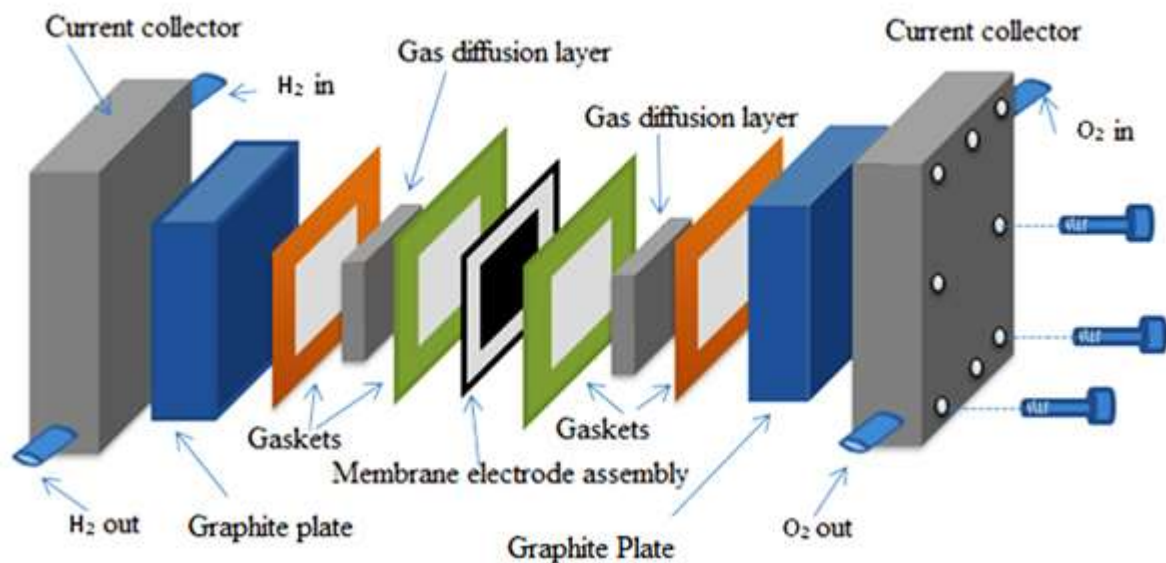


Figure 8 The different components that make up the fuel cell [18]

2.1 Bipolar plates

The fuel is inserted through the current collector, and then must be properly distributed inside the cell through the bipolar plates.

2.1.1 Properties of bipolar plates

BPPs are one of the most important components of the stack with about 80% of the total weight and 30-40% of the cost. BPPs must perform many functions [25,26]:

- homogeneously distribute the gases on the cell area.
- separate the combustible and oxidizing gas and prevent gas leaks.
- collect current in electrochemical vicinity.
- discharge the produced water.
- guarantee the mechanical resistance of the cell
- guarantee the electrical connection between cells and electrical output to another row of cells;
- distribute the refrigerant fluid, remove the heat generated;
- remove the water in the flood, ensure good management of both moisture and heat;
- structurally support and separate each cell, including the separation of hydrogen and oxygen;

2.1.2 Materials for bipolar plate

The material to be used for the dishes must comply with the following conditions:

- high thermal conductivity (greater than $20 \left[\frac{W}{mK} \right]$ [25]): important for heat management;
- high purity or low content of volatile and extractable components;
- mechanical and chemical compatibility: each component must be able not to deteriorate over time and not to damage even the rest of the components. It is therefore very important to find the material that best suits the cell. The membrane and the catalyst are very sensitive and easily damaged areas.
- they must show little aging;
- highly polished surface;
- be easy to build: these last two points are related to the costs and the quality of the dish.

Initially, the material used was graphite, high-density graphite which included natural or synthetic graphite; graphite has an excellent corrosion resistance, high chemical stability and

the lack of components that can poison the membranes and catalysts and finally a good electrical conductivity during cell operation. However, its porous structure induces a fragile behaviour and allows the permeation of the gas through the channels formed after processing. The materials used for the bipolar plates are generally based on stainless steel, or titanium. These metal bipolar plates have high conductivity and thermal properties, good mechanical properties and negligible gas permeability.

A set of features to be complied with according to the "United States Department of Energy (DOE)" by the BPP regarding performance and cost targets [27].

Technical Targets: Bipolar Plates for Transportation Applications

Characteristic	Units	2015 Status	2020 Targets
Cost ^a	\$/kW _{net}	7 ^b	3
Plate weight	kg/kW _{net}	<0.4 ^c	0.4
Plate H ₂ permeation coefficient ^d	Std cm ³ /(sec cm ² Pa) @ 80°C, 3 atm, 100% RH	0 ^e	<1.3x10 ^{-14,f}
Corrosion, anode ^g	µA/cm ²	no active peak ^h	<1 and no active peak
Corrosion, cathode ⁱ	µA/cm ²	<0.1 ^c	<1
Electrical conductivity	S/cm	>100 ^j	>100
Areal specific resistance ^k	ohm cm ²	0.006 ^h	<0.01
Flexural strength ^l	MPa	>34 (carbon plate) ^m	>25
Forming elongation ⁿ	%	20-40 ^o	40

Figure 9 A set of features to be complied with according to the "United States Department of Energy (DOE)" by the BPP regarding performance and cost targets [27]

2.2 The gas diffusion layer

2.2.1 Properties of the layer

The diffusion layer (gas diffusion layer, GDL) is a crucial component in the cell because it offers the following functions and properties [28]:

- helps to distribute the reagent gases from the flow channels of the bipolar plates to the catalysis layer; therefore, the GDL must be porous enough to make the gas flow without too much trouble;

- helps to remove the water produced and accumulated in the catalysis layer towards the flow channels; therefore, it must have pores wide enough so that the water moves without blocking the pores;
- provides a mechanical support to the catalyst layer and the membrane so that they resist the pressure exerted by the bipolar plates; therefore, the GDL must be constructed with a material that does not deform;
- allows the conduction of electrons from the catalysis layer to the bipolar plates and vice versa with a low electronic resistance; therefore, the material must have a good electronic conductivity;
- helps to transfer the heat produced by the catalysis layer to the plates in order to keep the cell at a desired temperature; therefore, the material must have a high thermal conductivity.

2.2.2 Materials for the gas diffusion layer

The layer is usually composed of carbon sheets, i.e. carbon fibers pressed or in carbon fabric, i.e. carbon fibers woven into a fabric-like material. The latter has a higher permeation rate than the carbon sheets. However, the carbon sheet supports provide greater stiffness and stability to the electrode. There are two type of gas diffusion layer [29].

- Carbon Paper Gas Diffusion Layers (GDL) (e.g. Sigracet, Freudenberg, Toray, etc) tend to be thinner and more brittle than Carbon Cloth Gas Diffusion Layers. Each type has a different mass transport, porosity, hydrophobicity, and conductivity.
- Papers such as Toray are quite hard and brittle, with very little compressibility. These are good for designs where a tighter tolerance is permitted in the compression and where the thin GDL is a critical factor. Since they are so brittle, care must be taken when handling them in order to not break corners or otherwise damage the GDL.

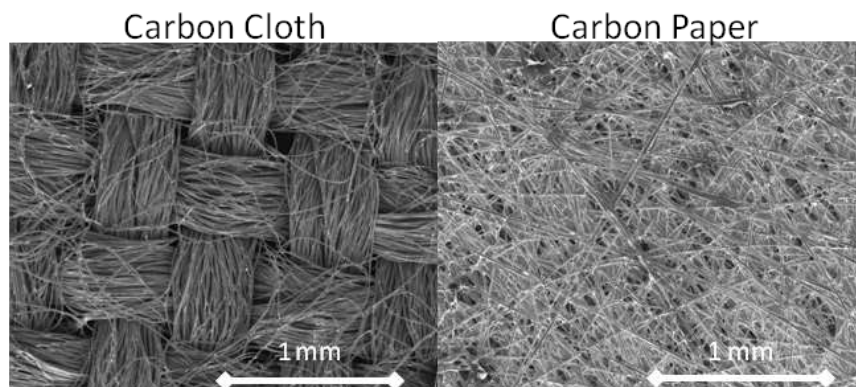


Figure 10 The two type of GDL [29]

- The Carbon Cloth based GDL materials (see Fig. 10) are the most flexible and are generally quite mechanically robust but are also the thickest. These are typically designed to

have a fair amount of compression when assembled in the stack (anywhere from ~10% to 60% of the GDL thickness) and can act somewhat as compressible “springs” in the stack design.

2.3 The catalyst layers

The catalysis layer (catalyst layer, CL) is found between the PEM and the diffusion layer of the gas (gas diffusion layer, GDL); the H^+ protons move between the catalysis layer and the PEM, and the electrons move between the catalysis layer and the GDL. On the CL, electrochemical reactions occur for the generation of electric power; the reactions are on the anode-side catalyst layer and on the cathode-side catalysis layer and both are active or three-phase boundary sites where the reacting gases [31,32], protons and electrons react on the surface of catalysis, thanks to the presence of platinum. A representation of how the catalyst is composed is shown in Fig. 11. Regarding the reaction to the cathode, a factor influencing the performance of the catalyst is the removal of reaction water in the liquid phase. On the one hand, an excess of water hinders the transport of oxygen that fails to reach the cathode and consequently, by not completing the reaction, the cell performance decreases; on the other hand, a lack of water causes a decrease in the proton conductivity of PEM and Nafion in the catalysis layer, leading also in this case to a deterioration in cell performance [30,33]. The basic requirements of a CL are:

- many active sites;
- an efficient transport of protons from the catalysis layer of the anode to that of the cathode;
- easy transport of reagent gases;
- high electrical conductivity between the reaction sites and the current collector;

- high mechanical strength;
- corrosion resistance.

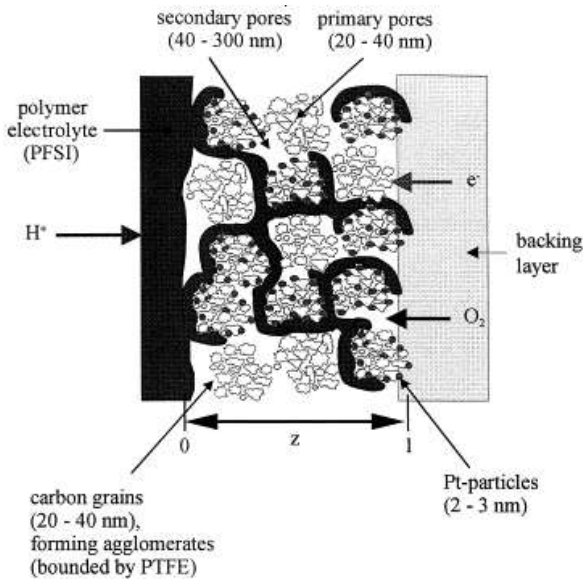


Figure 11 Schematic picture of the catalyst layer geometry and its composition, exhibiting the different functional parts. The typical catalyst layer thickness l is 10 mm [29].

2.3.1 Properties of the catalysis layers

Current catalyst technology involves using platinum Pt nanoparticles (typically 2-3 nm), supported by a carbon surface. The best catalyst for anode and cathode is platinum. In general, the higher the platinum content, the greater the performance, but there are also higher costs, which are a factor impeding the marketing of PEM. For this reason, we try to reduce the platinum content without compromising performance and durability. In terms of performance, platinum levels of $0.01 - 0.02 \left[\frac{mg}{cm^2} \right]$ have arrived in the laboratories, but with such low values, durability becomes problematic; at present, an optimum value of platinum loading, both in terms of performance and durability, is around $0.2 \left[\frac{mg}{cm} \right]$ [18]. The Nafion content in the catalyst affects the performance of MEA, since it affects gas permeability and ionic strength. Another characteristic of the catalysis layer is the porosity, necessary for the transport of gas to active sites; unfortunately, the performance of the cell is not proportional to the porosity: if this is high, the mass flow increases but the proton and electrons decrease.

2.3.2 Types of catalysis layers

There are two principal types of thin film catalyst layers: one in which the layer is placed on the gas diffusion layer (catalyst-coated gas diffusion electrode CCGDL), and one where the layer is deposited on the proton exchange membrane (catalyst -coated membranes, CCM) [24,34]. For the CCGDL you can have:

- a distribution of Nafion and of the uniform catalyst through the catalysis layer This method demonstrates excellent performance.
- an uneven distribution of the catalyst or Nafion or both. In the first case, you can have a platinum gradient or along the cross section of the layer (i.e. from the PEM / CL interface to the CL / GDL interface) or along the longitudinal section of the layer (i.e. along the path of the reacting gases from the entrance to the exit); in the second case, only one direction is used, along the cross section. For the CCM we have:

- Conventional CCM: currently a platinum - Nafion mixture applied to the membrane is used;
- nanostructured thin film electrode; platinum is deposited on thin films and then placed on the membrane surface.

2.4 The proton exchange membrane

Nafion is a tetrafluoroethylene sulfonate and is constituted (Fig.12) by a main sequence of -CF₂- CF₂-CF₂- molecules linked together and by a chain of -O-CF₂-CF-O-CF-CF₂- which connects the region preceding a group of SO_3^- and H^+ ions. So, it is obtained by adding to the molecule of Teflon a lateral branch which ends with a hydrogen sulphite (HSO_3^-). In this chemical group there is a very weak bond linking H^+ and SO_3^- . This gives rise to high mobility of H^+ in polymer. The way in which the H^+ ions are conducted across the electrolyte is called “hopping mechanism”, and it is a procedure by which H^+ ions jump from one SO_3^- site to the next one [35,6].

drag) and back diffusion (water back diffusion): the first is due to the fact that each proton H^+ in the motion of migration from the anode to the cathode carries some molecules of water; the second mechanism occurs because the cathode accumulates many more water molecules than the anode, due to the fact that electro-osmotic drainage occurs and that the water is produced at the cathode so this different concentration causes the back diffusion from the cathode to the cathode anode. As the current density increases during the operation of the cell, electro-osmotic drainage increases; as a consequence, the level of dehydration at the anode increases so much that the membrane's ability to exploit backscattering to balance the water content on the two faces of the membrane is lost. Furthermore, the accumulation of water at the cathode leads to an increase in concentration losses since oxygen finds it more difficult to reach the cathode.

The necessity to maintain the membrane hydrated involves the necessity to operate at $T < 100^\circ\text{C}$. So, there are some consequences [18]:

- 1) Low T involves low rates of electrochemical reaction. Therefore, it will be necessary to introduce good quality catalyst, like Platinum. Then since platinum suffers from poisoning effect, especially of carbonaceous molecules, there will be low CO (Pt becomes ineffective if $[\text{CO}] > 100$ ppm).
- 2) Pemfc can recover heat to produce thermal power. However, the low T of operation will involve low exergies for such thermal fluxes. Therefore, Pemfc can be coupled only with low T terminals at high surface.
- 3) Low T means fast start up and shutdown down and fast varying load (automotive, residential applications)

The thin membranes have a low mechanical resistance and therefore tend to get damaged in a short time; some of the factors that induce a decline in mechanical performance are hydrolysis, oxidative attack, depolymerization. Groups containing hydrogen have an influence on the thermal and chemical stability of fluoropolymers; for example, hydrogen peroxide (H_2O_2), the formation of which may be due to the oxygen crossover or to an incomplete reduction of oxygen on the surface of the catalyst, reacting with metallic contaminants (due to the presence of metallic bipolar plates) like Fe_2^+ or Cu_2^+ , a form of radicals that attack PEM [18].

3 Water Management in a fuel cell

During the operation of a fuel cell, because of the electrochemical reactions that combine hydrogen and oxygen, there is the production of water. In PEM cells it is essential to humidify the membrane, in order to guarantee the proton conductivity necessary to offer a good functioning of the cell without causing excessive voltage losses due to a high ionic resistance. It has already been discussed that due to the temperatures involved in this type of cells it is difficult to maintain an adequate humidification of the electrolyte membrane. In fact, at temperatures higher than 50 ° C the effect of evaporation of the water contained in the membrane is noticeable, which becomes insufficient if produced only by electrochemical reactions. An excessive dehydration of the same, in addition to causing a decrease in performance, can also be detrimental to the structural integrity of the membrane that is likely to break. Furthermore, the electrolytic membrane allows the transport of water in both directions: due to the structure of the polymers that constitute it, there is a good uniformity in the distribution of the water molecules inside it; however, particularly extreme operating conditions can cause a lack of uniformity in the water content and therefore concentration gradients can be found that significantly affect the cell performance, causing unevenness in the current, voltage and temperature values [35].

It is therefore clear that sufficient water must be contained in the polymeric electrolyte, otherwise the conductivity may decrease. In a PEMFC, water is formed at the cathode. In the ideal case, this water would bring the electrolyte to have the correct level of hydration. The air fed to the cathode should be able to dry out any excess water. Since the electrolyte membrane is very thin, the water would diffuse from the cathode to the anode, and in each region of the entire electrolyte an appropriate level of hydration would be realized.

3.1 The problem of membrane drying

The electrolyte membrane allows the transport of water in both directions: due to the structure of the polymers that constitute it, there is a good uniformity in the distribution of the water molecules inside it. However, there should not be as much water to flood the electrode, preventing the transport of the gaseous reactants in the diffusion layer up to the catalyst layer (Blocking). However, certain particularly extreme operating conditions can cause non-uniformity in the water content inside the membrane, and therefore concentration gradients can

be found that significantly affect cell performance, causing current, voltage and very different temperatures inside the cell itself [36].

If the cell is at different temperature values, then the relative humidity can change considerably as it is a function of temperature. If it exceeds 100% then the water condenses and will be found in the liquid form (multiphase flow). Water can partially block some channels and lead to an uneven distribution of the reagents, reducing efficiency.

The first problem is the drying effect caused by the flow of cathode air, especially at high temperatures. In fact, at temperatures higher than 60 ° C, the air will always be dried faster than water is produced by the reaction between H_2 and O_2 [36,18]. A very practiced method to solve these problems is to humidify the air, the hydrogen, or both, before their entry into the fuel cell. This process is often necessary and increases notably the efficiency of the fuel cell.

Yet another complication is that the water balance in the electrolyte must be correct in every region of the cell. In concrete, some parts could be hydrated in the desired way, others too dry. For example, dry air can enter the cell, but passing over the electrodes can become so saturated that it cannot dry them from excesses of water.

The air will always be fed through the flow cell greater than is necessary to provide stoichiometric oxygen. Problems arise because the drying effect of the air is nonlinear in relation to the temperature. To understand this phenomenon the effects must be considered quantities of the term's relative humidity, water content and vapor pressure saturated. The amount of water vapor in the air varies greatly, depending on the temperature, from the position, climatic conditions and other factors. A simple method of measurement and description of the amount of water vapor in the air is to supply the ratio of water to other gases (nitrogen, oxygen, argon, carbon dioxide and others that make up dry air). This quantity is known otherwise as percentage of humidity, absolute humidity or specific humidity and is defined as:

$$x = \frac{m_w}{m_a} \quad (20)$$

where m_w is the mass of water present in the mixture, and m_a is the mass in dry air. The total mass of moist air is the sum of the two.

However, this does not give a good representation of the drying effect air. Air at high temperature, even if with a high-water content, can look very dry, and have a very strong drying effect. On the other hand, the air at low temperature, even if with a low water content, can be perceived as very humid. The reason for this is due to the variations in the pressure of vapor

saturated water vapor. This saturated vapor pressure is the partial pressure of the water when a mixture of air and liquid water are in equilibrium. If saturated, air cannot retain additional water vapor in a mixture.

To determine how much water is needed to supply the inlet gas, the water produced during the operation of the fuel cell must be carefully analysed. If the relative humidity of the outlet air is much less than 100%, then the effect could be the drying of the cell, and the PEM would cease its operation. The only way to overcome this problem is to humidify one or both reagent gases. On the other hand, a relative humidity of more than 100% is impossible, and the flow of air would contain condensed water drops [37].

3.2 Transport of water in the membrane

The proton conductivity of the membrane decreases as the water content decreases within it. The amount of water molecules that Nafion can retain depends on its molecular structure, but the overall membrane water content may vary due to various factors [38,53]:

- Transport of water molecules from the anode to the cathode due to electro-osmotic drag (EOD).
- Transport of water molecules from the cathode to the anode due to back-diffusion
- Water loss due to evaporation phenomena
- Water formation at the cathode for electrochemical reaction.
- Transfer of water by permeation due to pressure gradients between anode and cathode

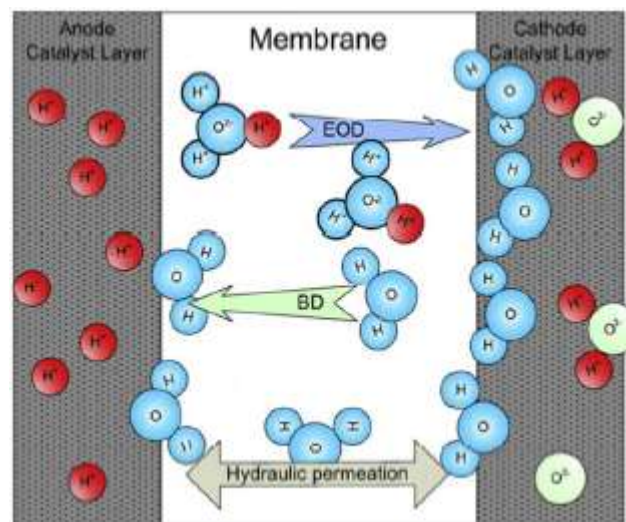


Figure 14 Typical movements of water through the membrane

Some of these aspects are represented in Fig. 14.

3.2.1 Electro-osmotic drag

The passage of the water molecules from the anode to the cathode linked to ionic transport is called electroosmotic drag (electro-osmotic drag). The electrolyte membrane is normally crossed by H^+ protons that move from the anode to the cathode to complete the electrochemical reaction characteristic of the operation of the fuel cells. In practice, due to the molecular structure of water, some molecules of H_2O are bound to the hydrogen ion to form a new ion called hydronium (H_3O^+) [39]. This ion crosses the membrane as normally happens with the H^+ proton. The result of this phenomenon is the transport of water from the anode to the cathode. The factors that govern this passage are many, but the main conditions are the humidification of the membrane and the cell temperature. Therefore, this phenomenon is indirectly influenced by the humidification temperatures of the hydrogen and air flows and by the current to which the cell is made to work.

As mentioned previously, through the hopping mechanism, the H^+ ion has the possibility to cross the membrane. The more the membrane is hydrated the more efficient this process is. Basically, the conducted ion is not only H^+ , but rather one it is possible to form the ions of the type between H_3O^+ , $H_5O_2^+$, $H_7O_3^+$ [18].

At the cathode the H^+ ions are combined with oxygen and with the electrons that have passed through the external electric circuit and there is the production of water.

3.2.2 Back diffusion

The formation of water at the cathode due to the electrochemical reactions and the different water intake through the two streams cause a concentration difference of water at both ends of the electrolyte membrane. Usually the concentration at cathode is greater because it has the production of water and moreover, having air flow rates more due to the need for a considerable excess of this to get good cell performance, a considerable amount is introduced through the gaseous flow if this is humidified. The difference in concentration leads to a transport of water for the natural tendency of the system to bring itself into equilibrium conditions. The transport takes place according to the rules of diffusion through porous means. Usually the water that is moved due to this phenomenon goes from the cathode to the anode. For this reason, we speak of back diffusion. This phenomenon is also greatly influenced from the working conditions and

therefore from the degree of humidification of the membrane and from the working temperature [15].

3.2.3 Transfer of water due to pressure gradients between anode and cathode

This is achieved by increasing the pressure in both chambers. In the event of flooding problems, the cathode pressure is kept lower than that of the anode, to allow a faster escape of water. While if the pressure in the cathode is greater than that of the anode, the water will move towards the anode. The motion of water is determined by Darcy's law:

$$\mathbf{u} = -\frac{k}{\mu} \nabla P \quad (21)$$

Where u is the velocity of water displacement, μ is the viscosity of the membrane, k the permeability of the membrane. This factor is very important. In case of excessive flow of water due to the osmotic drag electrode, if the pressure in the cathode chamber is greater than that of the anode, the quantity of water passing from the cathode to the anode is increased, with the useful effect of keep the membrane more hydrated. So, you can play with the pressure of the chambers in case of drying (increase cathode pressure) and in case of high production of water, you can increase the pressure of the anode to allow a faster escape of water.

3.2.4 Water loss due to evaporation phenomena

The amount of water inside the membrane also changes due to evaporation. At the anode this phenomenon can be harmful because it leads to the membrane dehydration and decreased performance due to excessive resistance to the passage of protons. On the contrary, at the cathode this phenomenon can be positive because it is partly able to limit the phenomenon of flooding. This is indeed the reason for the considerable excess of air supplied to the cathode. To avoid an excessive accumulation of water on the cathode side which causes a lowering of the performance because it prevents the passage of oxygen to the reaction sites, it comes send an excess amount of air to facilitate the expulsion of water either through the evaporation of part of this, both through transport phenomena. It is difficult to quantify the water that

evaporates and the one that is transported outside the cell. It is possible to carry out balances on the flow of water entering and leaving the cell and, evaluating its performance during operation under various conditions, hypothesize situations of dehydration or flooding if performance declines. Fuel cells are often made to work at higher pressures than that environment because performance is improved as expressed from the Nernst equation [40]. Because of the problems of flooding usually the pressure on the cathode side is kept lower than that of the anodic side. In fact, one back pressure on the air side prevents the expulsion of water. If you want to apply a high back pressure to the cathode, there must be further increased excess air. Different pressures on the two sides of the membrane lead to a transport of water due to pressure gradient.

4 Computational model of PEMFC

The fuel cell model that will be represented is a 2D model. The model then cuts the cell with a plane x, y in order to represent both the chambers and the membrane and not to consider the thickness along the z plane. Usually all the layers of the cell have the same thickness except the channel, which is narrower than the membrane and the porous medium. A 3D representation of the fuel cell is given by the Fig. 15:

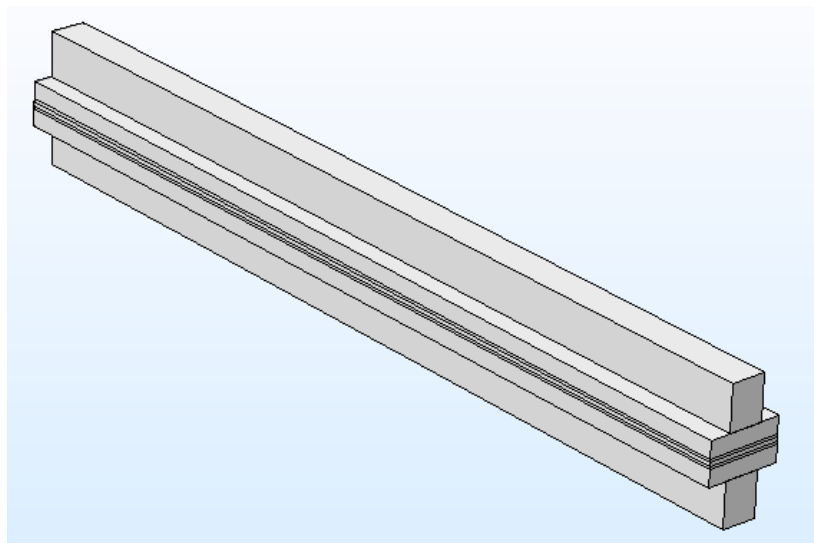


Figure 15 A 3D representation of fuel cell

A plane that cuts perfectly along the z axis as shown in Fig. 16, so as to obtain a 2D representation of the problem that includes all the main components of the cell, even in the 3D study because of the symmetry that has the cell along this plane it is possible to represent only half a cell to save on the computational cost of the calculation. Through the 2D representation, however, we do not lose any main aspect for the study of the cell if not that of the different behaviour in the corners of the cell.

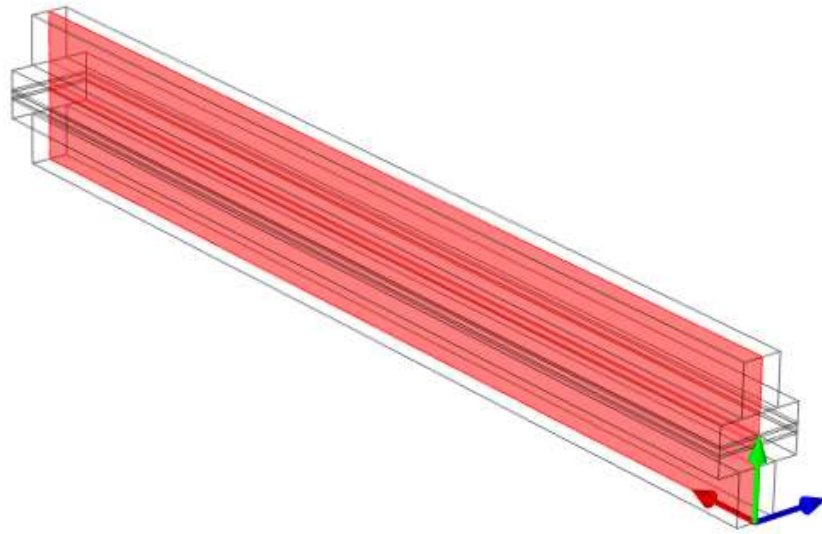


Figure 16 Cut plane along z directions

In the end the geometry of the problem and their respective domains are shown in Fig. 17:

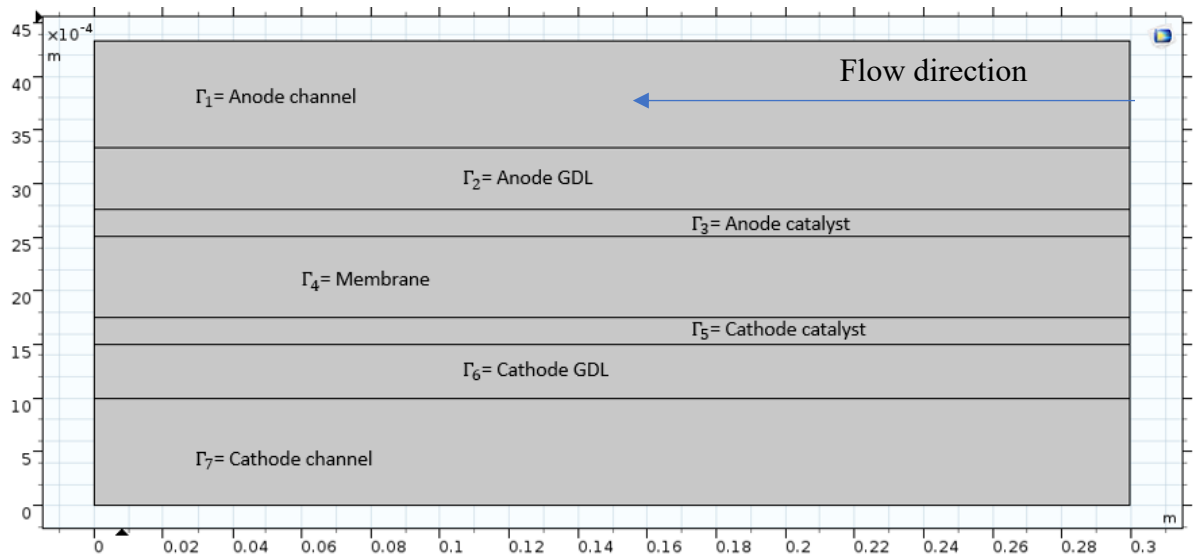


Figure 17 2D representation of fuel cell (Not in scale)

While for the boundary conditions are explained in Fig. 18.

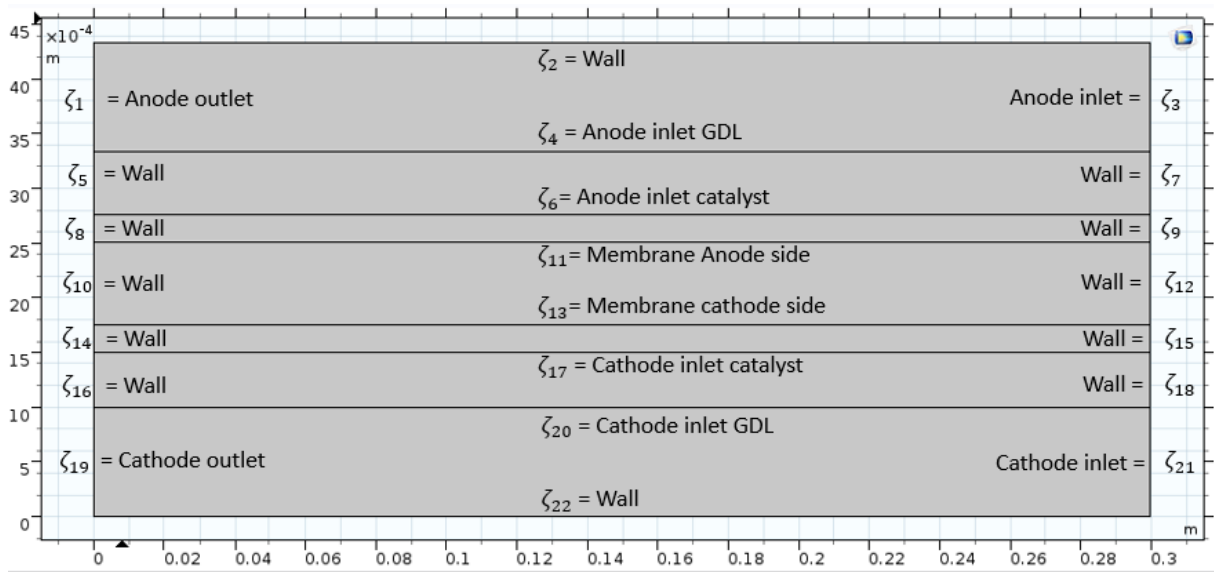


Figure 18 Nomenclature of boundary conditions (not in scale)

As we will see later, the 2D study was done with geo-data and the physical conditions of input and equilibrium taken from the article by Seigel et al. [41]. From here on it will be explained how the model was solved.

4.1 Introduction to computational model

To solve the fuel cell model, we must first analyse the different domains within it then identify the physical phenomena that take place inside the cell and find and the right equations to represent them. Every physical phenomenon is therefore represented by an equation and is applied only in the area of the cell where the physical one takes place. The cell model includes the reactants distribution channels, the porous medium with the catalyst zone, and the membrane. The bipolar plate and the manifold are not shown. Assuming this we can divide the cell into different domains, where different physics are present. The different domains are represented in a 2D view in Fig. 17.

The fuel cell can be divided into different domain:

1. Channel anode: where hydrogen mixed with water, all in gaseous form, enter in the fuel cell.
2. GDL anode: the reagent (H_2) enters in the porous medium and diffuses through it in order to approach the catalyst.
3. Catalyst anode: the reagent reacts thanks to the presence of the catalyst (platinum) realizing of electrical charges.
4. Electrolytic membrane: where H^+ are transferred.
5. Catalyst cathode: In this zone takes place the oxygen reduction reaction with formation of H_2O .
6. GDL cathode: the other reactants (O_2) enters the porous medium and diffuses through it. It is humidified.
7. Channel cathode: Here comes the needed to provide the oxygen to the reaction, and where the exhaust gases are expelled.

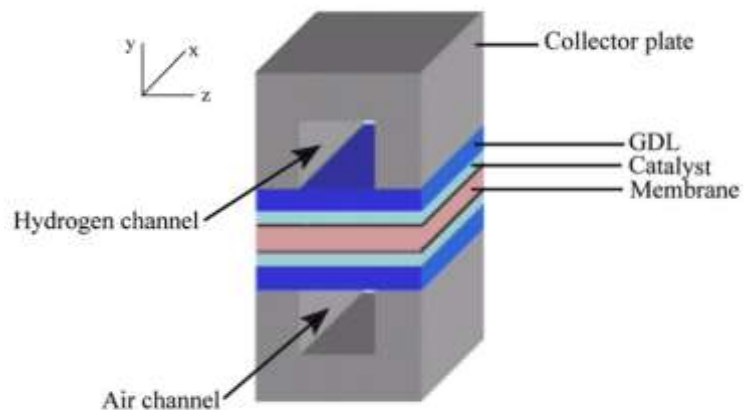


Figure 19 External fuel cell diagram [35]

On the anode side, humidified hydrogen gas (with steam water) is inserted, while on the cathode side, a moist air is inserted (then containing O_2 , N_2 and H_2O). Inside the cell we also have two other water phases:

- 1) dissolved water i.e. absorbed by the membrane, which is affects the ionic conductivity of the nafion
- 2) Liquid water, formed when its pressure can exceed the saturation value

Therefore, to represent water in its different forms, it is necessary to use different physics (and therefore equations) since its physical behaviour changes a lot.

4.2 Assumptions for the fuel cell model

Hypotheses to study the cell are necessary to simplify the problem. The study carried out on the fuel cell is in the steady state condition. Thanks to their low working T, fuel cells have a fast start up and switch on/off. So, studying the steady state is a reasonable method because the transient time is very fast [42].

Other hypotheses adapted for the model are:

- The reactant and production in gaseous form are assumed to be ideal gas mixture.
- The electrode is treated as an isotropic and homogenous porous medium and the porosity and permeability are constant in all cell.
- The flow in channel is laminar, therefore low Reynolds values.
- The membrane is impermeable for gas phase. In ideal cases, there are losses since the polymer membrane is not perfectly impermeable to molecules and electrons. But this kind of losses are not represented in the model.
- The electrical losses in the GDL and bipolar plate are negligible.

4.3 Governing equations

There are several physics to be applied inside the cell (refer to Tab. 2 for more information regarding how they should be applied).

	Channel anode	GDL anode	Catalyst anode	Membrane	Catalyst cathode	GDL cathode	Channel cathode
Continuity and Brinkman	X	X	X		X	X	X
Chemical species transport	X	X	X		X	X	X
Conservation of charges		X	X	X	X	X	
Dissolved water			X	X	X		
Liquid Water transport	X	X	X		X	X	X

Table 2 Governing equations and their application domains

4.4 Equations for the gaseous species

4.4.1 Continuity's equation

The reagent gases are inserted into the cell through the channels that transport the gas into the GDL, so that they can spread in the porous medium. Inside the channel enters a flow of fluid and it is essential that the conservation of the mass is respected. The continuity equation prescribes the mass conservation of the gaseous species.

Thus, the first equation to be inserted is the continuity equation. Conservation is applied to both the entire anode compartment and the cathode compartment.

$$\nabla \cdot (\rho \mathbf{u}) = S_{H_2} + S_{O_2} + S_{LV} + S_{wp}\gamma_{LV} + S_{wd}\gamma_{wd} \quad (22)$$

Where:

ρ is the average density of the components $\left[\frac{kg}{m^3s}\right]$, \mathbf{u} the velocity of fluid $\left[\frac{m}{s}\right]$, S_{LV} represent the condensation or evaporation value of water $\left[\frac{kg}{m^3s}\right]$, γ_{LV} it is the function of gasses-liquid water switch, which we will see in section 4.3.3, S_{wd} is the water in the dissolved phase that include EOD and back diffusion given by the difference of pressure $\left[\frac{kg}{m^3s}\right]$, γ_{wd} it is the function of dissolved-liquid water switch, which we will see in section 4.3.3, S_{wp} is the water product by the reaction $\left[\frac{kg}{m^3s}\right]$.

In the two electrodes we have H_2 and H_2O for the anode, and O_2 , N_2 and H_2O for the cathode. The source terms in the continuity equation can be different from zero, due to the electrochemical reactions in the catalyst layer, and they are zero in other parts of the computational domain.

They can be computed as follows

- Cathode catalyst layer

$$S_{O_2} = -\left(\frac{i_c}{4F}\right)|R_{eff}| \quad (23)$$

$$S_{wp} = \left(\frac{i_c}{2F}\right) |R_{eff}| \quad (24)$$

- Anode catalyst layer

$$S_{H_2} = -\left(\frac{i_a}{2F}\right) |R_{eff}| \quad (25)$$

Where:

R_{eff} is the reaction rate $\left[\frac{A}{m^3}\right]$, F the Faraday constant $\left[\frac{C}{mol}\right]$, M_i it is the molar mass of each species $\left[\frac{kg}{mol}\right]$.

The continuity equation maintains the conservation of all species present in the cell except for liquid water and dissolved water. For these two forms of water additional equations will be added to take account of their motion and their production.

4.4.1 Brinkman's equation

Within the channel and the porous medium, the reactants move both for the speed imposed on the gas due to the difference in pressure between the inlet and the outlet of the channel, and by diffusion due to the difference in concentration.

To calculate the velocity of gas within a channel, the Navier stokes equation is usually used. But inside the cell there is not only the channel but also the porous medium. To represent the speed inside the porous medium it is not suitable to use the Navier stokes, but it must be modified to take into account the porosity of the medium which reduces its permeability. Therefore, a modified version of Navier stokes, the Brinkman equation, is used.

The Brinkman equation takes into account the additional friction due to the porous media. It appears as a mix of Darcy's law and the Navier-Stokes equations. They extend Darcy's law to account for dissipation of kinetic energy by viscous shear as in the Navier-Stokes equation and we also take into consideration convective transport [43].

As in the Navier Stokes equations, the dependent variables in the Brinkman equations are the directional velocities and pressure. The flow field determined by the Brinkman equations comes from balancing momentum in the x , y and z direction.

Putting the term of porosity ε equal to 1, Navier stokes is obtained.

- Navier stokes:

$$\rho(\mathbf{u} \cdot \nabla)\mathbf{u} = \nabla \cdot [-\rho I + \mu(\nabla\mathbf{u} + (\nabla\mathbf{u})^T)] + \mathbf{F} \quad (26)$$

Combined with the Darcy equation seen in Eq. (21) we obtain:

- Brinkman:

$$\rho_f \left[\frac{1}{\varepsilon} (\mathbf{u} \cdot \nabla) \frac{\mathbf{u}}{\varepsilon} \right] = \nabla \left[-P_f + \frac{\mu_f}{\varepsilon} (\nabla\mathbf{u} + (\nabla\mathbf{u})^T) \right] - \left(\frac{\mu_f}{K} + (\rho_f \nabla \cdot (\mathbf{u})) \frac{1}{\varepsilon^2} \right) \mathbf{u} + \mathbf{F} \quad (27)$$

Where

\mathbf{u} is the velocity of fluid $\left[\frac{m}{s} \right]$, ε is the porosity of the GDL, μ_f is the viscosity $\left[\frac{kg}{m \cdot s} \right]$, K is the permeability $[m^2]$, ρ_f is the density of fluid mixture $\left[\frac{kg}{m^3} \right]$, P_f is the pressure $[Pa]$.

We use the Brinkman equation to calculate the transport and the velocity of the incoming fluid calculating as if it were a single fluid with a medium rho that depends on the components of the fluid and their concentrations.

Finally, to complete the equation it is necessary to provide the appropriate boundary conditions. In this case it is necessary to impose the pressure or the speed at the inlet of the fluid and to make the flow null along all the walls. It is very important that the boundary conditions are set correctly to create a laminar condition.

This physics too must be applied on domain Γ_1, Γ_2 and Γ_3 for the anode, and Γ_5, Γ_6 and Γ_7 for the cathode. While the boundary conditions are:

$$\text{Wall} \quad \mathbf{u} = 0 \quad \text{On } \zeta_2, \zeta_5, \zeta_6, \zeta_7, \zeta_8, \zeta_9, \zeta_{13}, \zeta_{14}, \zeta_{15}, \zeta_{16}, \zeta_{18}, \zeta_{22} \quad (28)$$

$$\text{Inlet anode} \quad u_{a,avg} = 1.547 \left[\frac{m}{s} \right] \quad \text{On } \zeta_3 \quad (29)$$

$$\text{Inlet cathode} \quad u_{c,avg} = 3.747 \left[\frac{m}{s} \right] \quad \text{On } \zeta_{21} \quad (30)$$

Outlet
 anode, $P = 30[*pisg*]$ On ζ_1, ζ_{19} (31)
 cathode

4.4.2 Chemical species transport's equation

Species transport was derived for the reactant and product gases on the anode and cathode sides. For the gas transport we use the Maxwell-Stefano diffusion model. Species transport was solved for H₂ and H₂O on the anode side and O₂, N₂ and H₂O on the cathode side.

While generally we use the Fick equation in order to study the transport by diffusion of an element, in this case it's required a different kind of approach. The Maxwell-Stefan equation is used to treat the diffusion along the canal and the porous medium. This is a model that describes diffusion in multicomponent systems. It is necessary to calculate the diffusion of the element within the channel, while also considering the presence of other elements.

The Binary diffusion coefficient (BDC) of gas species can be calculated by [44]:

$$D_{ij} = a \left(\frac{T}{T_{ref}} \right)^{1.75} \left[\frac{m^2}{s} \right] \quad (32)$$

Where:

$$a = 9.15e - 5, T_{ref} = 307.1 \text{ for H}_2\text{-H}_2\text{O}$$

$$a = 2.56e - 5, T_{ref} = 307.15 \text{ for N}_2\text{-H}_2\text{O}$$

$$a = 2.2e - 5, T_{ref} = 293.2 \text{ for O}_2\text{-N}_2$$

$$a = 2.82e - 5, T_{ref} = 308.1 \text{ for O}_2\text{-H}_2\text{O}$$

This will allow us to construct a symmetric matrix with all the BDC coefficient, and, consequently, to obtain the diffusion value of each single component.

For both the anode and cathode, the number of species equations is less than the number of species. More precisely the number of equations to insert is given by the number of species present minus one. This is given by the fact that the last equation representing the last species is resolved by difference together with the overall gas phase conservation equation, which is to say that since the sum of all the species is already calculated, the last will be derived by simple

difference. At the anode, only the equation of species for water vapor is resolved. The hydrogen mass is calculated from the solution to the water vapor equation and to the overall conservation of the gaseous phase equation. At the cathode, both the equations of the oxygen and vapor species are resolved, while the nitrogen mass fraction is then determined from the difference. The BDC coefficient for all component of the flow is obtain in the porous regions, with a modification due to porosity and tortuosity factors [36].

The specie equations are divided into two terms: the first is equal to the product of velocity, mixture density and gradient of the mass fraction, while the second term is the product of the mass fraction and the divergence of the total mass flow.

The general form of Maxwell-Stefan is [45]:

$$\rho^g \mathbf{u} \cdot \nabla w_i - \nabla \cdot \left(\rho^g w_i \sum_j D_{ij}^{eff} \left(\nabla x_j + \frac{1}{P_f} [(x_j - w_j) \nabla P_f] \right) \right) = S_i \quad (33)$$

$$S_{Tot, H_2O} = S_{LV} + S_{wp} \gamma_{LV} + S_{wd} \gamma_{wd}$$

$$S_{Tot, O_2} = S_{O_2}$$

Where $x_j = \frac{w_j}{M_k} M_n$ and $M_n = \left(\sum_i \frac{w_i}{M_i} \right)^{-1}$, s is the saturation of the liquid water, w_i is the mass fraction of species “ i ”, M_i is the molar mass of species “ i ”, w_i is the molar concentration, D_{ij} is the BDC, and S_i is the source term for species.

For simplicity we consider that:

$$\mathbf{N}_{i,max} = \rho^g w_i \sum_j D_{ij}^{eff} \left(\nabla x_j + \frac{1}{P_f} [(x_j - w_j) \nabla P_f] \right) + \rho^g \mathbf{u} w_i \quad (34)$$

To calculate the BDC value, we must take into account, the porosity and tortuosity when we are in the medium. The diffusion of the material is slowed down, in this case.

Therefore, the diffusion in a porous media is calculated as follows:

$$D_{ij,p} = \left(\frac{\varepsilon}{\tau}\right)^n D_{ij} \quad (35)$$

Where ε is the porosity of the porous media and τ is the tortuosity factor.

Due to the presence of water, the gas has a further difficulty in spreading in the porous medium and this could reduce the concentration of the reagent in the vicinity of the catalyst, and consequently reduce the performance of the cell. The presence of water reduces diffusion according to the following equations [36]:

$$D_{ij}^{eff} = (1 - s)D_{ij,p} \quad (36)$$

The source terms are different according to the species treated.

For the oxygen we have only the term seen in Eq. (23). As far as oxygen is concerned, the source term represents the oxygen consumption due to the chemical reaction between the reagents. The amount of reacting mass depends on the reaction rate, which calculation mode will be explained later. Regarding the water, the concept is a bit more complicated. We have three terms $S_{LV} + S_{wp}\gamma_{LV} + S_{wd}\gamma_{wd}$ that were also present in Eq. (22). The terms source represents in writing order:

- condensation-evaporation of water (S_{LV})
- the production of water from the reaction (S_{WP} only in the cathode)
- transition from dissolved steam (S_{WD})

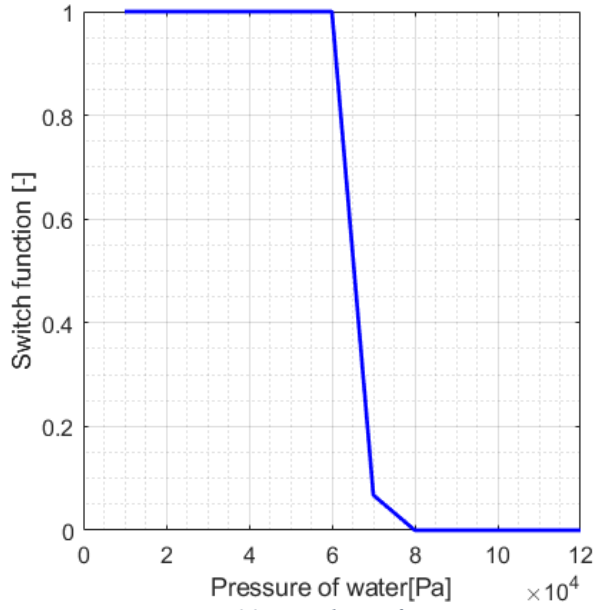


Figure 20 switch γ_{LV} function

The S_{LV} will be discussed in section 4.6.2. The mass quantity of water produced depends on the rate of reaction and is given by the sum of the mass of O_2 and by the mass of H_2 reacting within the cell. The γ_{LV} coefficient that multiplies the source term separates the water that is produced as vapor and the water produced as liquid. The switch function shown in Fig. 20 shows the rapid change in value depending on the steam pressure value. If the pressure in the cathode is very high and reaches the saturation, the water will be produced

directly in the liquid form, instead of steam. This is calculated with the γ_{LV} coefficient which is represented as follows [41]:

$$\gamma_{LV} = 1 - 0.5 \left[1 + \tanh \left(\frac{\rho_{wv}^g}{\rho_{SAT}^g} - 59 \right) \right] \quad (37)$$

Therefore, when the density is greater than the saturation ($\frac{\rho_{wv}^g}{\rho_{SAT}^g} > 0.98$), the coefficient takes the value of 0 and no steam is produced, but only liquid water. The quantity of water produced by the reaction can be seen from Eq. (24).

The last term concerns the transition from steam to dissolved water. The phase change that can take place is only from steam to dissolved and never the opposite. The hypothesis made is that water, evaporating from the dissolved phase, passes directly from the vapor phase into the liquid one [41]. Thus, steam water can only be absorbed by the membrane in both chambers, and the source term can only be negative. The γ_{wd} coefficient is defined as follows (it will later be explained in the section 4.6.1).

$$\gamma_{wd} = 0.5 + \frac{(\rho_{wv}^g - \rho_{wv}^p)}{2|\rho_{wv}^g - \rho_{wv}^p|} \quad (38)$$

it is a switch function that can only assume the values 0 and 1. When the density of the water is greater than that of the dissolved water, the value of γ_{wd} is equal to 1, otherwise it is 0. When the term γ_{wd} is equal to 1 then the term source will be negative and there will be passage of water from dissolved steam. Like the Brinkman's equation, this physics must be applied on domain Γ_1, Γ_2 and Γ_3 for the anode, and Γ_5, Γ_6 and Γ_7 for the cathode.

In this case, as a boundary condition, different conditions must be imposed on entry and exit. At the entrance it is imposed the initial concentration (or even the mass or molar fraction) of at least n-1 species, so that the last one is calculated accordingly. It is necessary, instead, to impose that the diffusive flow of all the components of the fluid is equal to 0 at the output. To this in all the other wall is added the usual "no flux" condition.

$$\text{Wall} \quad \mathbf{n} \cdot \mathbf{N}_{i,max} = 0 \quad \text{On } \zeta_2, \zeta_5, \zeta_6, \zeta_7, \zeta_8, \zeta_9 \quad (39)$$

$$\begin{array}{l} \text{Inlet} \\ \text{anode} \end{array} \quad w_{H_2O} = 0.62 \quad \text{On } \zeta_3 \quad (40)$$

$$\begin{array}{l} \text{Inlet} \\ \text{cathode} \end{array} \quad \begin{array}{l} w_{H_2O} = 0.1 \\ w_{O_2} = 0.21 \end{array} \quad \text{On } \zeta_{21} \quad (41)$$

$$\begin{array}{l} \text{Outlet} \\ \text{anode} \end{array} \quad \nabla w_{H_2O} = 0 \quad \text{On } \zeta_1, \zeta_{19} \quad (42)$$

$$\begin{array}{l} \text{Outlet} \\ \text{Cathode} \end{array} \quad \begin{array}{l} \nabla w_{H_2O} = 0 \\ \nabla w_{O_2} = 0 \end{array} \quad \text{On } \zeta_1, \zeta_{19} \quad (43)$$

Where \mathbf{n} is the normal unit vector orthogonal to the surface.

4.5 Energy equations of the cell

In this section we will discuss the equations that determine the energy and the useful effects of the cell, i.e. electric and thermal power.

4.5.1 Charge transport's equation

The generation of electrical energy is calculated by studying the motion of the charges, both positive ions H^+ within the membrane, and of the electrons along the GDL and the bipolar plate. To study this phenomenon, it is enough to calculate the conservation of the charge along the application domain. Protons travel through the membrane Catalyst, while electrons transfer through the Catalyst and GDL too. Conservation of charge is performed for both proton and electrons.

1. The solid phase potential equation represents transport of electrons in the solid conductive regions (GDL and catalyst layer):

$$\nabla \cdot (\sigma_e \nabla \phi_e) + S_{\phi,e} = 0 \quad (44)$$

2. The membrane phase potential equation depicts transport of protons in the MEA that consists of both catalyst layers and the membrane itself, expressed by:

$$\nabla \cdot (\sigma_p \nabla \phi_p) + S_{\phi,p} = 0 \quad (45)$$

In the above equations ϕ_s and ϕ_p denote electrical potential of solid phase (electron) and membrane phase (proton) respectively, σ_e the electrical conductivity of the solid phase and σ_p is the protonic conductivity of the membrane phase. The terms $S_{\phi,e}$ and $S_{\phi,p}$ are the volumetric source terms, which exist only in the catalyst layer and are determined based upon the transfer current densities.

The local current densities in anode and cathode can be obtained by the Butler–Volmer equation. Due to the different characteristics of anodic and cathodic electrochemical reaction, the polarization potential loss is minor in anode and relatively great in cathode. Also, the effect of the reactant concentration on the reactive rate, i.e. current density, should be taken into account. So, the original Butler–Volmer equation is modified for calculating the anodic and cathodic local current density, in order to find the cell reaction rate expressed as follows [46]:

$$R_{agg,i} = \theta (1 - s) A_v i_{o,k} \left(\frac{C_k^p}{C_{k,ref}^p} \right)^j \left[e^{\left(\frac{\alpha_a F}{RT}\right)} - e^{-\left(\frac{\alpha_c F}{RT}\right)} \right] \quad (46)$$

Where the general subscript “*i*” is “*a*” representing anode with *k*” representing H_2 , or “*i*” is “*c*” representing cathode with *k*” representing O_2 representing cathode. $i_{o,k}$ is the exchange current density, *s* is the saturation water, η_a and η_c are activation overpotentials of the anode and cathode, respectively, C_{H_2} and C_{O_2} are the molar concentrations of hydrogen and oxygen dissolved in the membrane phase, α the cathode transfer coefficient, n_a the electron number of anode reaction, n_c is that of cathode reaction and θ is the agglomerate effectiveness. In the anode side the ratio between the concentrations is elevated to $j = 0.5$. The source’s terms

$$\begin{aligned} \text{Cathode catalyst} \quad S_{\phi,p} &= R_{agg,c}, S_{\phi,e} = -R_{agg,c} \\ \text{Anode catalyst} \quad S_{\phi,p} &= -R_{agg,a}, S_{\phi,e} = R_{agg,a} \end{aligned} \quad (47)$$

The ionic and electronic conductivity are very different. The electronic conductivity is much higher than the ionic one and is assumed constant throughout the GDL and catalyst. While the ionic conductivity that applies only to the two catalyst and the membrane is a function of the degree of humidification of the membrane according to the following formula [36]:

$$\sigma_p = (0.5139\lambda - 0.326) \exp \left[1268 \left(\frac{1}{303} - \frac{1}{T} \right) \right] \left[\frac{S}{m} \right] \quad (48)$$

λ is the ratio between the moles of water contained in the membrane and the moles of SO_3^- , that will be discussed in the section 4.6.1, the more water there is in the membrane, the better the conduction will be (as seen in section 3.4).

An important factor that reduces the rate of reaction is liquid water. The greater the amount of liquid water, the lower the rate of reaction and the performance of the cell, too. Therefore, a term that takes into account the amount of water is added to the equation of $R_{agg,i}$.

The dissolved molar concentration of species in the polymer phase is given by Henry’s law [36]:

$$C_{i,m} = H C_i^g \quad (49)$$

where H is the Henry constant, C_i^g and $C_{i,m}$ are the molar concentrations of species existing in gas phase and in membrane phase (or Nafion, polymer phase), respectively.

The value of current in anode and in cathode is the same, so it is possible to determine the value of η_c and η_a : After that the activation over voltage is calculated like:

$$\eta_{act} = \eta_a + \eta_c = E_{th} - \Phi_e - \Phi_p \quad (50)$$

Where E_{th} is the open circuit voltage, defined as follows [47]:

$$E_{th} = 1.229 + 0.85 \times 10^{-3}(T - 298.15) + 4.3085 \times 10^{-5}T \times \left(\ln(P_{H_2}) + \frac{1}{2} \ln(P_{O_2}) \right) \quad (51)$$

It's important to consider that the catalyst layer is porous and made up of clumps of carbon-supported Platinum catalyst, surrounded by a thin layer of Nafion [52]. The gaseous reactants must dissolve into the polymer phase and diffuse through the polymer film to reach the reaction sites. In order to account for the effect of diffusion resistance through the catalyst with porous and agglomerate structure, the reaction rate is modified by an effectiveness factor, θ , which is a measure of how readily reactants diffuse through the catalyst grain. We define $R_{d,i}$ reaction rate without agglomerate effects as follows:

$$R_{d,i} = \frac{R_{agg,i}}{\theta} \quad (52)$$

Where “ i ” can be “ a ” representing anode, or “ c ” representing cathode $\theta(\leq 1)$ can be determined by following equation:

$$\theta = \frac{3}{\beta_{agg,i}} \left(\frac{1}{\tanh(\beta_{agg,i})} - \frac{1}{\beta_{agg,i}} \right) \quad (53)$$

Where β_{agg} is Thiele's modulus, defined as follows [49]:

$$\beta_{agg,i} = L_{agg} \sqrt{\frac{R_{d,i}}{D_i^m C_k^p F}} \quad (54)$$

where L_{agg} the characteristic length of catalyst particle, $R_{d,i}$ is the reaction rate without agglomerate effects and D_i^m is species diffusivity of reactant in the polymer phase.

The term of effectiveness reduces the rate of reaction of the cell and consequently leads to a lower production of electricity. The term of effectiveness is used in order to measure how rapidly reactants react across spherical agglomerates.

Obtaining an effectiveness of 1.0 means that the diffusion of the reagents through the agglomerates does not meet resistance, while an efficiency of less than 1.0 means that the agglomerate resists the limitation of reactor distribution at reaction rate. So, we know that values lower than 1 reduce the rate of reaction and therefore the efficiency of the cell [52].

This physics must be applied on domain Γ_2, Γ_3 for the anode, Γ_5, Γ_6 for the cathode and in the membrane Γ_4 .

As for the boundary conditions, this time they are at the two ends of the GDL and in the whole cell contour (composed of GDL, catalyst and membrane).

The anode electrode is considered as the electric ground ($\phi_p = 0$). Also, the electrical potential of the cathode electrode is assumed as the cell voltage. ($\phi_p = V_{oc}$). So, the value of voltage of the cell is known.

The insulation boundary condition is applied for the other walls.

$$\begin{array}{l} \text{Wall} \end{array} \quad \begin{array}{l} \mathbf{R}_{agg,a} \cdot \mathbf{n} = 0 \\ \mathbf{R}_{agg,c} \cdot \mathbf{n} = 0 \end{array} \quad \text{On } \zeta_5, \zeta_8, \zeta_{10}, \zeta_{14}, \zeta_{16}, \zeta_7, \zeta_9, \zeta_{12}, \zeta_{15}, \zeta_{18} \quad (55)$$

$$\begin{array}{l} \text{Anode} \\ \text{inlet} \\ \text{GDL} \end{array} \quad \phi_e = 0 \quad \text{On } \zeta_1, \zeta_{19} \quad (56)$$

$$\begin{array}{l} \text{Cathode} \\ \text{inlet} \\ \text{GDL} \end{array} \quad \phi_e = V_{cell} \quad \text{On } \zeta_1, \zeta_{19} \quad (57)$$

4.6 Equations for water management

Dissolved phase moves through the membrane due to difference in concentration, and because of the effect of electroosmotic drag. In the cathode the water passes from the dissolved phase to the vapor phase, and if its pressure is greater than the saturation pressure, then the water can condense and pass to the liquid phase. The liquid phase is present only in the cathode, because in the anode, due to the passage of water due to the EOD at higher currents, there is an anode dehydration (because in the anode the passage of water occurs at higher currents, determining its dehydration).

It is assumed that all 3 phases are in equilibrium. Source's terms are defined using high mass transfer rates in such a way to maintain the equilibrium between the 3 phases [41].

The amount of current generated depends on the degree of hydration of the membrane, so the amount of dissolved H_2O present in the membrane. At higher currents, part of the membrane dehydrates and the current falls.

The water dissolved is calculated with the parameter “ a ” (water vapour activity) that depend by the polymer water content λ .

4.6.1 Dissolved water's equation

To treat the passage of water both for electro-osmotic drag, both for back-diffusion, and for hydraulic permeability the Eq. (59) is used. it is important to know that inside the catalyst, there is a fraction of polymer that is able to absorb water and transport it inside/outside the membrane.

The membrane can be treated as a fluid with infinite viscosity and where there is no mass diffusion. The concentration of water C_{WD}^p in the membrane is calculated through the Polymer water content λ parameter which depends on the type of membrane (Nafion 1100) [53,55].

$$\lambda = \frac{C_{WD}^p M_{mem}}{\rho_{mem}} \left[\frac{mol H_2O}{mol SO_3^-} \right] \quad (58)$$

It can be modelled with the Nernst Planck equation. The Fick law is combining with Ohm's law, and the current density of an electromechanical potential is obtained.

$$n_d \nabla \cdot (\varepsilon_p \lambda \nabla \phi_p) - \nabla \cdot (D_{DW}^p \nabla c_w^d) - \nabla \cdot \left(\frac{K_{p,m} c_w^d}{\mu_w} \nabla P_f \right) = S_{wd} \quad (59)$$

For simplicity we consider that:

$$N_{dis} = n_d (\varepsilon_p \lambda \nabla \phi_p) - (D_{DW}^p \nabla c_w^d) - \left(\frac{K_{p,m} c_w^d}{\mu_w} \nabla P_f \right) \quad (60)$$

Where n_d is a constant that represents the number of water molecules carried per unit of proton transferred, ε_p is the polymer fraction present in the catalyst, λ represents the amount of water present in the membrane, σ_m is the ionic conductivity, Φ_p is the potential of the membrane, D_{DW}^p is the diffusivity of water in the membrane, c_w^d is the water concentration in $\left[\frac{mol}{m^3} \right]$ in the membrane, $K_{p,m}$ is the permeability of water in the membrane and μ_w is the viscosity of the liquid water.

The first term represents the EOD that depends by a constant [11]:

$$n_d = \frac{2.5}{22F} \quad (61)$$

The water is carried by the current from the anode to the cathode, and the force, direction is given by the gradient of potential $\nabla \Phi_p$. The mobility of water along the membrane, however, depends on the amount of water already present λ and ionic conductivity. Moreover, in the two catalyst because the polymer is not present in the whole domain but with a certain fraction ε_p , the mobility is less than the membrane.

After that, the second term represent the diffusivity (which characterizes the back diffusion). Inside the membrane the water diffuses due to the difference in concentration through the D_{DW}^p calculated with Eq. (62):

$$D_{DW}^p = 1.3 \times 10^{-10} \exp \left[2416 \left(\frac{1}{303} - \frac{1}{T} \right) \right] \left[\frac{m^2}{s} \right] \quad (62)$$

The last term represents the hydraulic permeability. In case of different pressure between the two chambers the water undergoes a further thrust in the direction where the pressure is lower. The passage of water also depends on the viscosity μ_w and the permeability that is a function of the amount of water already present in the membrane [50]:

$$K_{p,m} = 2.5 \cdot 10^{-20} \lambda \text{ [m}^2\text{]} \quad (63)$$

The dissolved phase is maintained in equilibrium by S_{wd} that is present only in the catalyst layers in both chambers, and is calculated as follows:

$$S_{wd} = h_m (\rho_{wv}^g - \rho_{wv}^p) \quad (64)$$

The source term (that is defined in $\left[\frac{kg}{m^3s}\right]$) depends on the constant coefficient h_m (chosen large enough to maintain equilibrium) and the difference in density between the steam water in the channel and the density of the steam water in equilibrium with the polymer. The equilibrium density depends on the saturation density (hence the operation T) and the coefficient a . The latter is the vapor water activity that can be calculated according to the degree of humidification of the membrane [41]:

$$\rho_{wd}^p = \rho_{wv}^g a \quad (65)$$

$$a = 1.76e^{-6}\lambda^{-4} + 2.17e^{-4}\lambda^{-3} - 8.80e^{-3}\lambda^{-2} + 0.16\lambda - 0.12 \quad (66)$$

If the polymer is not very wet, the value of “ a ” will be less than 1 and will try to absorb the water, otherwise if it is very wet the value of “ a ” will be greater than 1 and will tend to be watered with dissolved water. So, the value of “ a ” will be less than 1 in the area of the anode because it dehydrates, and greater than 1 in the area of the cathode where it accumulates and is expelled. The trend of “ a ” as a function of λ is shown in the figure Fig.21. Anode dehydration leads to a reduction in cell performance as it reduces electrical conductivity according to Eq. (46).

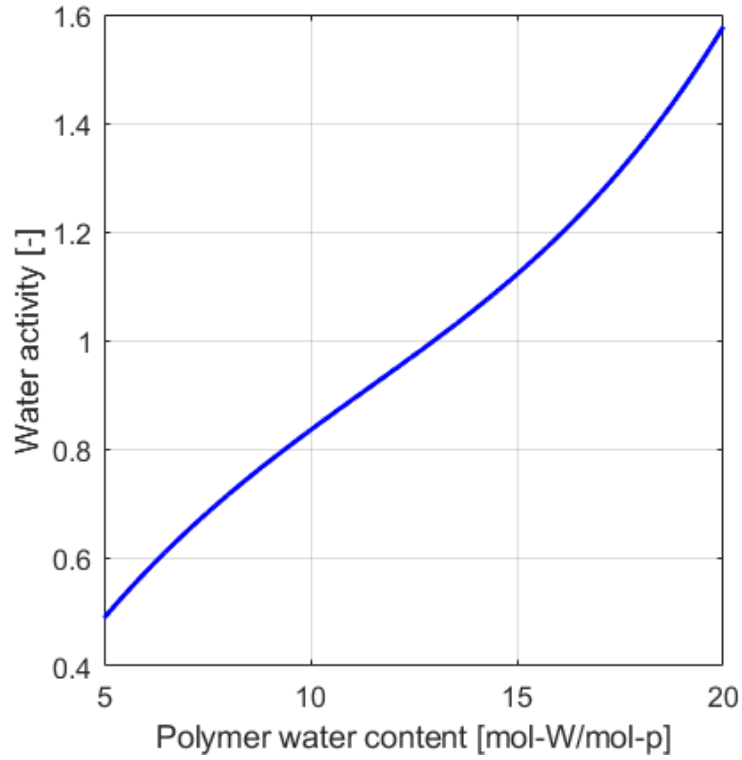


Figure 21 Water activity as function of λ

Water that leaving the dissolved phase passes directly and into the liquid as show by the term $S_{wd}(1 - \gamma_{wd})$. Water passes to the dissolved phase from the vapor phase as shown in $\gamma_{wd}S_{wd}$ (seen Eq. (22)) [36]. The variable γ_{wd} is a switch term, that becomes 1 when water is leaving the dissolved phase and zero otherwise. And lastly, water entering or leaving the dissolved phase is reflected by the term S_{wd}/M_w in the equation for dissolved water transport, in both areas, anode and cathode. Because of S_{wd} is in $\left[\frac{kg}{m^3s}\right]$ dividing by the molar mass I find the $\left[\frac{mol}{m^3s}\right]$ that is used to calculate c_w^d .

The domain of application of this physical is only the zone comprising the two catalyst Γ_3 and Γ_5 and the membrane Γ_4 . For the boundary conditions the outflow and non-flux are present in this physics.

$$\begin{array}{ll} \text{Outlet Anode and} & \\ \text{cathode side} & -\mathbf{n} \cdot \nabla c_w^d = 0 \quad \text{On } \zeta_6, \zeta_{17} \quad (67) \end{array}$$

$$\begin{array}{ll} \text{Wall} & -\mathbf{n} \cdot \mathbf{N}_{dis} = 0 \quad \text{On } \zeta_8, \zeta_{10}, \zeta_{14}, \zeta_9, \zeta_{12}, \zeta_{15}, \quad (68) \end{array}$$

4.6.2 Liquid water's equation

By applying the volume average approach to the continuity equation and then using Darcy's law for both the liquid and gas phases, the governing equation of the liquid water transport is expressed as follow [54,41]:

$$\rho_{WL}\mathbf{u} \cdot \nabla s - \rho_{WL}\nabla \cdot (D_{wl}^{cp}\nabla s) = -S_{LV} + S_{wp}(1 - \gamma_{LV}) - S_{wd}(1 - \gamma_{wd}) \quad (69)$$

For simplicity we consider that:

$$\mathbf{N}_{wat} = \mathbf{u}s - (D_{wl}^{cp}\nabla s) \quad (70)$$

The degree of freedom in this physics is the variable "s" that represents the saturation of water. This variable is dimensionless and represents the ratio between the volume of liquid water and the volume of pores in the section in which it is located.

$$s = \frac{V_{WL}}{V_{pore}} \quad (71)$$

To obtain the mass then it is necessary to first obtain the quantity of volume of water formed knowing the porosity of the medium, and then to multiply by the density of the liquid.

The expected result is the formation of liquid water inside the porous medium in the cathode side, while in the anode it is practically nil (due to the electro-osmotic effect).

In this study it is assumed that the liquid water velocities are null in the porous media, but in other studies, this hypothesis remains debated especially when large liquid water droplets are present [36]. In other articles the speed of water is considered instead. However, the speed of the water can never be the same as that of the gas, but it is very reduced due to its high viscosity and the difficulty of moving inside the porous medium.

Within the porous medium, the speed is neglected, and therefore the liquid is transmitted only by capillary diffusion, since the movement of fluids in unsaturated porous media is limited due to the surface tension and adhesive forces.

Considering only the porous medium, then the convective term is neglected, and the capillary diffusion is calculated with the following formula [56]:

$$D_{WL}^{cp} = \frac{\rho_{wl}g}{\mu_{WL}} K(s) \frac{\partial P_c}{\partial s} \quad (72)$$

Where:

μ_{WL} is the water viscosity $\left[\frac{kg}{ms}\right]$

$K(s)$ the permeability of liquid water $[m^2]$

P_c is the capillary pressure [Pa]

The diffusion of the liquid (see Fig.22) and the variation of the capillary pressure as a function of its saturation are written using empirical equations as a function of water saturation [51]:

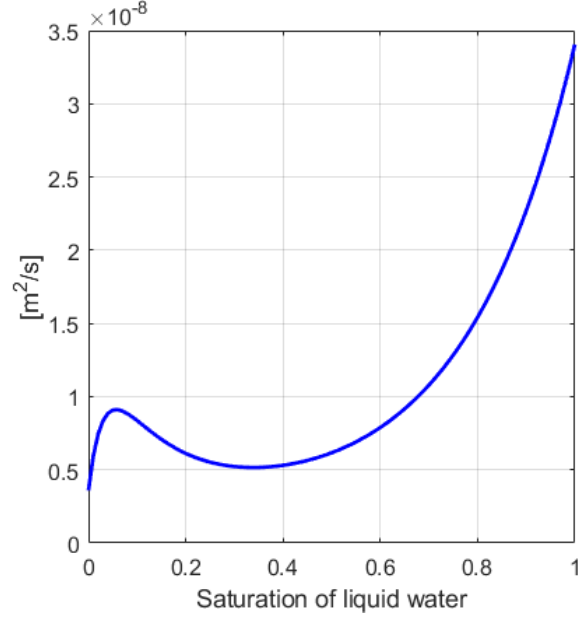


Figure 22 Capillary diffusion of liquid water according to saturation

$$K(s) = K_{1,abs} s \quad (73)$$

$$\frac{\partial P_c}{\partial s} = -A \times D [e^{-A(s-C)} + e^{A(s-C)}] \quad (74)$$

While the constant coefficients are calculated in centimetres as it follows [51]:

- $A = 3.7$
- $C = 0.494$
- $D = 0.0173$

In the channel, however, I consider the velocity of the liquid equal to that of the gas, since there is no resistance to the motion of the liquid as the velocity of the gas is very high, the liquid that has formed or has arrived in the canal is rapidly transported out of the cell. Therefore, in the channel the presence of liquid will be very low and will not modify the gaseous motion.

Liquid water, that is generated within the channel, it is given by the three source terms. Liquid water is formed either by condensation of the steam water, or by the passage of the water from dissolved to liquid, or by the production, due to the reaction of the hydrogen, of water directly in the liquid phase.

The first term is the of condensation and evaporation. This term is defined as:

$$S_{LW} = \psi s \gamma_{LV} - \psi (1 - s) (1 - \gamma_{LV}) \quad (75)$$

Where γ_{LV} is a switch function which depends on the ratio between the vapor density and the density saturation of the water (see Eq. (37)), ψ it is a constant coefficient chosen wide enough to maintain the balance between the three phases of the water.

The ρ_{SAT}^g it is obtained by knowing the value of the saturation pressure with the variation of the temperature as given in Tab. 3 [57].

Temperature [K]	P_{sat} [Pa]
298.15	0.031698e5
308.15	0.056291e5
318.15	0.095953e5
328.15	0.15763e5
338.15	0.25043e5
348.15	0.38597e5
358.15	0.5786e5
368.15	0.84609e5

Table 3 Saturation pressure as a function of temperature

If the pressure of water exceeds the saturation pressure, then it condenses and passes to the liquid state. Vice versa, if the formation of liquid water is excessive, and the pressure of the liquid is below that of saturation, the liquid evaporates and goes back to the vapor phase.

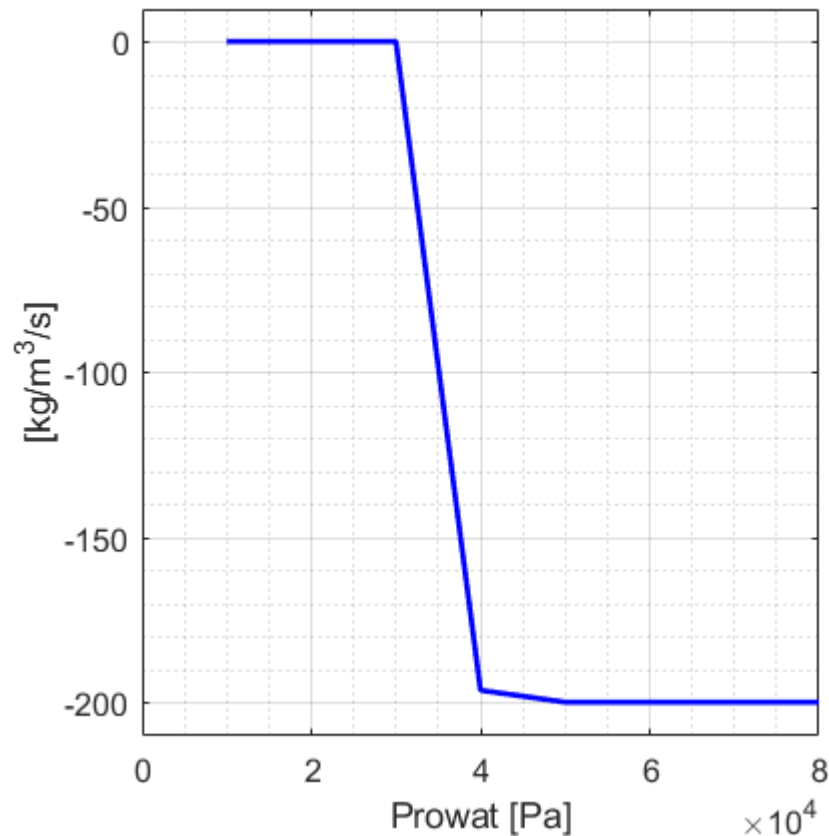


Figure 23 Behaviour of the S_{LW} source term as a function of saturation pressure

The first source term, the condensation-evaporation (see Fig. 23), is applied throughout the compartment of both chambers (catalyst-GDL-channel), while the other two source terms are calculated only in the catalyst of each chamber.

We have already spoken before of the term source for the production of liquid water. The difference lies only in the multiplicative coefficient next to it, so that the source term is applied only if the steam water pressure is saturated. This way, instead of producing steam, from the reaction, directly liquid water will be produced.

The last source term is the one governing the passage from dissolved water to liquid water. As we already said before, the water that leaves the dissolved phase goes directly to the liquid state. When the γ_{wd} coefficient is 1 the source term is 0, while when it is 0, we have the liquid water formation.

Like the continuity equation and chemical species transport equation, this physics must be applied on domain Γ_1, Γ_2 and Γ_3 for the anode, and Γ_5, Γ_6 and Γ_7 for the cathode.

As boundary conditions, it is assumed that the reactants flow rate that entering the chambers are dry. So, this condition is set via a Dirichlet condition. While at the exit the convection is considered dominant and the diffusion is neglected. Throughout the rest of the domain the No-flux condition is imposed.

$$\text{Wall} \quad \mathbf{n} \cdot \mathbf{N}_{wat} = 0 \quad \text{On } \zeta_2, \zeta_5, \zeta_6, \zeta_7, \zeta_8, \zeta_9, \zeta_{13}, \zeta_{14}, \zeta_{15}, \zeta_{16}, \zeta_{18}, \zeta_{22} \quad (76)$$

$$\begin{array}{l} \text{Inlet at anode} \\ \text{and cathode} \end{array} \quad s = 0 \quad \text{On } \zeta_3, \zeta_{21} \quad (77)$$

$$\begin{array}{l} \text{Exit at anode} \\ \text{and cathode} \end{array} \quad \nabla s = 0 \quad \text{On } \zeta_1, \zeta_{19} \quad (78)$$

4.7 Numerical methods

4.7.1 Method and program used

The equations have been solved using the COMSOL Multiphysics[®] software which uses the finite element method (FEM). To solve the problem of convergence, the study was divided into 6 segregated steps:

1. Velocity and pressure of anode side
2. Mass fraction of water in the anode side
3. Velocity and pressure of cathode side
4. Mass fraction of water and oxygen in the cathode side
5. Electrolyte potential, Electrode potential
6. Saturation water in anode compartment, saturation water in cathode compartment

The Newton method is used to find solutions to the problem. it is an iterative model that generates a succession of points starting from an initial point X_0 which after a certain number

of iterations converges to an approximation of the root of the function. The damping factor for each segregated step was chosen in order to obtain the convergence of the problem [58].

In order to avoid computational error during the study, changes were made to the equations to avoid numerical errors. Often some variables reached null values, or too high that led to the lack of convergence of the simulation. For example, Eq. (38) was written as:

$$\gamma_{wd} = 0.5 + \frac{(\rho_{wv}^g - \rho_{wv}^p)}{1e^{-6} + 2|\rho_{wv}^g - \rho_{wv}^p|} \quad (79)$$

in order to avoid computational problem with the value of $\gamma_{wd} = 0$, a very small value is added which does not change the effects of the equation but avoids computational problems. The Eq. (53) and Eq. (73) have been modified following the same criterion in order to reach the convergence of the problem.

4.7.2 Parameters and variables

The relevant design and operating parameters are summarizing on Tab. 4 and Tab. 5. The comparison with the Seigel's problem is possible thanks to the presence of the same geometry and physics' inputs. The cell was run at a cell temperature of 80 °C with the reactant gases on both the anode and cathode zones maintained at temperatures of 80 °C throughout the cell, the pressure outlet of 30 [Psig] and relative humidity of 100% at the inlet, exactly like done in Seigel. Mass flow rate, at both the anode and cathode, corresponded to a stoichiometric ratio of 6 at a current density of $1 \left[\frac{A}{cm^2} \right]$ [41]. In Tab. 6, boundary conditions are indicated which solve the problem and their field of application. Subsequently, Tab. 7 represents the domains in which the source terms of each physics are applied. Finally, Tab. 8 shows the degrees of freedom of the problem and the domains in which they are calculated.

Property	Value	Description	Reference
μ_a	2e-5 [Pa s]	Anode viscosity	[41]
μ_c	1e-5 [Pa s]	Cathode viscosity	[41]
κ_{gdl}	1.8E-11 [m ²]	Permeability of GDL	[59]
μ_{WL}	4E-4 [kg/ (m s)]	Liquid viscosity	[60]
D_{O_2}	2E-7 [m/s]	Diffusivity of Oxygen in polymer	[41]
D_{H_2}	7.9E-7 [m/s]	Diffusivity of hydrogen in polymer	[61]
i_{0,H_2}	30 [A/m ²]	Current reference in anode	[15]
i_{0,O_2}	0.0041 [A/m ²]	Current reference in cathode	[41]
C_{0,O_2}	1.18 [mol/m ³]	Reference concentration of oxygen	[41]
C_{0,H_2}	26.6 [mol/m ³]	Reference concentration of hydrogen	[41]
F	96487 [s A/mol]	Faraday's constant	[59]
h_{da}	0.64	Solubility coefficient for the anode	[41]
h_{dc}	0.19	Solubility coefficient for the cathode	[41]
α_a	0.5	Anodic transfer coefficient	[15]
α_c	0.55	Cathodic transfer coefficient	[15]
g	9.81 [m/s ²]	Gravity	[-]
ρ_{WL}	970 [kg/m ³]	Density of liquid water at 80°C	[57]
R	8.314 [J/mol/K]	Universal constant of gas	[-]
ρ_m	2000 [kg/m ³]	Density of membrane	[63]
M_{nafion}	1.1 [kg/mol]	Molar mass of membrane	[63]

Table 4 Physical properties

Property	Value	Description
W_{gc}	30 [cm]	Width channel
L_{gc}	0.001 [m]	Length channel
H_{gc}	0.001 [m]	Height channel
t_{col}	2.9E-4 [m]	Collector thickness
t_{agd1}	2.9E-4 [m]	Thickness GDL anode
t_{cgdl}	2.54E-4 [m]	Thickness GDL cathode
t_{cat}	1.65E-5 [m]	Catalyst
t_m	5.08E-5 [m]	Membrane thickness
ϵ_{void}^{gdl}	0.375	Degree of vacuum in GDL
ϵ_{void}^{cat}	0.31	Degree of vacuum in catalyst
T	353 [K]	Temperature
P_{in}	310 [kPa]	Inlet pressure
E_{th}	1.19[V]	Theoretical open circuit voltage
Ψ	20 [kg/ (m ³ s)]	Evap/Cond mass transfer coefficient
σ_e	600 [S/m]	Electric conductivity
A_v	6.99E6 [1/m]	Specific reaction area of catalyst
V_{cell}	Varies [V]	Operating voltage of cell
w_{H_2}	0.38	Mass fraction at inlet of hydrogen
M_{H_2O}	0.018 [kg/mol]	Molar mass of water
h_m	500 [1/s]	Dissolved/water mass transfer
P_{an}	2.0684E5 [Pa]	Relative pressure outlet anode
P_{cat}	2.0684E5 [Pa]	Relative pressure outlet cathode
ϵ_C^{cat}	0.24	Polymer volume fraction in the catalyst
L_{agg}	4E-7 [m]	Mean agglomerate size
T	3.5	Tortuosity
$w_{H_2O_a}$	0.60	Mass fraction at inlet of water in anode
M_{H_2}	0.002 [kg/mol]	Molar mass of hydrogen
M_{O_2}	0.032 [kg/mol]	Molar mass of oxygen
M_{N_2}	0.028 [kg/mol]	Molar mass of nitrogen
w_{O_2}	0.21	Mass fraction at inlet of oxygen
$w_{H_2O_c}$	0.1	Mass fraction at inlet of water in cathode
U_{an}	1.547 [m/s]	Inlet velocity anode
U_{cat}	3.747 [m/s]	Inlet velocity cathode

Table 5 Design and operating parameters for validation study

Boundary's condition	Anode inlet	Anode inlet GDL	Anode inlet Catalyst	Anode outlet	Cathode outlet	Cathode inlet Catalyst	Cathode inlet GDL	Cathode inlet
Momentum's equations	$u_{a,avg} = 1.547 \left[\frac{m}{s} \right]$	/	/	$P = 30[psig]$	$P = 30[psig]$	/	/	$u_{c,avg} = 3.747 \left[\frac{m}{s} \right]$
Oxygen	/	/	/	/	$\nabla w_{O_2} = 0$	/	/	$w_{O_2} = 0.21$
Water vapour	$w_{H_2O} = 0.62$	/	/	$\nabla w_{H_2O} = 0$	$\nabla w_{H_2O} = 0$	/	/	$w_{H_2O} = 0.1$
Dissolved water	/	/	No Flux	/	/	No Flux	/	/
Liquid water	$s = 0$	/	/	$\nabla s = 0$	$\nabla s = 0$	/	/	$s = 0$
Membrane potential	/	$\phi_p = 0$	/	/	/	/	$\phi_p = V_{cell}$	/
Thermal Energy	$T = 353 [K]$	/	/	/	/	/	/	$T = 353 [K]$

Table 6 Value of the boundary conditions

Source's terms	Channel Anode	GDL Anode	Catalyst Anode	Membrane	Catalyst Cathode	GDL Cathode	Channel Cathode
S_{O_2}					X		
S_{H_2}			X				
$S_{\phi,i}$			X		X		
S_{WP}					X		
S_{wd}			X		X		
S_{LW}	X	X	X		X	X	X

Table 7 Source terms present in the model and their application domains

Degree of freedom	Channel Anode	GDL Anode	Catalyst Anode	Membrane	Catalyst Cathode	GDL Cathode	Channel Cathode
Continuity and Brinkman	P_f, \mathbf{u}	P_f, \mathbf{u}	P_f, \mathbf{u}	P_f, \mathbf{u}	P_f, \mathbf{u}	P_f, \mathbf{u}	P_f, \mathbf{u}
Fick's Diffusion	C_{H_2}, C_{H_2O}	C_{H_2}, C_{H_2O}	C_{H_2}, C_{H_2O}		C_{O_2}, C_{H_2O}	C_{O_2}, C_{H_2O}	C_{O_2}, C_{H_2O}
Charge's		ϕ_e	ϕ_e, ϕ_p	ϕ_p	ϕ_e, ϕ_p	ϕ_e	
Nernst-Planck			C_{wd}	C_{wd}	C_{wd}		
Liquid Water	s	s	s		s	s	s

Table 8 Degrees of freedom

5 Result and discussion

5.1 Model verification

A mesh convergence study was conducted to select the required degree of precision, see fig. (24). The mesh created is a "Mapped meshing" suitable to maintaining good mesh density across the domain. In the most important areas, for example the two catalyst, it has been made finer because in these domains there are great gradients. The final mesh, represented in Fig. 25, chosen divides the domain into 140 x 242 elements and it was acceptable because the error with respect to the first mesh is less than 1%, as you can see in the Tab. 9 and Tab. 10 and in Fig. 24.

Number of elements	Relative error respect to the most precise mesh (52500 elements)
2989	78.3%
8470	24.4%
16065	9.5%
33880	1.05%

Table 9 Oxygen relative error

Number of elements	Relative error respect to the most precise mesh (52500 elements)
2989	19.3%
8470	8.15%
16065	3.23%
33880	0.84%

Table 10 Liquid water relative error

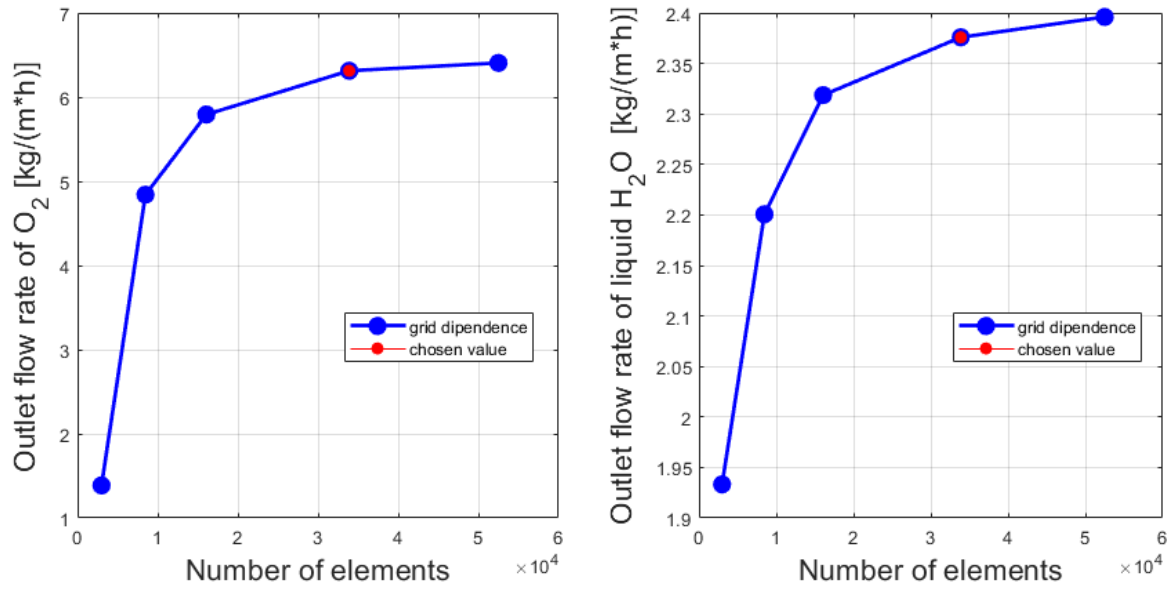


Figure 24 Grid independence of oxygen (relative error=1.05%) and water (relative error=0.84%)

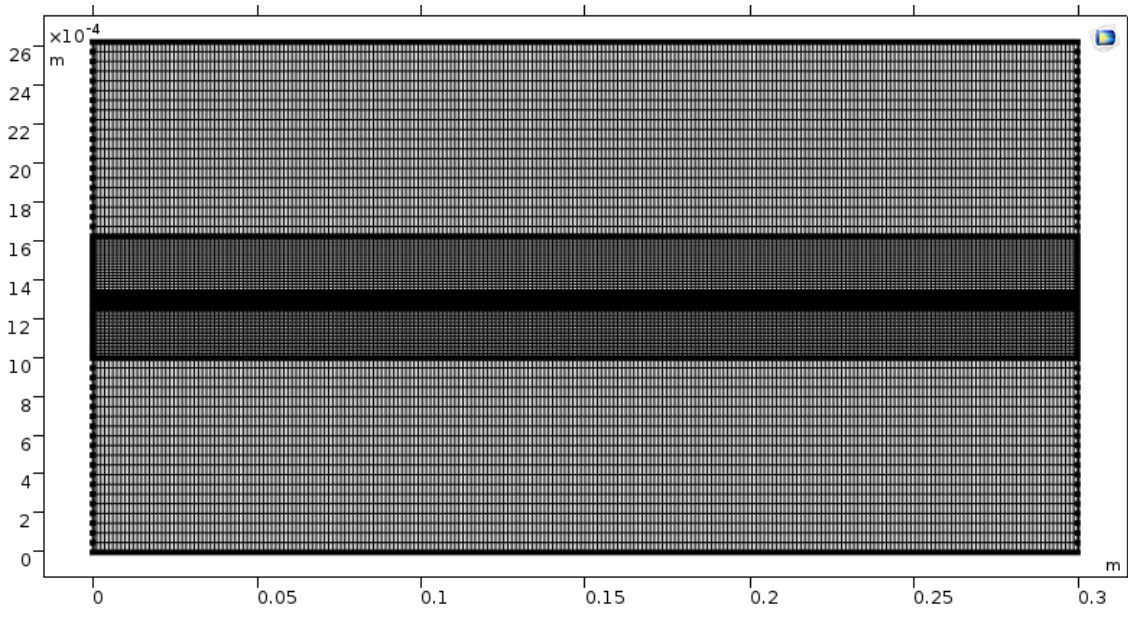


Figure 25 Final mesh chosen

5.2 Model validation

In order to validate the numerical model, we compare the polarization curve we obtained with the one obtained by Seigel et Al [41] in their study, which compares their model with experimental results. The comparison is shown in Fig. 26 for the polarization curve, and in Fig.27 for the power curve.

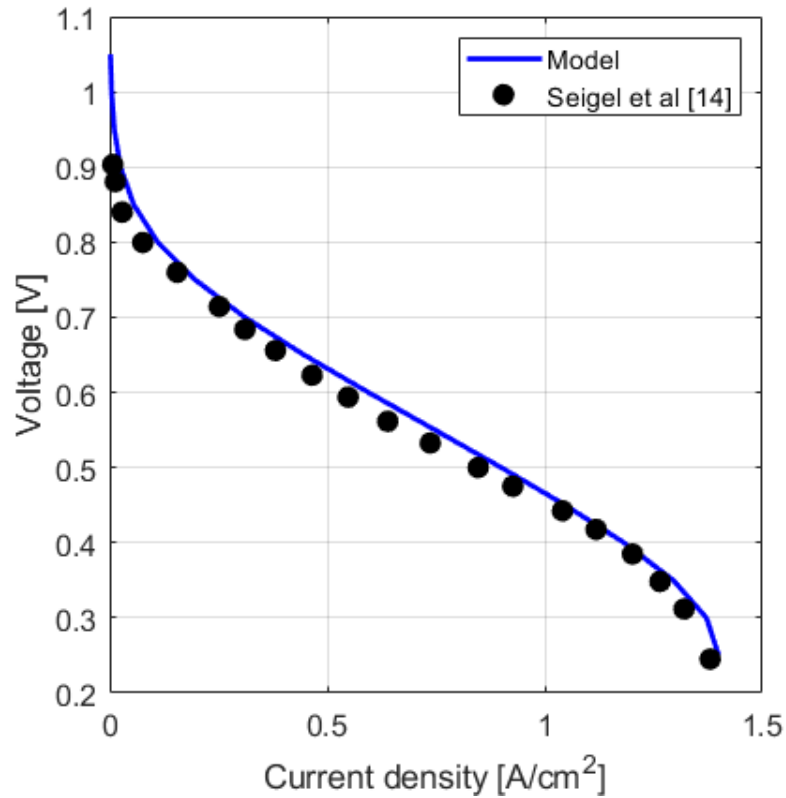


Figure 26 The comparison between the polarization curve obtained from the model, and that obtained from the Seigel model

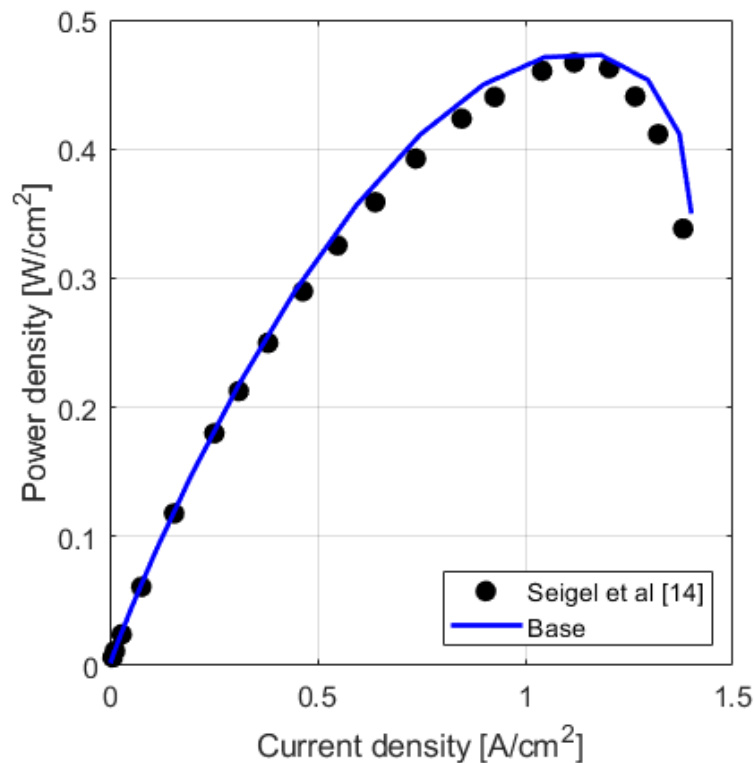


Figure 27 Comparison of the power curve of the Pemfc, with the reference curve taken from the article by Seigel et al [41].

From the Fig. 26 curve it is also possible to note the 3 different behaviours of the cell according to the voltage, exactly as we said in the section 1.5:

- In the first part the losses are due to the activation energy
- In the second part are due to the ohmic effect
- In the third part the reduction is due to diffusion difficulties

The biggest difficulty is that of representing the diffusion losses, because to be represented it must necessarily take into account the multi-phase flow of water. This trend is reproduced with high accuracy thanks to the formation of liquid water, which reduces both the diffusion of the reactants and the rate of reaction.

An analysis without considering the formation of liquid water, yields a large difference between the two-polarization curve. The model without water formation cannot reproduce the diffusion difficulties of the reagents, as shown in Fig. 28.

On the other hand, if we do not even consider the water flowing along the membrane, but we take the membrane completely humidified, the losses are reduced. So not considering the water inside the PEMFC leads to a big error of evaluation.

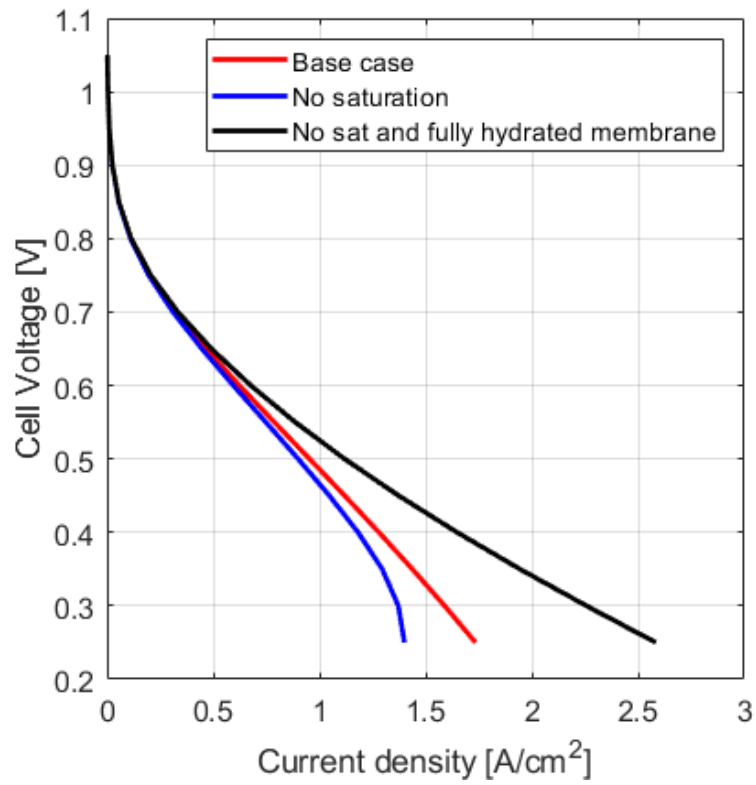


Figure 28 In red the polarization curve without formation of liquid water, in blue the model curve considering also the water.

5.3 Analysis in nominal conditions

Where there is no porous medium, the velocity of the gas is greater, whereas in the porous medium, the velocity becomes almost negligible and the phenomenon becomes prevalently diffusive. The velocity along the height of the channel is represented in Fig.29.

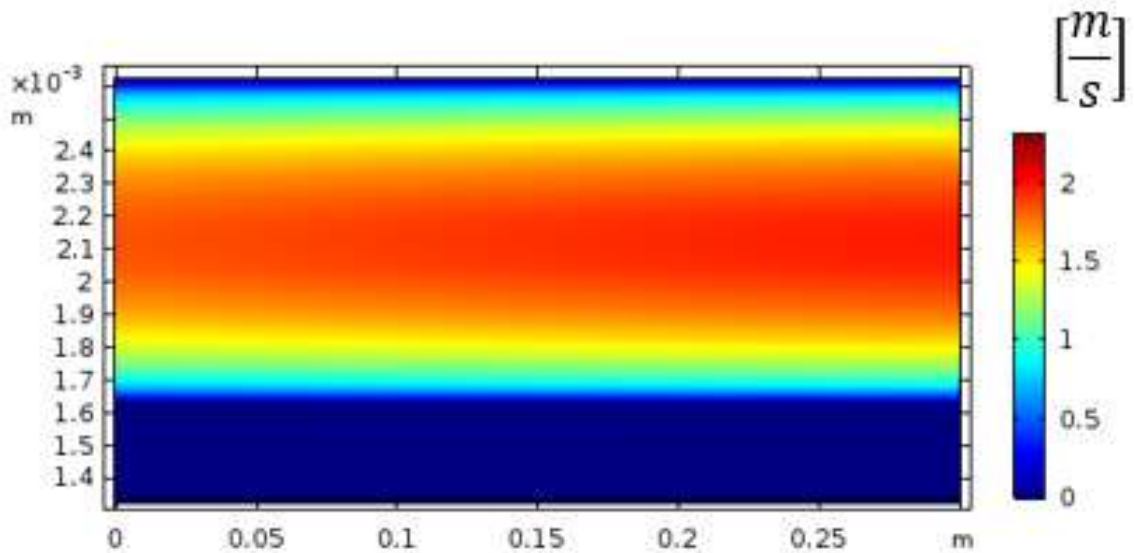


Figure 29 The anode velocity profile inside the fuel cell. It is present only in the anode compartment.

The Fig. 29 shows the trend of the velocity along the perpendicular direction of the cell more precisely. Note how along the channel the velocity is that of the classic parabolic profile, while along the porous medium the fluid is very slowed down until it stops at the end of the catalyst (see Fig.30).

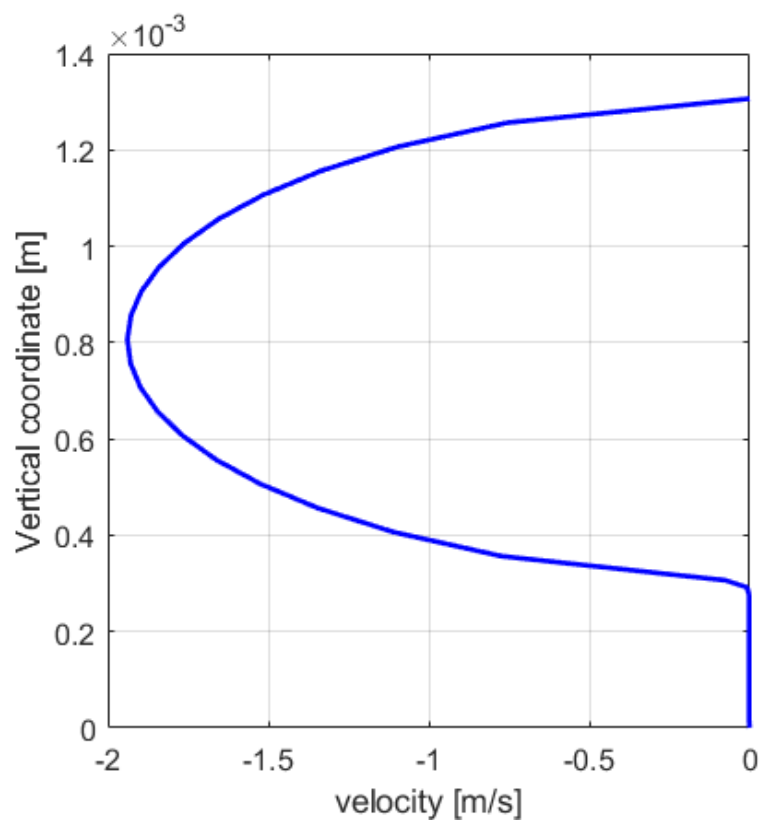


Figure 30 Velocity profile at 0.4 Volt in the anode side

The concentration of oxygen along the channel (Fig. 31) tends to decrease as it reacts, and therefore its concentration will be lower near the catalyst where the reaction takes place.

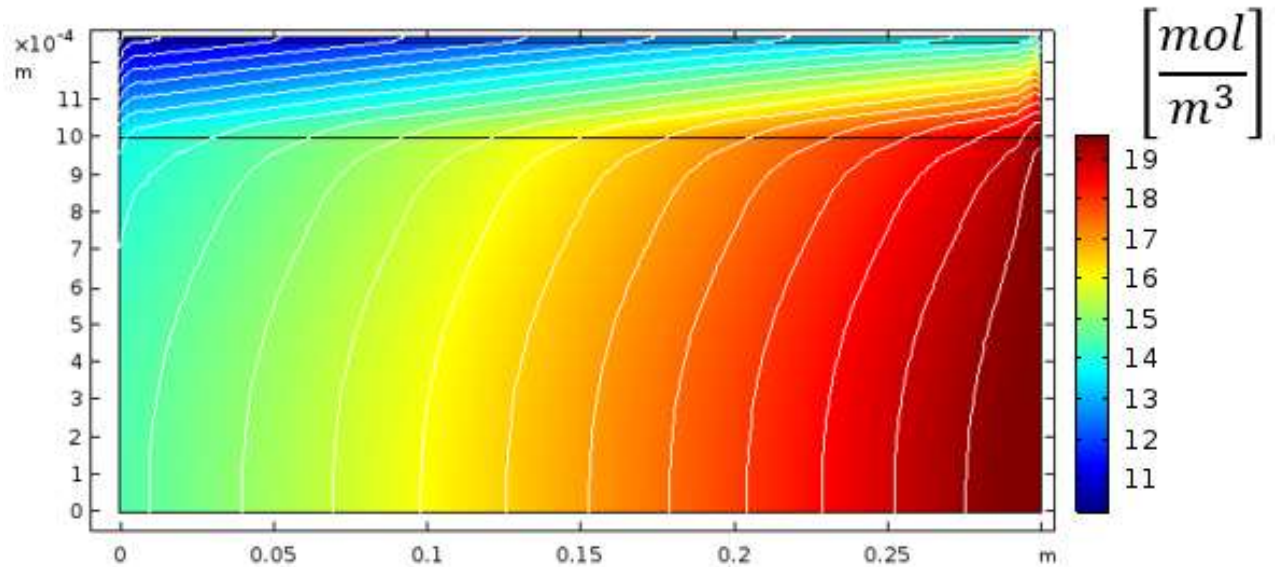


Figure 31 Molar concentrations of oxygen at 0.4 Volt

The iso-lines of oxygen concentration have different slopes in the three zones. This is due to the different value of diffusivity in the 3 zones. In the porous medium the diffusion is more dominant than convection, but especially in the catalyst, the diffusion is greatly reduced both for the lower degree of vacuum and for the greater quantity of water.

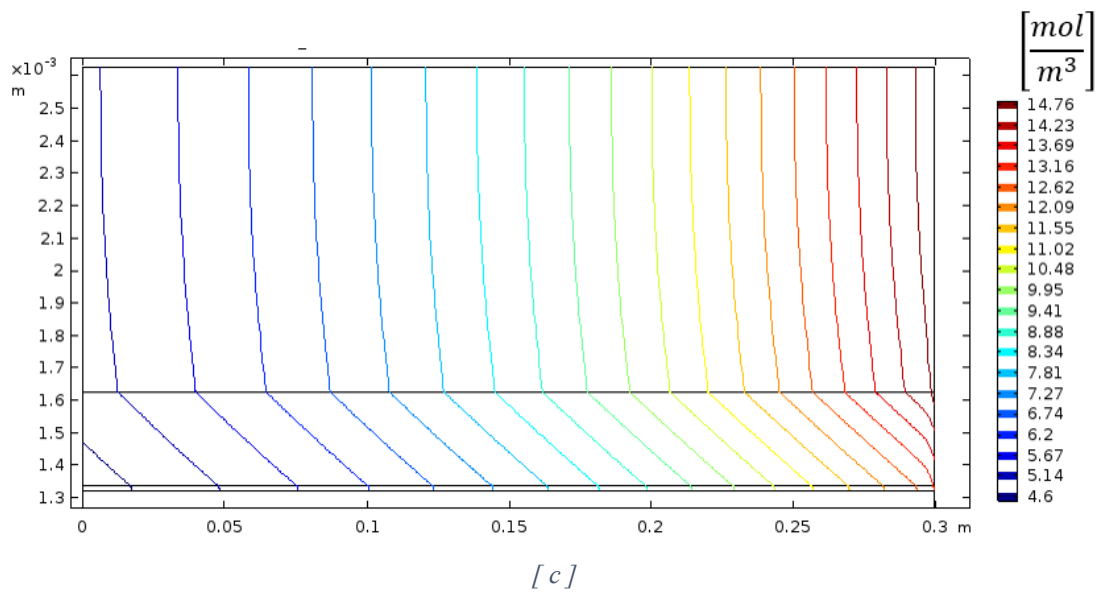
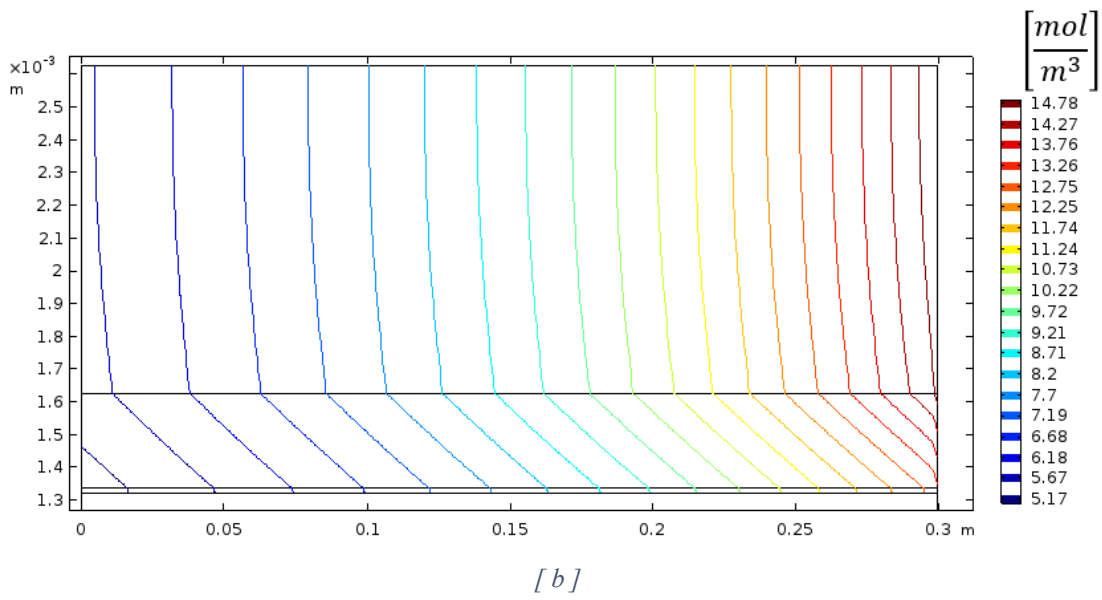
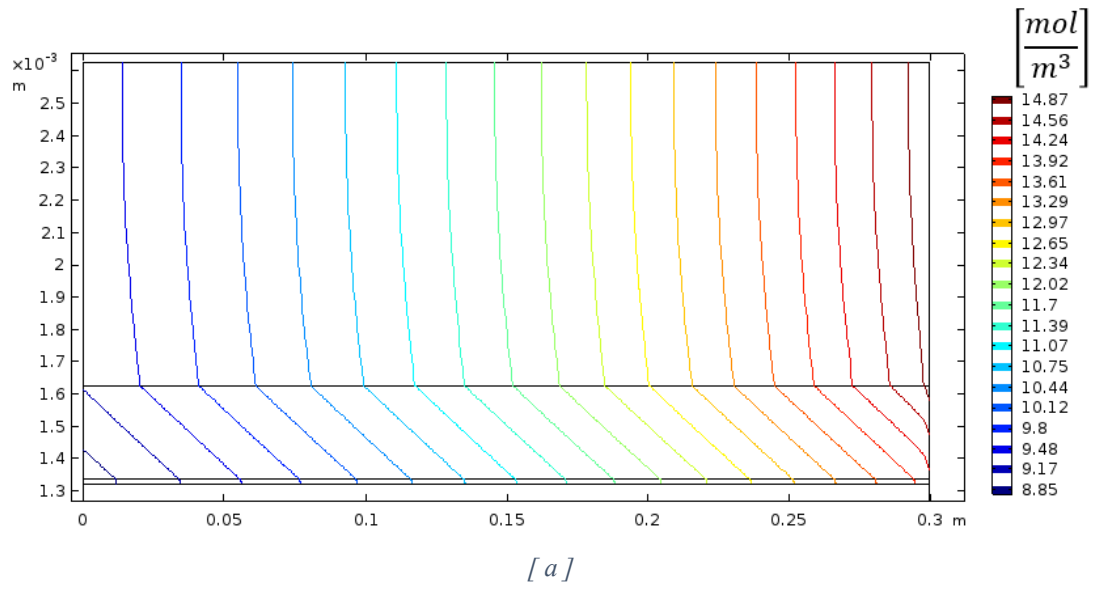


Figure 32 Water anode concentration in 3 different voltage cases. [a]: 0.6 V; [b]: 0.4 V; [c]: 0.25V

In the anode side the steam water is absorbed by the membrane, hence its concentration decreases as visible in Fig. 32. As at low voltages the current is greater, and the effect of EOD is more relevant.

The concentration of steam water along the cathode decreases and begins to dehydrate. We can see in Fig. 33 how the water absorbed by the membrane is distributed along the thickness of the membrane. This figure represents the water content along a vertical line positioned at $x=0.15$ m and crossing the cathode catalyst, the membrane and the anode catalyst. We can see that the distribution of water in the membrane is regulated by the three factors seen in the equation 63. The motion due to EOD is prevalent at high value of current and the water will tend to move towards the cathode and at the anode side the membrane will be drier.

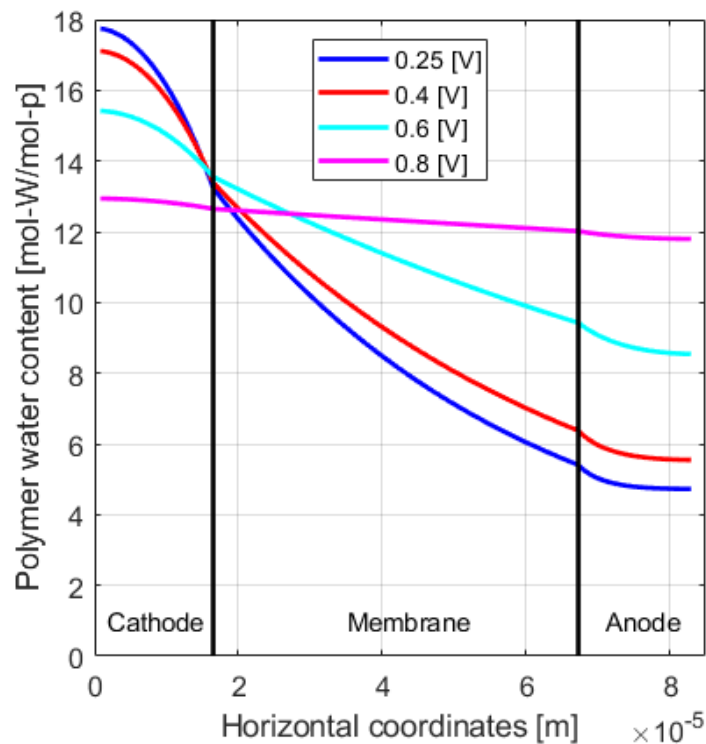


Figure 33 Variation of water within the membrane at different voltages at $x=0.15$ m

Near the catalyst there is a large production of steam water due both to the completion of the reaction and the evaporation of liquid water. The steam water concentration in the cathode is shown in Fig. 34 and its pressure relative to the saturation pressure is shown in Fig.35.

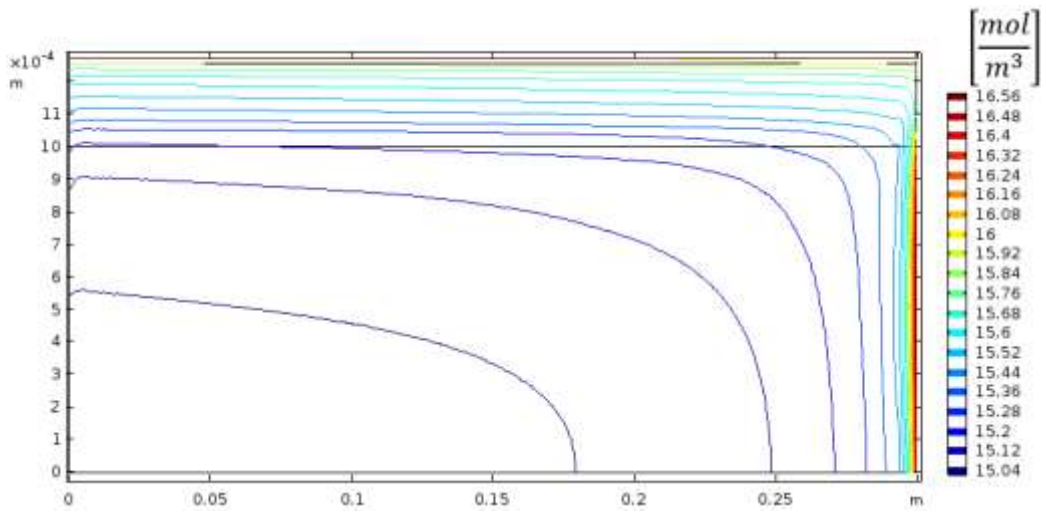


Figure 34 Molar concentration of steam water at the cathode

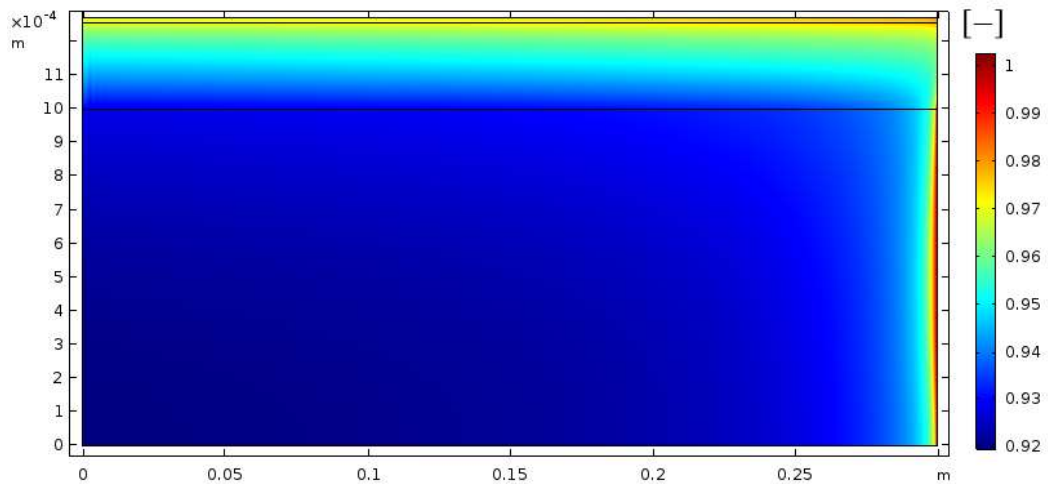


Figure 35 Ratio between the steam water pressure in the cathode and its saturation pressure.

As we have already said the liquid water is created by the dissolved water released by the membrane, or by the chemical reaction. From the fig. 36 we note that most of the water is produced in the catalyst near the cathode entrance. This is because the reaction rate has the maximum value near the inlet where the concentrations of the reagents are greater. Also, for the membrane, the concentration of dissolved water is higher at the entrance, higher currents result in more water transported by EOD. The contribution of both lead to a peak of liquid water in the catalyst and at the inlet side. As can be seen in the cathode channel, the value of discharge is zero, so the amount of water to be studied is only found in the porous medium, in fact the iso-line in Fig. 37, represent only the GDL and catalyst layer.

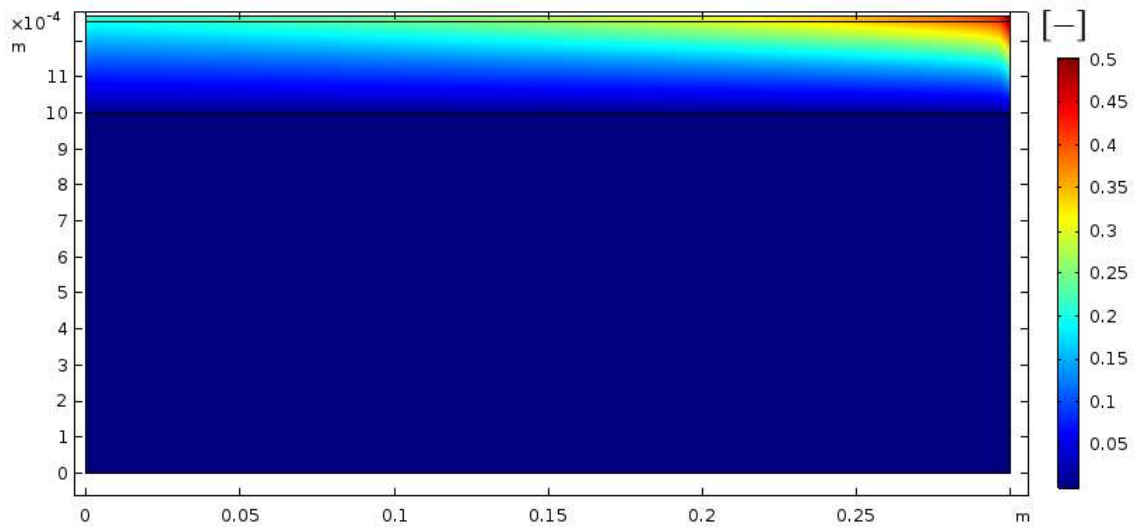


Figure 36 Surface plot of saturation water in cathode compartment.

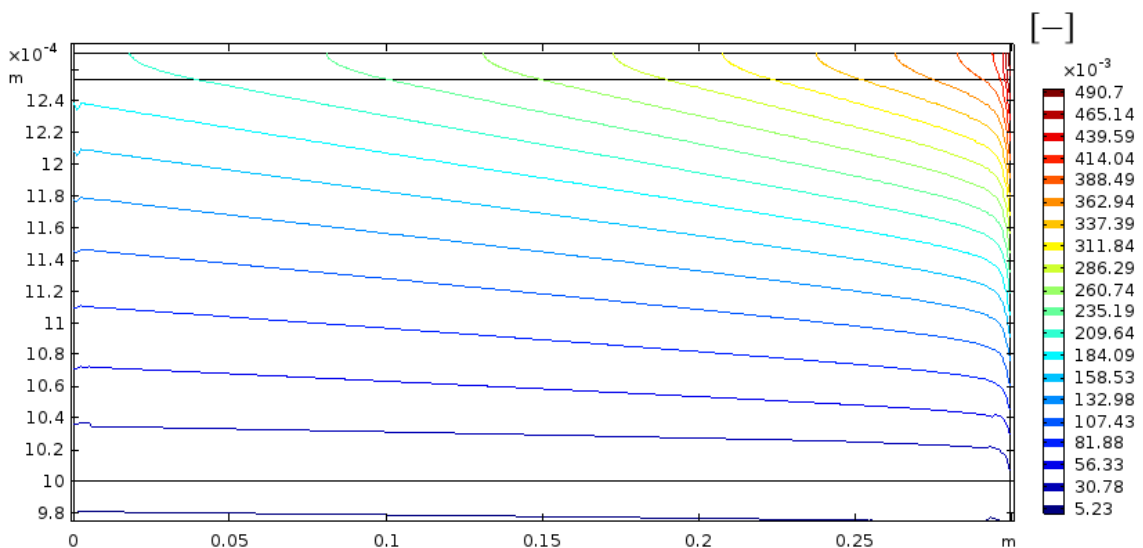


Figure 37 Iso-lines of the saturation curve.

The importance of water and its movements along the cell are all represented in the model. As for the ohmic losses (i.e. the slope of the polarization curve), when at high currents the anode dehydrates too much leads to a reduction in the performance of the cell, since it increases the resistivity of the cell to the ions. Moreover, at high currents, the formation of too much liquid water leads to a reduction of both the diffusion of the reagents and therefore to a consequent reduction in the rate of reaction.

Since no liquid water enters the cell inlet, the production rate of the liquid water must be equal to the quantity that is expelled from the cell. To see this, it is calculated a simple balance

between the water produced in the whole cell domain, and the one that comes out. The results are shown in Tab. 11.

Property	Value	Description
Volt [V]	0.4	Voltage of cell
$S_{LW} \left[\frac{kg}{m \ h} \right]$	0.685	Evaporation- condensation term
$S_{WD}(1 - \gamma_{WD}) \left[\frac{kg}{m \ h} \right]$	0.577	From dissolved to liquid
$S_{WP}(1 - \gamma_{LV}) \left[\frac{kg}{m \ h} \right]$	1.115	Water product in liquid form
$\rho \int su \left[\frac{kg}{m \ h} \right]$	2.399	Total amount of water leaving the cell

Table 11 Mass balance of the liquid water, calculated in $\frac{kg}{mh}$

Water sources must be equal to the one that comes out. From the sum of the first three we obtain that the relative error between produced water and outlet water is less than 1%. Thus, suggest that conservation of liquid water is enforced with sufficient accuracy.

5.4 Parametric analysis

Once a model that representing all the physical aspects of the cell has been obtained, we can move to a parametric analysis of some variables to see how these influences the power generated and the efficiency of the cell. Among the changes made to the cell, we consider variations in operating parameters, and variations of design parameters.

5.4.1 Variation of operating parameters

The two most important parameters that regulate the amount of water present in the cell are pressure and temperature.

For each variation in pressure and temperature, the two fully humidified reagent gases must always be maintained (100% relative humidity and reconsider the new value of Open circuit

voltage. The open circuit voltage is calculated with the Nernst equation seen in equation Eq. (51) and the respective values used in the various conditions are shown in Tab. 12 and Tab. 13.

Property	Description	Value		
		$T = 70^{\circ}C$	$T = 80^{\circ}C$	$T = 90^{\circ}C$
$E_{th} [V]$	Open circuit Voltage	1.1972	1.1900	1.1800
$w_{H_2O,a}$	mass fraction of water at the anode entry	0.535	0.62	0.73
$w_{H_2O,c}$	mass fraction of water at the cathode entry	0.066	0.1	0.152

Table 12 Change of input parameters when temperature changes

The temperature range, however, cannot vary too much [62]. The operating temperatures of a Pemfc cell of this type are from 60 to 80 degrees. Raising its temperature too much should be avoided, otherwise the membrane and other materials could be damaged [18,20].

As we can see in Fig. 38, with increasing temperature, the activation losses increase. At low voltages the high T curve has lower current values, while the ohmic losses are reduced. In the part of the diffusion losses, however, in all three cases of T the situation does not change, therefore the temperature does not influence the diffusion losses.

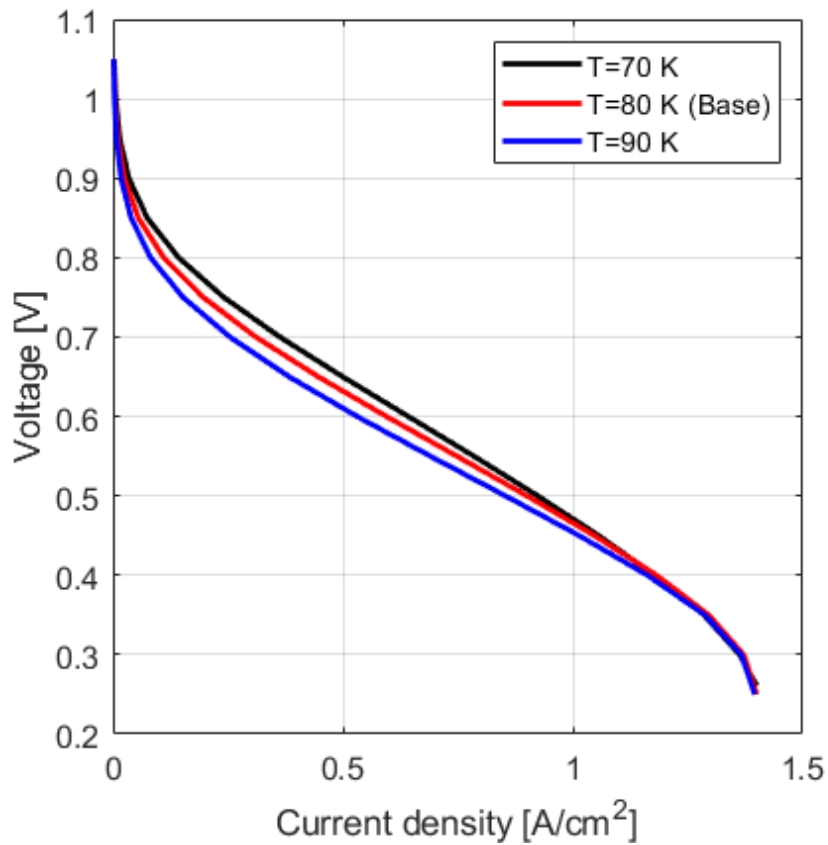


Figure 38 Different polarization curves by varying the temperature.

In the case of pressure, however, if we increase the pressure value of the reagents, the concentrations near the catalyst will be greater, and therefore an increase in the power will be produced, but at the same time the high pressure prevents the water from evaporating, and this increases the losses by diffusion. . At low pressures the reactant concentrations decrease, but the diffusion losses decrease as we can see in the Fig. 39.

Property	Description	Value		
		$P = 30 \text{ Pisg}$	$P = 20 \text{ Pisg}$	$P = 10 \text{ Pisg}$
$E_{th} [V]$	Open circuit Voltage	1.1900	1.1811	1.1693
$w_{H_2O,a}$	mass fraction of water at the anode entry	0.62	0.71	0.78
$w_{H_2O,c}$	mass fraction of water at the cathode entry	0.1	0.13	0.185

Table 13 Change of input parameters when pressure changes

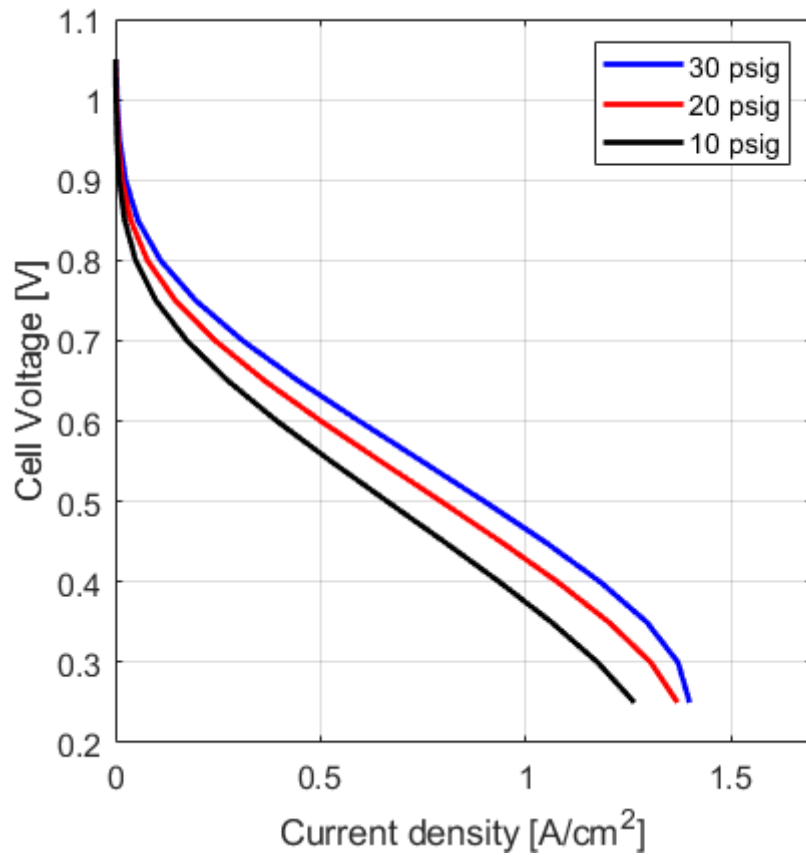


Figure 39 Polarization curve for different values of pressure

To reduce diffusion losses at higher voltages, the formation of liquid water must be avoided. The percentage of water to be inserted is calculated in order to have the reactants with a lower percentage of humidification.

The values entered in the model, in order to have a degree of humidification of 80%, are indicated in the Tab. 14.

Property	Description	Value
$w_{H_2O,a}$	mass fraction of water at the anode entry	0.57
$w_{H_2O,c}$	mass fraction of water at the cathode entry	0.077

Table 14 Value of inlet mass fraction of water in the case study with lower humidity

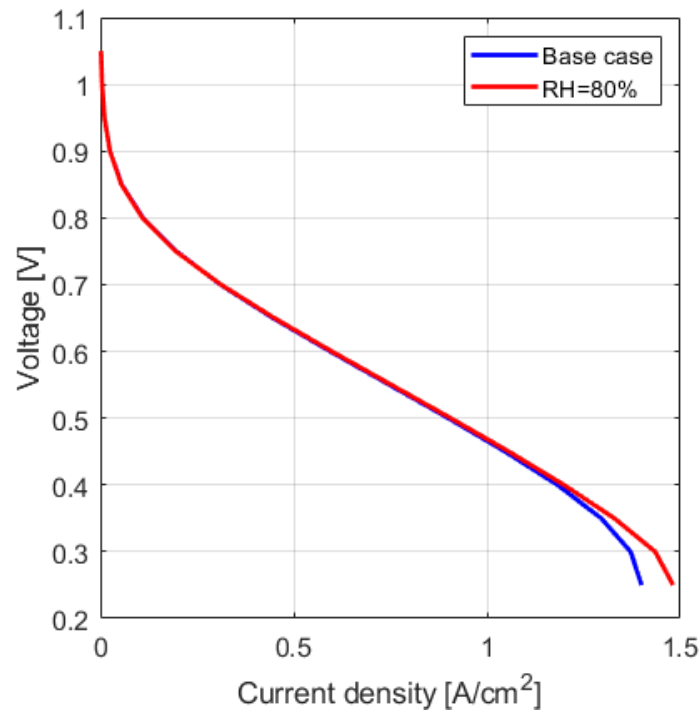


Figure 40 Comparison between the polarization curves with different relative humidity in input

From Fig. 40 we can notice that when entering with relative humidity of 80%, the diffusion losses are reduced, when the air manages to "capture" part of the liquid water that is in the cell. Thus, the performance of the low voltage cell is improved.

5.4.2 Variation of design parameters

As the reactants pass through the pores, they arrive near the catalyst where they complete the electrochemical reaction. For a fixed volume of carbon of the catalyst layer, a decrease in the catalyst layer void fraction was obtained by adding ionomer. The result as shown in Fig. 41.

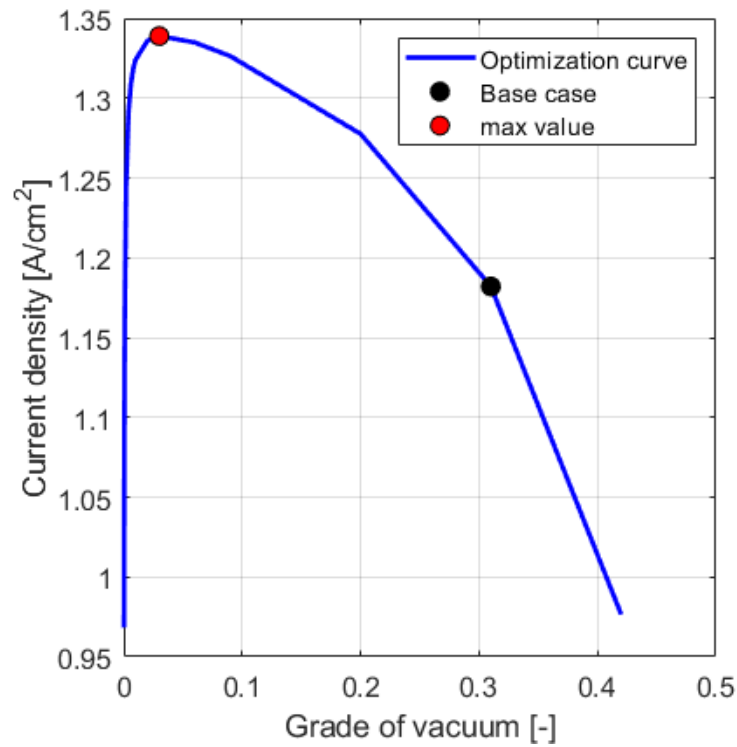


Figure 41 Variation of the current intensity by varying the degree of vacuum at a constant voltage of 0.4 V

The optimal catalyst layer void fraction at this voltage is 0.03. At even smaller values of vacuum we have a very sharp reduction in current. This is due to rapidly increasing concentration overpotential. As the void fraction and permeability decrease, reactant transport by diffusion and advection within the catalyst layer drops very quickly. If the degree of vacuum is reduced too much, the reagent gas and the water vapor cannot permeate in the catalyst, and this leads not only to a reduction in concentration, but also to the reduction of water in the membrane. Since there is less water vapor near the catalyst, the membrane will be less humidified, as we can see in Fig. 42. The losses by diffusion at high currents are less clear, because due to the reduction in concentration, the rate of reaction is limited and there is not a too high production that limits the diffusion of the reagents (see Fig.43).

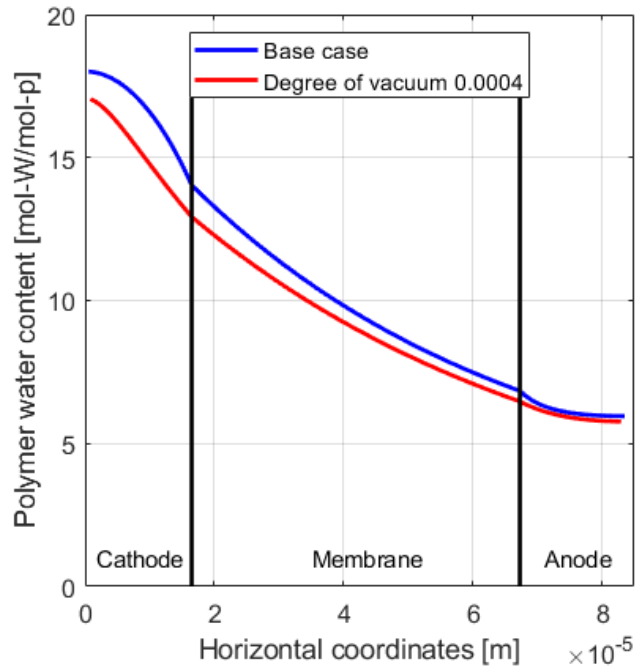


Figure 42 Polymer water content at 0.4 Volt and at $x=0.25$ m.

Instead, in the opposite direction, if the degree of vacuum increases too much, the ionomeric fraction must decrease, the porous medium is no longer able to connect the reactant gas and current production is reduced. The increase in porosity improves mass flow and reduces concentration overpotential, and it also increases the ohmic overpotential [52].

A comparison with the polarization curve is made with respect to the base case with the optimal value of ϵ_{void}^{cat} and a much lower value ($\epsilon_{void}^{cat} = 0.0003$) is show in Fig. 43 and in Fig. 44 for the power-curve.

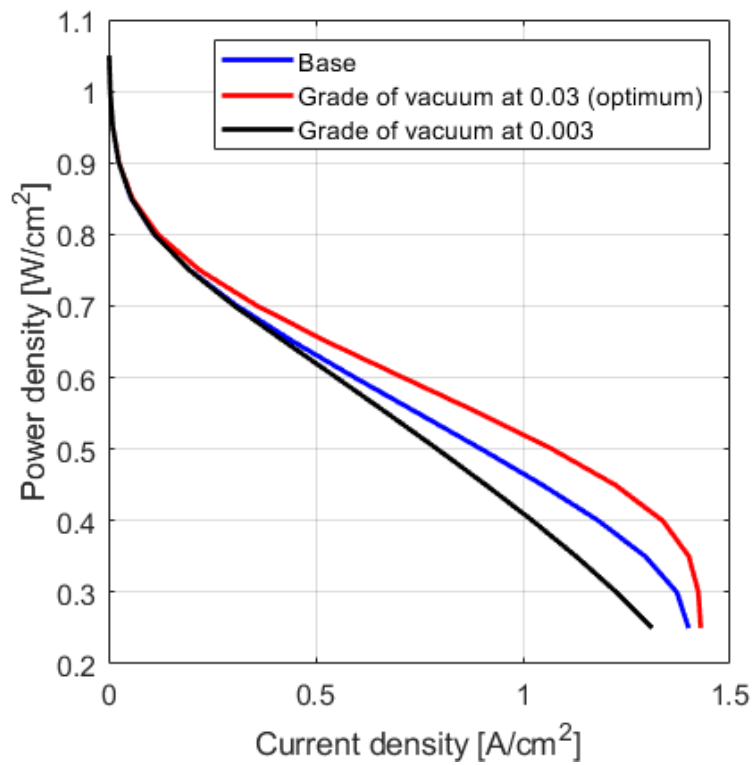


Figure 43 Polarization curves to the various " ϵ_{void}^{cat} ". At very low values of " ϵ_{void}^{cat} " the losses of diffusions are very high, and the efficiency of the cell is lower than the base case.

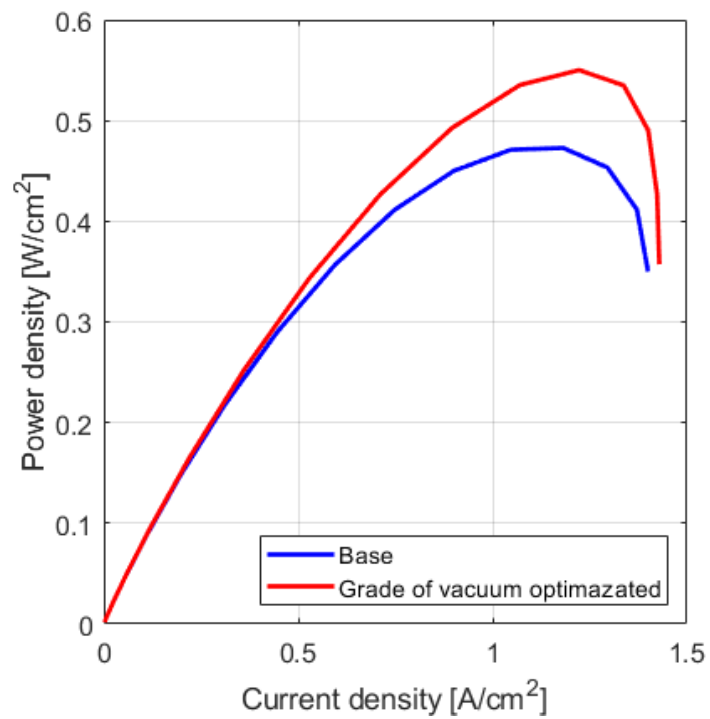


Figure 44 Comparison of the power curves considering the case with the optimal degree of vacuum

Another parameter of interest that can be modified is the catalyst layer distribution of platinum particles [64]. When calculating the rate of reaction, Butler-Volmer current is multiplied by A_v in order to obtain the rate of reaction. In the base case of the model, the value of A_v has been assumed to be constant throughout the domain of the catalyst. Its value can be modified in order to have a different distribution along the surface of the catalyst, making sure that its absolute quantity does not change value. The modification is made to the catalysts (both anode and cathode) in order to have the highest possible increase.

To understand the physical trend, it is important to study how the rate of reaction along the x-axis and the y-axis varies.

The variation along the x direction is different according to the height at which we take the measure. In general, however, the variation along the x-direction is not very relevant as shown in Fig. 45.

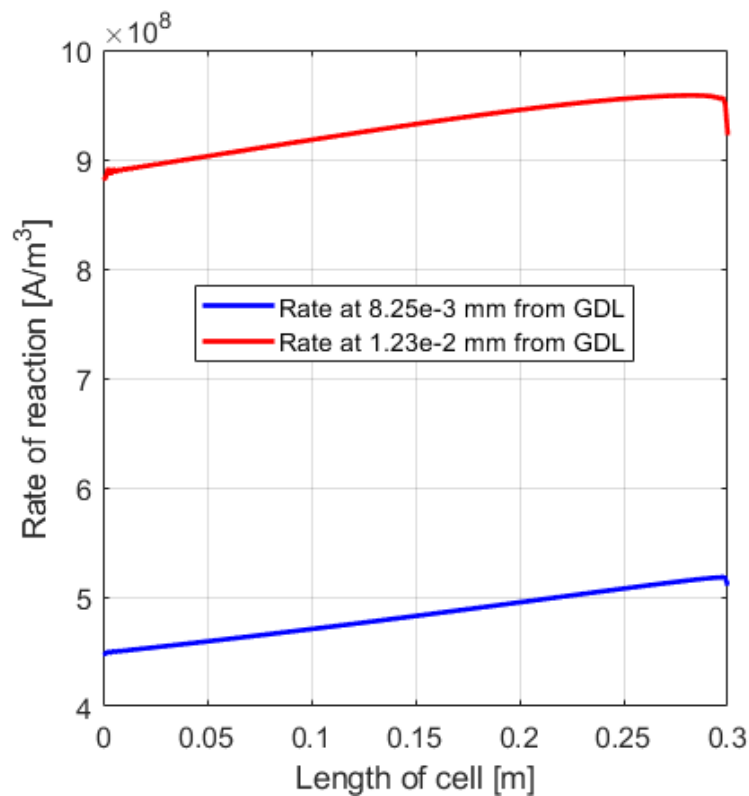


Figure 45 Reaction rate along the anode x direction.

The red curve located closer to the membrane is at a height y closer to the membrane, and has a higher value, but the initial part is affected by the presence of water and the value closer to the entrance is lower.

To understand how the performance of the cell is affected by A_v along x direction we consider the following straight. The variable x varies the length of the cell, while P_1 indicates the slope of the line.

$$A_v = A_{v_{ref}} \left(1 + \frac{P_1}{\frac{W_{gc}}{2}} \left(x - \frac{W_{gc}}{2} \right) \right) \quad (80)$$

Parameter $P_1 = [-1; 1]$ varies the slope of the line, and 13 inclinations have been tested to see which the best is. The straight line is applied in the same way to both the catalyst of the anode and to that of the cathode at 0.4V.

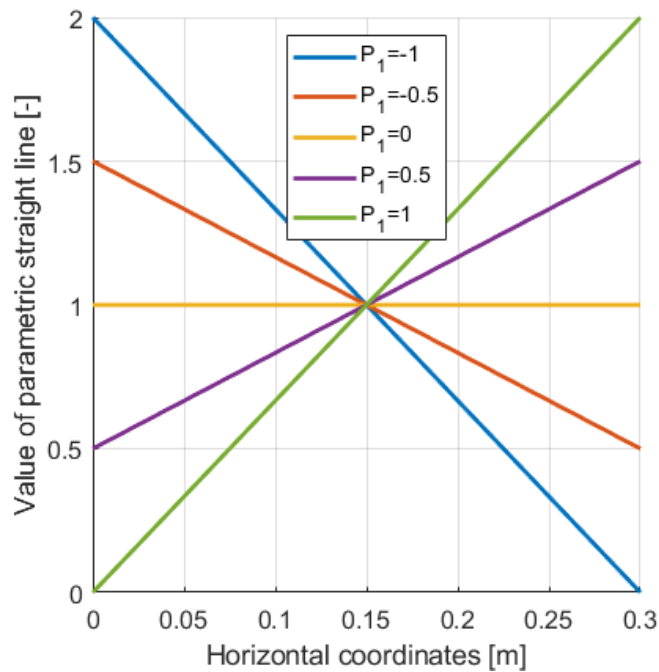


Figure 46 Representation of the lines to some values of P_1

From the Fig. 46 it is noted that when the value P_1 is positive, the line is decreasing from input to output, while when P_1 is negative vice versa.

The variation of the produced current has been studied at every variation of inclination of the line, and the result is shown in the Fig. 47.

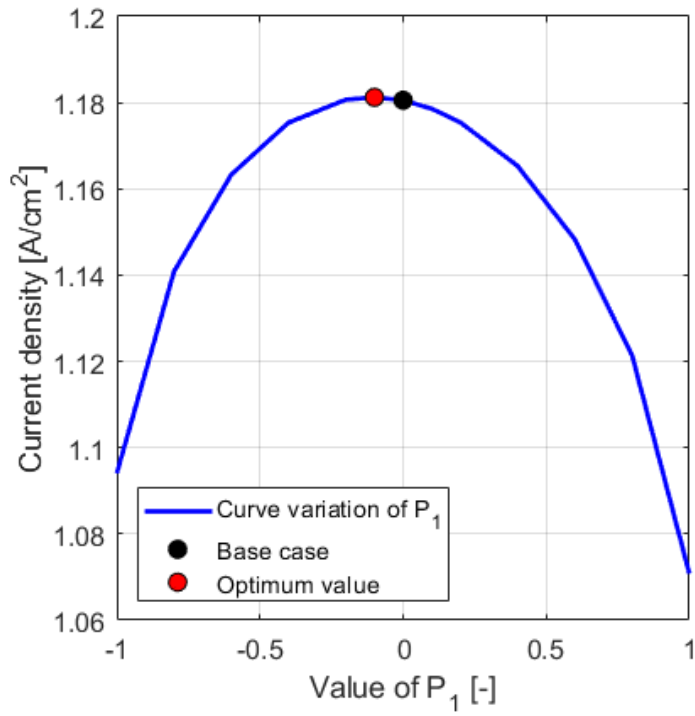


Figure 47 Current values when parameter P_1 changes.

We note that the maximum is obtained for $P_1 = -0.1$, ie for a straight line with a slight decrease. This is since the rate of reaction at the entrance is much lower due to the presence of the liquid water formed.

Studying the case without formation of liquid water we obtain different result, seen in Fig. 48.

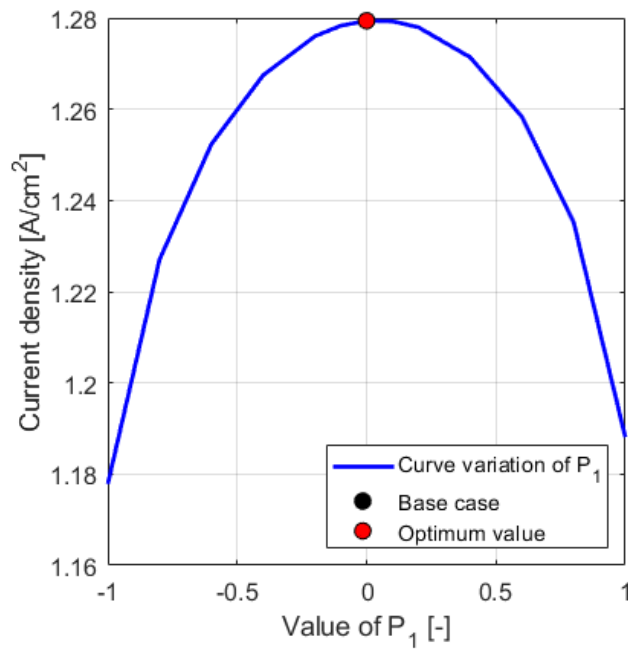


Figure 48 Current values when parameter P_1 changes in case of no formation of water

So, we understand that, the best distribution of A_v is obtained, putting more platinum catalyst loading where the rate of reaction is higher. The presence of liquid water leads to a reduction in rate especially at the entrance where the formation of liquid is greater. Furthermore, a case was studied in which the value of A_v was higher than the referment A_v and the study of the distribution along the x-direction of the cell was repeated and shown in Fig. 49.

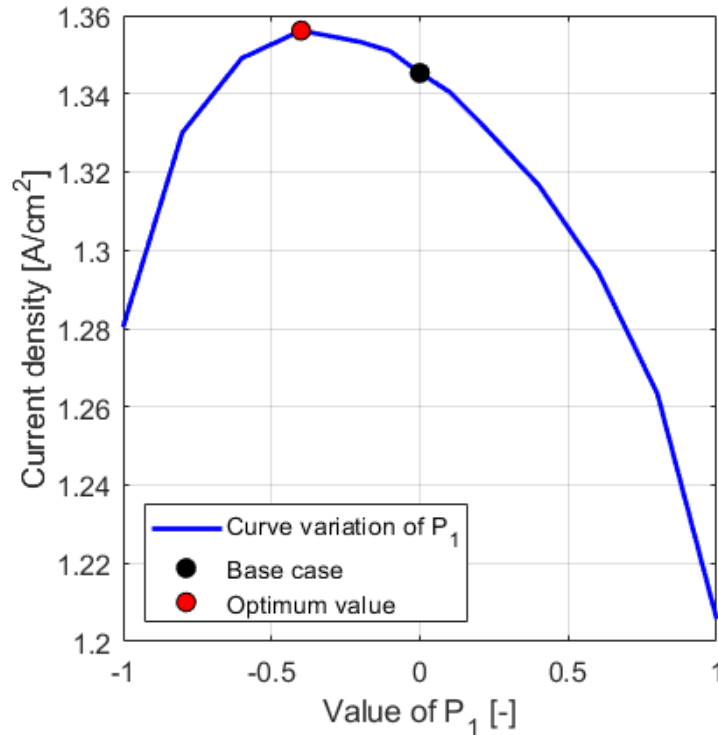


Figure 49 Current values when parameter P_1 changes. Case when $A_v=15000 \left[\frac{1}{mm}\right]$

The best distribution is obtained for $P_1 = -0.4$. This is because, as A_v is higher, the reaction rate increases, and more water is produced at the entrance. This leads to a better solution when A_v is more outgoing.

In both cases (both with referment A_v and with increased A_v) the variation of performance is not very high. With an optimal distribution where the progress of A_v along the length follows the trend of the reaction rate the maximum possible increase can be obtained. The percentual increase in performance from the base case to the best case is calculated in the Tab. 15.

Property	Description	Value
$I_{base\ case} \left[\frac{A}{cm^2} \right]$	Current density	1.179
$I_{best\ case} \left[\frac{A}{cm^2} \right]$	Current density	1.1812
$\frac{\Delta I}{I_{base\ case}} [-]$	% of variation	0.068%
$I_{Av=15000} \left[\frac{1}{mm} \right] \left[\frac{A}{cm^2} \right]$	Current density	1.345
$I_{Av=15000}^{Best\ case} \left[\frac{1}{mm} \right] \left[\frac{A}{cm^2} \right]$	Current density	1.356
$\frac{\Delta I}{I_{Av=15000}} [-]$	% of variation	0.811%

Table 15 Variation of cell performance from the basic case to the best case

From the Tab. 15 we understand that the variation of the rate along the x-direction is not very relevant. While in Fig. 50 is shown that along the thickness of the catalyst there is a large variation in the rate of reaction. The value increases by almost one order of magnitude along the thickness of the catalyst.

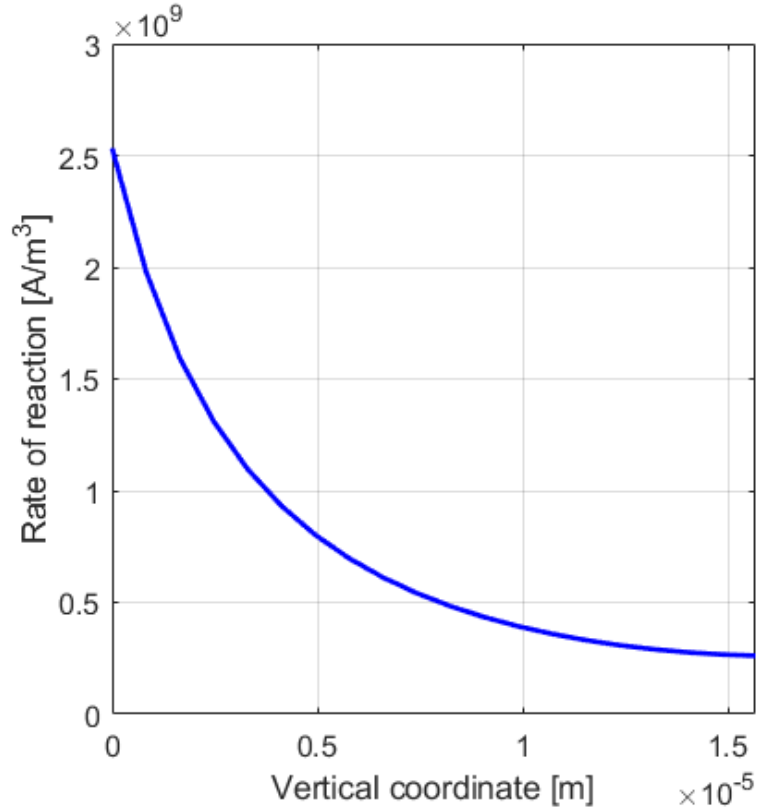


Figure 50 Variation of the rate of reaction along the thickness of the catalyst. Starting from the membrane until reaching the interface between GDL and catalyst.

To understand how the performance of the cell is affected by Av along y direction we consider the following trend:

$$Av = Av_{ref} \frac{y - \left(H_{gc} + t_{cgl} + \frac{t_{cat}}{2}\right)}{H_{gc} + t_{cgl} - \left(H_{gc} + t_{cgl} + \frac{t_{cat}}{2}\right)} P_2 + 1 \quad (81)$$

Exactly as before, a straight line with variable slope is considered to study how the performance of the cell varies in the different configurations. We analyse the cell for 13 different value in the range $P_2 = [-1;1]$ with voltage of cell at 0.4 Volt. The distribution is applied to both catalysts, for positive P_2 we have a decreasing line up to the interface with the membrane, while for negative P_2 vice versa.

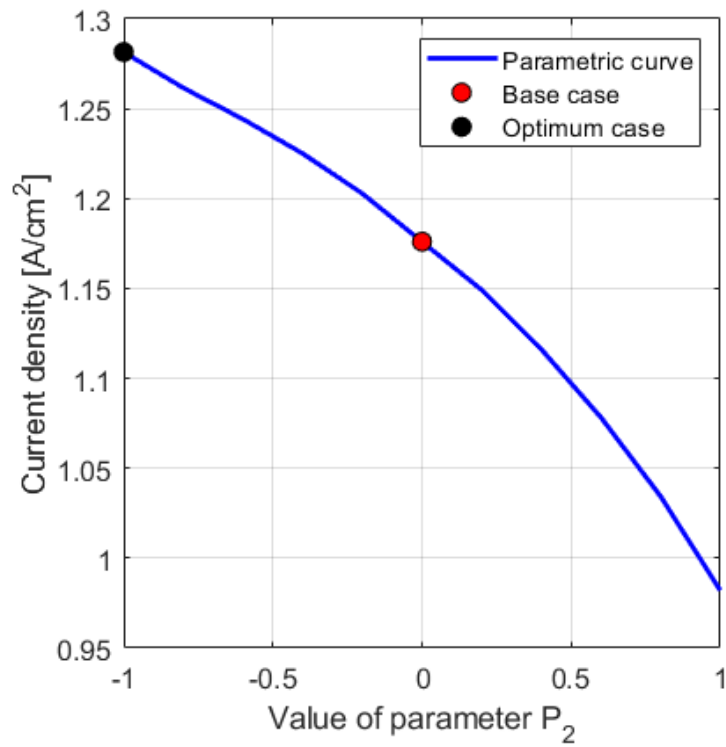


Figure 51 Study of the current production trend, by varying the slope of the distribution function of the platinum catalyst loading at $x=0.15$ m

From Fig. 51 it is clear that the best configuration result is $P_2 = -1$, that is when the straight line has its highest possible value near the membrane.

Property	Description	Value
$I_{base\ case} \left[\frac{A}{cm^2} \right]$	Current density	1.179
$I_{best\ case} \left[\frac{A}{cm^2} \right]$	Current density	1.281
$\frac{\Delta I}{I_{base\ case}} [-]$	% of variation	8.68%

Table 16 Variation of cell performance from the basic case to the best case

Also, from this study we understand that it is more convenient to add more catalyst, where the reaction rate is higher. We also note that the cell performance variation is more significant than the x direction case, as we can see from the Tab. 16.

Changing the distribution of A_v reduces the ohmic losses, but not those of distribution. As you can see in fact the cell fails to go beyond the current value of $1.4 \text{ [A/cm}^2\text{]}$ because the high rate of reaction at some point produces too much water, which becomes liquid, and begins to slow down and block reactions, as shown in Fig. 52, while in Fig. 53 there is the graph of power.

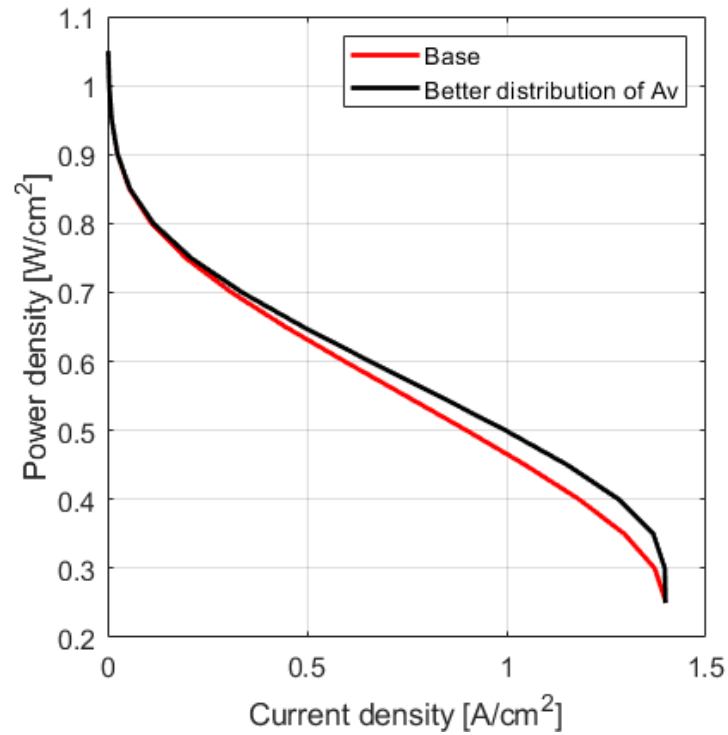


Figure 52 Difference of the polarization curve with different distribution of catalyst loading.

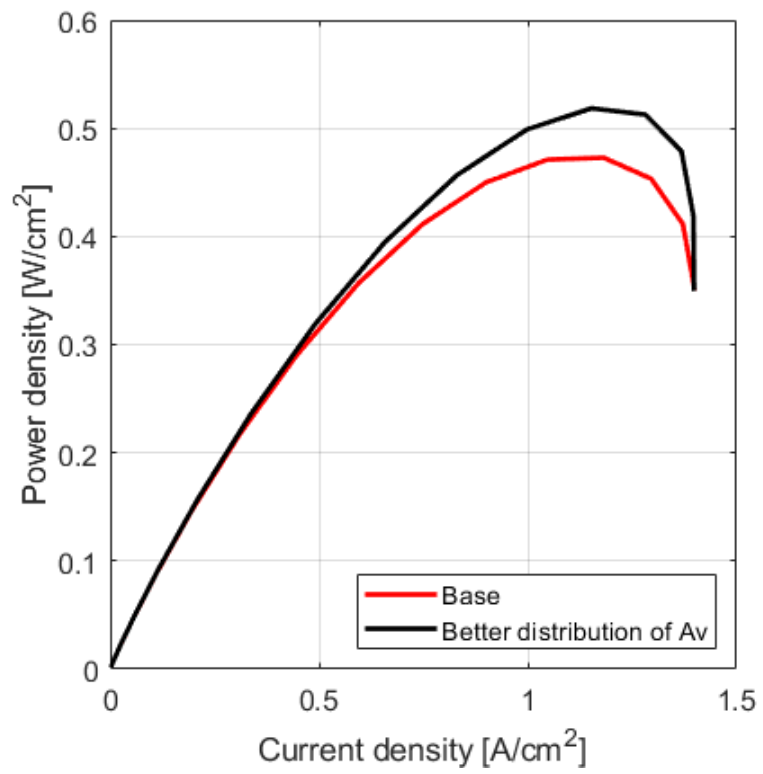


Figure 53 Difference of the power curve with different distribution of catalyst loading.

6 Conclusion

In this work, the elementary physics of a polymer membrane fuel cell was illustrated, showing all the aspects related to the motion of the water and how it changes the performances of the cell. A fuel cell model has been developed to predict the main physical phenomena involved and identify design trends and guidelines. We considered gas dynamics, species transport, water mass transfer between all its forms and ions and electrons transport.

To understand better how the water influences the performances of the cell, we have considered three different states of water, and each of them has its own physics, and therefore is resolved with a different equation. Many articles from literature model the fuel cell in single phase mode: they study all aspects of the fuel cell without taking into account the motion of water both in the membrane and in the liquid phase in the presence of excessive production. Through these models the losses due to activations and the ohmic drops can be well represented, but they do not correctly model the anode dehydration (with increase of ohmic losses) and the diffusion losses. The amount of water present in the model is able to influence both the ohmic aspects of the cell, and the diffusive aspects. In this way it is possible to take into account the behaviour of the cell at low voltages;

The governing equations are discretized using the finite element method and solved with a damped Newton method, using the commercial software COMSOL Multiphysics[®].

So, in this study, it was shown how the computational model of the cell was constructed, how it was validated and how it adequately reflects the behaviour of the cell, also by varying the operating parameters. Results show that the liquid water transport within the cell must take into account the loss of performance, due to reduction of rate of reaction even at low current densities. Moreover, the water transport through the Nafion and portions of the catalyst have an important role with respect to both ohmic losses and diffusion losses at the cathode.

A modification of the most significant design and operating parameters was carried out to investigate potential improvement of the device. It was demonstrated that the efficiency of the cell is strongly dependent on both the catalyst loading and porosity. This shows that in design studies, it is very important to study the optimum of these parameters, which can hardly be changed after installation. An optimal value of catalyst porosity has been found, which makes the concentration of reactants near the membrane. Concerning the catalyst loading, we analysed the effect of the specific active area per unit volume by varying its distribution along the domain of the catalyst. Using simple linear distributions, a 10% current density gain could be obtained.

In the future, one could think of optimizing the distribution of platinum through a topology optimization under costs constraints. This study must be done in order to optimize the rate of reaction to the working conditions that are more exploited in the cell. Noting from the study how the rate of reaction varies within the catalyst, it is possible to think of new Pemfc configurations where the catalyst has a different thickness and study how the rate and the consequent formation of water changes.

7 Bibliography

- [1] Robledo, C. B., Oldenbroek, V., Abbruzzese, F., & van Wijk, A. J. M. (2018). Integrating a hydrogen fuel cell electric vehicle with vehicle-to-grid technology, photovoltaic power and a residential building. *Applied Energy*, 215, 615–629. doi:10.1016/j.apenergy.2018.02.038
- [2] Djilali, N. (2007). Computational modelling of polymer electrolyte membrane (PEM) fuel cells: Challenges and opportunities. *Energy*, 32(4), 269–280. doi:10.1016/j.energy.2006.08.007
- [3] Siegel, C. (2008). Review of computational heat and mass transfer modeling in polymer-electrolyte-membrane (PEM) fuel cells. *Energy*, 33(9), 1331–1352. doi:10.1016/j.energy.2008.04.015.
- [4] Wang, Y., Chen, K. S., Mishler, J., Cho, S. C., & Adroher, X. C. (2011). A review of polymer electrolyte membrane fuel cells: Technology, applications, and needs on fundamental research. *Applied Energy*, 88(4), 981–1007. doi:10.1016/j.apenergy.2010.09.030.
- [5] Carton, J. G., Lawlor, V., Olabi, A. G., Hochenauer, C., & Zauner, G. (2012). Water droplet accumulation and motion in PEM (Proton Exchange Membrane) fuel cell mini-channels. *Energy*, 39(1), 63–73. doi:10.1016/j.energy.2011.10.023.
- [6] Ju, H., Meng, H., & Wang, C.-Y. (2005). A single-phase, non-isothermal model for PEM fuel cells. *International Journal of Heat and Mass Transfer*, 48(7), 1303–1315. doi:10.1016/j.ijheatmasstransfer.2004.10.004.
- [7] Wang, Y., & Wang, C.-Y. (2006). A Nonisothermal, Two-Phase Model for Polymer Electrolyte Fuel Cells. *Journal of The Electrochemical Society*, 153(6), A1193. doi:10.1149/1.2193403.
- [8] Teng, Y.-T., & Wang, F.-C. (2016). Cost analyses and optimization of a PEMFC electric vehicle model. 2016 IEEE/SICE International Symposium on System Integration (SII). doi:10.1109/sii.2016.7844112
- [9] Bavarian, M., Soroush, M., Kevrekidis, I. G., & Benziger, J. B. (2010). Mathematical Modeling, Steady-State and Dynamic Behavior, and Control of Fuel Cells: A Review†. *Industrial & Engineering Chemistry Research*, 49(17), 7922–7950. doi:10.1021/ie100032c.

- [10] Bajpai, H., Khandelwal, M., Kumbur, E. C., & Mench, M. M. (2010). A computational model for assessing impact of interfacial morphology on polymer electrolyte fuel cell performance. *Journal of Power Sources*, 195(13), 4196–4205. doi:10.1016/j.jpowsour.2009.12.121
- [11] O'Hayre, R., Cha, S.-W., Colella, W., & Prinz, F. B. (2016). *Fuel Cell Fundamentals*. doi:10.1002/9781119191766
- [12] Ahmed, D. H., & Sung, H. J. (2008). Design of a deflected membrane electrode assembly for PEMFCs. *International Journal of Heat and Mass Transfer*, 51(21-22), 5443–5453. doi:10.1016/j.ijheatmasstransfer.2007.08.037.
- [13] Shou, D., Fan, J., & Ding, F. (2013). Effective diffusivity of gas diffusion layer in proton exchange membrane fuel cells. *Journal of Power Sources*, 225, 179–186. doi:10.1016/j.jpowsour.2012.10.039
- [14] Hu, P., Peng, L., Zhang, W., & Lai, X. (2009). Optimization design of slotted-interdigitated channel for stamped thin metal bipolar plate in proton exchange membrane fuel cell. *Journal of Power Sources*, 187(2), 407–414. doi:10.1016/j.jpowsour.2008.11.047
- [15] Larminie, J., & Dicks, A. (2003). *Fuel Cell Systems Explained*. doi:10.1002/9781118878330
- [16] Gottesfeld, S., & Zawodzinski, T. A. (2008). Polymer Electrolyte Fuel Cells. *Advances in Electrochemical Science and Engineering*, 195–301. doi:10.1002/9783527616794.ch4
- [17] Kakati, B. K., & Deka, D. (2007). Effect of Resin Matrix Precursor on the Properties of Graphite Composite Bipolar Plate for PEM Fuel Cell. *Energy & Fuels*, 21(3), 1681–1687. doi:10.1021/ef0603582.
- [18] Appunti da lezione, Celle a combustibile a membrana polimerica. Descrizione generale della cella e dei suoi principi di funzionamento, Massimo Santarelli.
- [19] Zawodzinski, T. A. (1993). A Comparative Study of Water Uptake By and Transport Through Ionomeric Fuel Cell Membranes. *Journal of The Electrochemical Society*, 140(7), 1981. doi:10.1149/1.2220749.
- [20] Cunningham, B. D., Huang, J., & Baird, D. G. (2007). Review of materials and processing methods used in the production of bipolar plates for fuel cells. *International Materials Reviews*, 52(1), 1–13. doi:10.1179/174328006x102556
- [21] Liao, S.-H., Weng, C.-C., Yen, C.-Y., Hsiao, M.-C., Ma, C.-C. M., Tsai, M.-C., ... Liu, P.-L. (2010). Preparation and properties of functionalized multiwalled carbon

- nanotubes/polypropylene nanocomposite bipolar plates for polymer electrolyte membrane fuel cells. *Journal of Power Sources*, 195(1), 263–270.
doi:10.1016/j.jpowsour.2009.06.064.
- [22] Huang, C.-Y., Chen, Y.-Y., Su, C.-C., & Hsu, C.-F. (2007). The cleanup of CO in hydrogen for PEMFC applications using Pt, Ru, Co, and Fe in PROX reaction. *Journal of Power Sources*, 174(1), 294–301. doi:10.1016/j.jpowsour.2007.09.017
- [23] Sanz, O., Velasco, I., Pérez-Miqueo, I., Poyato, R., Odriozola, J. A., & Montes, M. (2016). Intensification of hydrogen production by methanol steam reforming. *International Journal of Hydrogen Energy*, 41(10), 5250–5259.
doi:10.1016/j.ijhydene.2016.01.084
- [24] Stefano Ferrarese. Upgrade e commissioning di un sistema di testa ad alte prestazioni per le celle a combustibile di tipo pem
- [25] Planes, E., Flandin, L., & Alberola, N. (2012). Polymer Composites Bipolar Plates for PEMFCs. *Energy Procedia*, 20, 311–323. doi:10.1016/j.egypro.2012.03.031
- [26] Alo, O. A., Otunniyi, I. O., Pienaar, Hc., & Iyuke, S. E. (2017). Materials for Bipolar Plates in Polymer Electrolyte Membrane Fuel Cell: Performance Criteria and Current Benchmarks. *Procedia Manufacturing*, 7, 395–401.
doi:10.1016/j.promfg.2016.12.011.
- [27] Garland, N., Benjamin, T., & Kopasz, J. (2007). DOE Fuel Cell Program: Durability Technical Targets and Testing Protocols. *ECS Transactions*.
doi:10.1149/1.2781004.
- [28] Chen, T., Liu, S., Zhang, J., & Tang, M. (2019). Study on the characteristics of GDL with different PTFE content and its effect on the performance of PEMFC. *International Journal of Heat and Mass Transfer*, 128, 1168–1174.
doi:10.1016/j.ijheatmasstransfer.2018.09.097.
- [29] Commercial Fuel Cell Components, Fuel Cells Etc, <https://fuelcellsetc.com>
- [30] Eikerling, M., & Kornyshev, A. A. (1998). Modelling the performance of the cathode catalyst layer of polymer electrolyte fuel cells. *Journal of Electroanalytical Chemistry*, 453(1-2), 89–106. doi:10.1016/s0022-0728(98)00214-9
- [31] Sui, P.-C., Chen, L.-D., Seaba, J. P., & Wariishi, Y. (1999). Modeling and Optimization of a PEMFC Catalyst Layer. *SAE Technical Paper Series*.
doi:10.4271/1999-01-0539.

- [32] Marr, C., & Li, X. (1999). Composition and performance modelling of catalyst layer in a proton exchange membrane fuel cell. *Journal of Power Sources*, 77(1), 17–27. doi:10.1016/s0378-7753(98)00161-x.
- [33] BROKA, K., & EKDUNGE, P. (1997). *Journal of Applied Electrochemistry*, 27(3), 281–289. doi:10.1023/a:1018476612810.
- [34] Genevey, D. B., von Spakovsky, M. R., Ellis, M. W., Nelson, D. J., Olsommer, B., Topin, F., & Siegel, N. (2002). Transient Model of Heat, Mass, and Charge Transfer as Well as Electrochemistry in the Cathode Catalyst Layer of a PEMFC. *Advanced Energy Systems*. doi:10.1115/imece2002-33322.
- [35] Dokkar, B., Settou, N. E., Imine, O., Saifi, N., Negrou, B., & Nemouchi, Z. (2011). Simulation of species transport and water management in PEM fuel cells. *International Journal of Hydrogen Energy*, 36(6), 4220–4227. doi:10.1016/j.ijhydene.2010.09.060
- [36] Jiao, K., & Li, X. (2011). Water transport in polymer electrolyte membrane fuel cells. *Progress in Energy and Combustion Science*, 37(3), 221–291. doi:10.1016/j.pecs.2010.06.002
- [37] Werner, C., Busemeyer, L., & Kallo, J. (2015). The impact of operating parameters and system architecture on the water management of a multifunctional PEMFC system. *International Journal of Hydrogen Energy*, 40(35), 11595–11603. doi:10.1016/j.ijhydene.2015.02.012.
- [38] Choi, K.-H., Peck, D.-H., Kim, C. S., Shin, D.-R., & Lee, T.-H. (2000). Water transport in polymer membranes for PEMFC. *Journal of Power Sources*, 86(1-2), 197–201. doi:10.1016/s0378-7753(99)00420-6.
- [39] Brandell, D., Karo, J., Liivat, A., & Thomas, J. O. (2007). Molecular dynamics studies of the Nafion®, Dow® and Aciplex® fuel-cell polymer membrane systems. *Journal of Molecular Modeling*, 13(10), 1039–1046. doi:10.1007/s00894-007-0230-7.
- [40] Moshtarikhah, S., Oppers, N. A. W., de Groot, M. T., Keurentjes, J. T. F., Schouten, J. C., & van der Schaaf, J. (2016). Nernst–Planck modeling of multicomponent ion transport in a Nafion membrane at high current density. *Journal of Applied Electrochemistry*, 47(1), 51–62. doi:10.1007/s10800-016-1017-2
- [41] Siegel, N. P., Ellis, M. W., Nelson, D. J., & von Spakovsky, M. R. (2004). A two-dimensional computational model of a PEMFC with liquid water transport. *Journal of Power Sources*, 128(2), 173–184. doi:10.1016/j.jpowsour.2003.09.072.

- [42] Chang, S.-M., & Chu, H.-S. (2006). Transient behavior of a PEMFC. *Journal of Power Sources*, 161(2), 1161–1168. doi:10.1016/j.jpowsour.2006.06.025.
- [43] Dehghan, H., & Aliparast, P. (2011). An Investigation into the Effect of Porous Medium on Performance of Heat Exchanger. *World Journal of Mechanics*, 01(03), 78–82. doi:10.4236/wjm.2011.13011.
- [44] Simulate Battery and Fuel Cell Designs with the Batteries & Fuel Cells Module, Comsol multi-physics®
- [45] Kubaczka, A. (2014). Prediction of Maxwell–Stefan diffusion coefficients in polymer–multicomponent fluid systems. *Journal of Membrane Science*, 470, 389–398. doi:10.1016/j.memsci.2014.06.055
- [46] Mann, R. F., Amphlett, J. C., Peppley, B. A., & Thurgood, C. P. (2006). Application of Butler–Volmer equations in the modelling of activation polarization for PEM fuel cells. *Journal of Power Sources*, 161(2), 775–781. doi:10.1016/j.jpowsour.2006.05.026
- [47] Liu, Z., Zeng, X., Ge, Y., Shen, J., & Liu, W. (2017). Multi-objective optimization of operating conditions and channel structure for a proton exchange membrane fuel cell. *International Journal of Heat and Mass Transfer*, 111, 289–298. doi:10.1016/j.ijheatmasstransfer.2017.03.120.
- [48] Futter, G. A., Gazdzicki, P., Friedrich, K. A., Latz, A., & Jahnke, T. (2018). Physical modeling of polymer-electrolyte membrane fuel cells: Understanding water management and impedance spectra. *Journal of Power Sources*, 391, 148–161. doi:10.1016/j.jpowsour.2018.04.070.
- [49] The optimization of channels for a proton exchange membrane fuel cell applying genetic algorithm, Xiangbing Zeng, Ya Ge, Jun Shen, Lingping Zeng, Zhichun Liu, Wei Liu
- [50] Zeng, X., Ge, Y., Shen, J., Zeng, L., Liu, Z., & Liu, W. (2017). The optimization of channels for a proton exchange membrane fuel cell applying genetic algorithm. *International Journal of Heat and Mass Transfer*, 105, 81–89. doi:10.1016/j.ijheatmasstransfer.2016.09.068
- [51] Natarajan, D., & Nguyen, T. V. (2003). A Two-Dimensional, Two-Phase, Multicomponent, Transient Model for the Cathode of a Proton Exchange Membrane Fuel Cell Using Conventional Gas Distributors [Journal of the Electrochemical Society 148, A1324 (2001)]. *Journal of The Electrochemical Society*, 150(3), L5. doi:10.1149/1.1554417

- [52] Siegel, N. P., Ellis, M. W., Nelson, D. J., & von Spakovsky, M. R. (2003). Single domain PEMFC model based on agglomerate catalyst geometry. *Journal of Power Sources*, 115(1), 81–89. doi:10.1016/s0378-7753(02)00622-5
- [53] Zawodzinski, T. A. (1993). A Comparative Study of Water Uptake By and Transport Through Ionomeric Fuel Cell Membranes. *Journal of The Electrochemical Society*, 140(7), 1981. doi:10.1149/1.2220749.
- [54] Yin, Y., Wang, X., Shangguan, X., Zhang, J., & Qin, Y. (2018). Numerical investigation on the characteristics of mass transport and performance of PEMFC with baffle plates installed in the flow channel. *International Journal of Hydrogen Energy*, 43(16), 8048–8062. doi:10.1016/j.ijhydene.2018.03.037.
- [55] Slade, S. M., Ralph, T. R., Ponce de León, C., Campbell, S. A., & Walsh, F. C. (2010). The Ionic Conductivity of a Nafion® 1100 Series of Proton-exchange Membranes Re-cast from Butan-1-ol and Propan-2-ol. *Fuel Cells*, 10(4), 567–574. doi:10.1002/fuce.200900118.
- [56] Abstracts from the Fall Meeting of the Comparative Cognition Society 2013, November 14, Toronto, Ontario. (2013). PsycEXTRA Dataset. doi:10.1037/e630982013-001
- [57] *Tabelle di Termodinamica Applicata e Trasmissione del Calore*, Marco Torchio
- [58] Quarteroni, A., & Saleri, F. (n.d.). Numerical methods for (initial-)boundary-value problems. *Scientific Computing with MATLAB and Octave*, 237–265. doi:10.1007/3-540-32613-8_8.
- [59] Um, S., Wang, C.-Y., & Chen, K. S. (2000). Computational Fluid Dynamics Modeling of Proton Exchange Membrane Fuel Cells. *Journal of The Electrochemical Society*, 147(12), 4485. doi:10.1149/1.1394090.
- [60] A review of: “Introduction to Fluid Mechanics” Fourth Edition SI Version R. W. Fox & A. T. McDonald, 1994 New York, Chichester, John Wiley and Sons ISBN 0471 59274 9 £19.95. (1994). *European Journal of Engineering Education*, 19(4), 513–513. doi:10.1080/03043799408928334.
- [61] Bernardi, D. M. (1992). A Mathematical Model of the Solid-Polymer-Electrolyte Fuel Cell. *Journal of The Electrochemical Society*, 139(9), 2477. doi:10.1149/1.2221251.

- [62] Nguyen, T. V. (1993). A Water and Heat Management Model for Proton-Exchange-Membrane Fuel Cells. *Journal of The Electrochemical Society*, 140(8), 2178. doi:10.1149/1.2220792.
- [63] Yang, Y., Guo, L., & Liu, H. (2012). Factors affecting corrosion behavior of SS316L as bipolar plate material in PEMFC cathode environments. *International Journal of Hydrogen Energy*, 37(18), 13822–13828. doi:10.1016/j.ijhydene.2012.04.026
- [64] Ebrahimi, S., Roshandel, R., & Vijayaraghavan, K. (2016). Power density optimization of PEMFC cathode with non-uniform catalyst layer by Simplex method and numerical simulation. *International Journal of Hydrogen Energy*, 41(47), 22260–22273. doi:10.1016/j.ijhydene.2016.07.247.